Non-linear terms in Delta Scuti stars power spectra
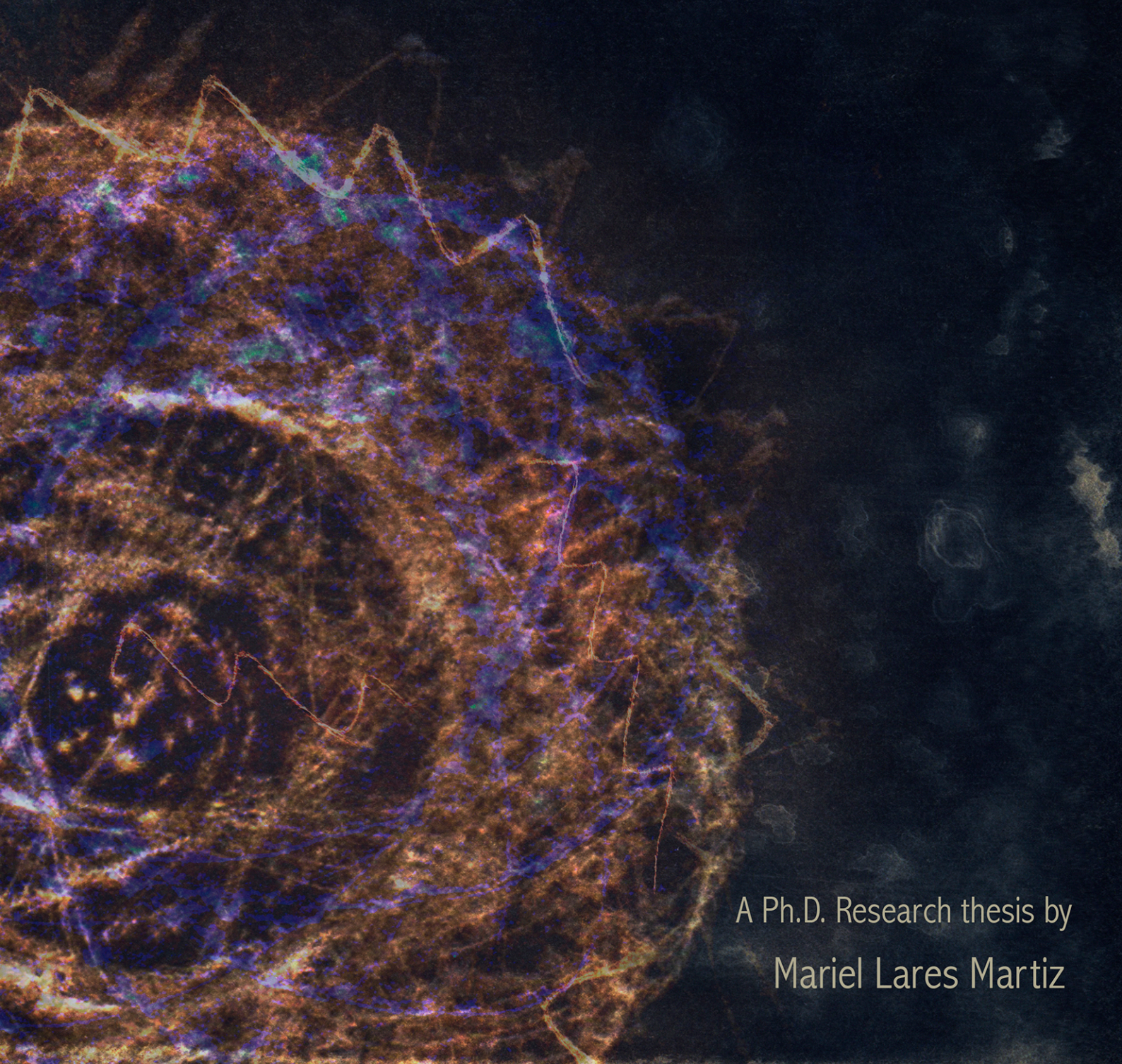
A Ph.D. Research thesis by

Mariel Lares Martiz

Non-linear terms in δ Scuti stars power spectra

By

Mariel Lares Martiz

A thesis submitted to
the University of Granada
for the degree of
DOCTOR OF PHYSICS AND MATHEMATICS

Asteroseismology Research Group
Department of Stellar Physics
Institute of Astrophysics of Andalusia-CSIC
University of Granada
April 2021

El doctorando / The *doctoral candidate* **Mariel Lares Martiz** y los directores de la tesis / and the thesis supervisor/s: **Rafael Garrido Haba y Javier Pascual Granado**

Garantizamos, al firmar esta tesis doctoral, que el trabajo ha sido realizado por el doctorando bajo la dirección de los directores de la tesis y hasta donde nuestro conocimiento alcanza, en la realización del trabajo, se han respetado los derechos de otros autores a ser citados, cuando se han utilizado sus resultados o publicaciones.

/

Guarantee, by signing this doctoral thesis, that the work has been done by the doctoral candidate under the direction of the thesis supervisor/s and, as far as our knowledge reaches, in the performance of the work, the rights of other authors to be cited (when their results or publications have been used) have been respected.
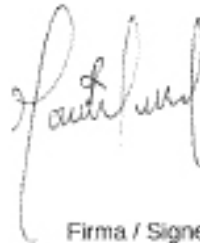
Lugar y fecha / Place and date: Granada, 5 de abril del 2021

Director/es de la Tesis / *Thesis supervisor/s;*

Doctorando / *Doctoral candidate:*

Firma / Signed

Firma / Signed

RESUMEN

Los modelos de pulsación estelar disponibles hasta la fecha no explican en su totalidad los espectros de potencias observados para las estrellas del tipo δ Scuti. Dichos espectros presentan una distribución en frecuencias muy diferentes, incluso para estrellas que poseen parámetros estelares muy similares. Este es el caso, por ejemplo, de las estrellas llamadas *híbridas*, que pulsan en un régimen tanto de modos p como de modos g, o la existencia de estrellas sin oscilaciones dentro de las bandas de inestabilidad de pulsación. Estos hechos sugieren que se han de revisar los mecanismos de excitación y de amortiguamiento que operan en estas estrellas, o introducir otros mecanismos causantes de la aparición de frecuencias en los espectros de potencias que los modelos actuales no son capaces de reproducir.

Uno de los mecanismos físicos que dan origen a máximos en los espectros de potencia y que los modelos actuales no tienen en cuenta, son los procesos no-lineales. Una respuesta no-lineal del medio estelar a la oscilación, debido a cambios de grosor de la capa convectiva, entre otros procesos, pueden causar distorsión en la forma sinusoidal de las curvas de luz. Como consecuencia, aparecen en los espectros de potencia frecuencias de combinaciones entre modos de oscilación propios de la estrella, llamadas términos no-lineales o no-linealidades.

En esta tesis, se estudian los términos no-lineales presentes en las estrellas δ Scuti con el objetivo de identificarlos inequívocamente. La motivación radica tanto en conseguir extraerlos correctamente de los espectros de potencia (para así explicar la distribución en frecuencia con los modelos de pulsación lineal disponibles), como en caracterizarlos, para en un futuro construir modelos no-lineales de pulsación.

Como resultado del trabajo de investigación, en esta memoria se presenta un método autoconsistente para extraer no-linealidades que garantiza residuos no correlados con dichos términos. El método permite identificar frecuencias con precisiones muy altas, del orden de las alcanzadas por el método O-C, en el caso de estrellas mono-periódicas. También permite,

en el caso de estrellas de doble modo o multi-periódicas, identificar estructuras de frecuencias ocultas en lo que, antes de la extracción, se consideraba ruido.

Además, se muestran resultados de una posible caracterización de los términos no lineales en estrellas High Amplitude δ Scuti. Se presenta un método basado en dicha caracterización de no linealidades que permitiría discriminar modos radiales en estrellas Low Amplitude δ Scuti, proporcionando así una restricción adicional que posibilitaría la identificación modal. Esta sería la primera vez que los términos no lineales son útiles, aunque indirectamente, para llevar a cabo un análisis astrosismológico en estrellas pulsantes de masa intermedia. Finalmente, se presentan también resultados para algunas estrellas variable del tipo γ Doradus, constituyendo el inicio de la caracterización de términos no lineales producto de la interacción de modos no radiales.

DEDICATORIA

Esta disertación/tesis está dedicada a mi yo del futuro. Para que recuerde y nunca olvide de lo que es capaz.

AGRADECIMIENTOS

En primer lugar, el mayor agradecimiento está dirigido a mis directores de tesis Rafael Garrido Haba y Javier Pascual Granado. Uno por sus ideas geniales que me sacaban de cualquier atasco y el otro por su meticulosas revisiones y precisas sugerencias. He obtenido de ellos tanto conocimiento y experiencia que me han permitido publicar en revistas científicas de alto nivel, cuestión que sin ellos no hubiera sido posible.

Quisiera agradecer también a los compañeros de grupo Antonio García Hernández, José Ramón Rodón, Juan Carlos Suárez y Andrés Moya por todas las veces que me habéis ayudado y acompañado en estos años. Estarán siempre en mis recuerdos esos congresos a los que hemos asistido, gracias por ayudarme a presentar mi trabajo a la comunidad internacional y a establecer los contactos cuya importancia he descubierto que es fundamental en el gremio.

Esta investigación fue financiada por la Agencia Estatal de Investigación y el Fondo Europeo de Desarrollo Regional bajo el proyecto con referencia ESP2017-87676-C5-5-R, titulado *"CONTRIBUCIÓN DEL IAA-CSIC A LA MISIÓN ESPACIAL PLATO2.0: FASES B2/C/D. OPERACION DE NOMAD-EXOMARS"* y fue realizada en las instalaciones del Instituto de Astrofísica de Andalucía, a cuyo personal extiendo mis agradecimientos por mantener un centro de investigación donde el ambiente de trabajo fue en todo momento más que agradable. Asimismo, me gustaría agradecer al departamento de Astrofísica de la Universidad Católica de Lovaina (IvS-KULeuven), por la calurosa acogida durante los 3 meses de estancia de investigación que allí realicé. Especialmente, a mi supervisor el Dr. Dominic Bowman y los demás miembros del grupo MAMSIE, con los que espero continuar la colaboración científica en el futuro.

Finalmente, quisiera agradecer a mis familiares, amigos y pareja, cuyos ánimos y consejos

durante todos estos años me impulsaron a continuar. Con un cariño especial, agradezco a Estefanía Casal López, el descubrimiento de estos años que más atesoro. ¡Por muchos más cafés juntas, amiga!.

PREFACIO

El presente trabajo forma parte de la actual línea de investigación que persigue el Grupo de Variabilidad Estelar (GVE) del Instituto de Astrofísica de Andalucía, donde se han estudiado las estrellas del tipo δ Sct desde sus inicios, en la década de los 70. Históricamente, el GVE comenzó sus aportaciones al entendimiento de estas estrellas pulsantes llevando a cabo observaciones desde tierra, más concretamente, en el Observatorio de Sierra Nevada (OSN), cuyas instalaciones proporcionan gran precisión en las observaciones posibilitando análisis astrosismológicos. Dicha precisión permitió al OSN posicionarse como uno de los centros de observación pertenecientes a la *Delta Scuti Network* (DSN), que fue una campaña de observación coordinada por diferentes observatorios en diferentes ubicaciones del mundo con el objetivo de obtener curvas de luz de mayor duración, traduciéndose en mayor resolución de las frecuencias correspondientes a las oscilaciones de las estrellas variables.

Pronto, los análisis realizados por el GVE a las curvas de luz proporcionadas por la DSN mostraron inconsistencias con los modelos disponibles. Con el fin de comprender el origen de estas discrepancias, se desarrollaron modelos teóricos incluyendo los efectos de la rotación y la no-adiabaticidad. Estos esfuerzos constituyen los modelos más efectivos disponibles hasta la fecha. Sin embargo, las discrepancias continuaban sin respuesta, por lo que la idea de que el origen de estas se debía al análisis de datos dado a las curvas de luz empezó a cobrar mayor peso en la línea de investigación del GVE.

Con la llegada de las misiones espaciales se obtuvieron por primera vez espectros de potencias ultraprecisos. La relación señal/ruido era tan superior a las alcanzadas por las observaciones desde tierra que muchos nuevos máximos fueron detectados. Paradójicamente, mayor precisión complicó el análisis: Las frecuencias originadas por la ventana espectral

en observaciones con un duty-cycle del 90% antes hubieran sido consideradas irrelevantes. Además, otras frecuencias, originadas por el funcionamiento del instrumento (e.g. variaciones térmicas), y que modulan la señal de las pulsaciones, antes eran indetectables. De la misma manera, aumentó la capacidad de detectar frecuencias correspondientes a la interacción entre modos de pulsación propios de la estrella, llamados términos no-lineales. La línea de investigación actual del GVE se centra en métodos para atenuar el efecto de las ventanas de observación sobre los datos y, con este trabajo de investigación, se pretende estudiar los términos no-lineales presentes en las estrellas del tipo δ Sct.

Dentro de este contexto, la investigación expuesta en esta memoria proporciona la base empírica necesaria para construir modelos no-lineales, además de la base general para la construcción del modelo analítico que explique la presencia de los términos no-lineales en estrellas variables. Asimismo, los métodos que aquí se describen para identificar sin ambigüedad estos términos, constituyen una consecución del GVE para estar un paso más cerca de comprender las, hasta ahora enigmáticas, estrellas δ Sct.

Contents

List of Figures

List of Tables

Chapter One

Introduction

1.1 Asteroseismology

The possibility of physically piercing into a star to measure the properties of its internal structure is very remote, even for the technology available nowadays. Scientific inference is the most obvious alternative to understand how are the stars like inside, and asteroseismology is providing satisfactory answers to this for half a century now. Asteroseismology is the field of astrophysics which provides density profiles, rotation profiles, interior chemical transport, and even ages of the variable stars, all through the study of their pulsations. Certainly, these contributions have been of great importance to the development of the knowledge of the stellar structure and evolution available at the present moment.

Variable stars are the stars whose measurements of their luminosity changes with time. They are divided in extrinsic variables, where the variability is owed to external causes (e.g. in a binary system, a transit of the companion causes periodic changes in the measurements of the luminosity), and intrinsic variables (or pulsating stars), where the variability is actually coming from the star itself. These pulsations, generate standing waves that travel trough the stellar medium, from which asteroseismology extracts all the information.

1.1.1 Historical overview

Methodical observations of the night sky, ever since the ancient times up to the establishment of the scientific method, have allowed to study pulsating stars for quite a long time. The first record of an astronomical observation of a variable star is the one made in 1596 by David Fabricius, when he discovered the Mira star (Jeffery, 2008). Later on (1785), John Goodrike was the first one to make photometric measurements of variability using reference stars. This comparison technique allowed him to discover the variability of the δ Cepheid star (Goodricke and Englefield, 1785).

It was not until the 20th century that astronomers discussed the possibility that light variation, observed for high amplitude and long periods variables, could have an intrinsic nature (Moulton, 1909). The work of Shapley (1914) backed up this assumption, considering the Cepheid stars variability in terms of radial oscillations as the most probable explanation. But it was not until Sir Arthur Stanley Eddington proposed that a star could be working as a Carnot engine in the thermodynamical sense, that sustained pulsation was physically understood. The Eddington mechanism would lead the star to pulsate in their natural oscillation modes, which are determined by the structure of the star. This explanation was first exposed in his *Pulsation Theory for Cepheid variables* (Eddington, 1917), later explained thoroughly in *The Internal Constitution of the Stars* (Eddington, 1920, 1926).

About the same time (1912), Henrietta Swan Leavitt found the period-luminosity relation observed for Cepheid stars, when studying a sample of them in the Magellanic cloud. By this time, it became clear that pulsating stars have considerable important applications in astrophysics. For example, to achieve high precision in distance measurements and to determine general properties of the stars (e.g. their density), by knowing the fundamental radial mode.

Over time, not only radial oscillations were studied, but also the presence of non-radial pulsations (Zhevakin, 1953) begins to be a possibility for explaining features that could

not have been explained before (e.g. width variations in β Canis Majoris spectral lines). Furthermore, the development of the perturbed equations of the stellar interior, together with technology improvement, allowed for what might be called the first asteroseismic study, where deeper layers than the photosphere could now be explored in greater detail for our nearest star, the Sun. The first integrated light observations of the entire solar disk, allowed Claverie et al. (1979) to interpret regular disturbances on the solar surface as the superposition of acoustic modes (see Section 1.1.3) trapped in different sections inside the solar cavity. This observing technique was applied to other types of variable stars, modelling their interiors with more or less success, consolidating asteroseismology as a growing research area at the service of improving current models of stellar evolution.

More recently, the field of asteroseismology experienced a boost in their findings in the light of space missions. In the 90's, many project proposals to take photometric observations from space were requested, but none of them approved (Stars, Prisma, Mons, Eddington). The first satellite dedicated to asteroseismology studies was the MOST spacecraft. It was launched in 2003 by the Canadian Space Agency (CSA). Although it enabled many discoveries, later proposals had to be attached to exoplanetary transits missions. For example, the CoRoT satellite (Auvergne et al., 2009), launched in 2006 by the French Space Agency (CNES) along with the European Space Agency (ESA). Its photometric measurements met the requirements of long observation with very high duty cycles of $\approx 90\%$, for obtaining ultra-precise data. The *Kepler* mission (Gilliland et al., 2010), led by the United States of America National Aeronautics and Space Administration (NASA), was launched in 2008. This mission also delivered extraordinary duty cycles and light curves of ultra-precise quality, still producing relevant discoveries.

Next, a brief summary of the theoretical framework of asteroseismology is presented with the purpose of facilitating the understanding of the content of this thesis. For further details, see Aerts et al. (2010) which is a very complete guide on asteroseismology, and Christensen-Dalsgaard (1997) that delves into the theory of stellar oscillations.

1.1.2 Perturbed linear equations of stellar structure and their solutions

Hydrodynamic equations can describe stars since the stellar medium is considered a continuum (in Eulerian description) of plasma in energy balance. The basic equations of such system, determining density (ρ), velocity ($\vec{v}$), and pressure p (or temperature T) are given by:

- Equation of continuity or mass conservation:

$$\frac{\partial \rho'}{\partial t} + \nabla(\rho \cdot \vec{v}) = 0, \tag{1.1}$$

- Equation of motion:

$$\rho \frac{\partial \vec{v}}{\partial t} + \rho \vec{v} \cdot \nabla \vec{v} = -\nabla p - \rho \nabla \Phi, \tag{1.2}$$

- Equation of Poisson:

$$\nabla^2 \Phi = 4\pi G \rho, \tag{1.3}$$

- Equation of energy or energy conservation:

$$\frac{\partial p}{\partial t} + \vec{v} \cdot \nabla \vec{p} = \frac{\Gamma_1 p}{\rho} \frac{\partial \rho}{\partial t} + \vec{v} \cdot \nabla \vec{\rho}, \tag{1.4}$$

When trying to model the intrinsic oscillations of a star, perturbation analysis is applied to the perturbed hydrodynamic equations. However, solving such equations can be a very complex task, so at this point to simplify considerably the solution it is possible to take the next reasonable approximations:

1. Amplitude of oscillations are small in comparison with global scales of the star (e.g. its radius).

2. Adiabaticity: oscillation periods often greater than the Kevin Helmholtz characteristic time of thermal adjustment.

3. Assume perfect spherical symmetry.

Here, the perturbed stellar structure equations are presented around the equilibrium state (labelled with the zero sub-index) and the perturbed variables represented with a prime (e.g. $\rho\prime$):

- Perturbed equation of continuity or mass conservation:

$$\frac{\partial \rho}{\partial t} + \nabla(\rho_0 \cdot \vec{v}) = 0, \tag{1.5}$$

- Perturbed equation of motion:

$$\frac{\partial \vec{v}}{\partial t} = -\frac{1}{\rho_0}\nabla p' + \frac{\rho'}{\rho_0}\nabla\Phi_0 + \nabla\Phi', \tag{1.6}$$

- Perturbed equation of Poisson:

$$\nabla^2\Phi' = 4\pi G\rho', \tag{1.7}$$

- Perturbed equation of energy or energy conservation:

$$\frac{\partial p}{\partial t} + \vec{v}\cdot\nabla\vec{p_0} = \frac{\Gamma_{1,0}p_0}{\rho_0}\frac{\partial \rho}{\partial t} + \vec{v}\cdot\nabla\vec{\rho_0}, \tag{1.8}$$

where orders higher than one for the perturbation variables are neglected, meaning that they are linearised.

Solutions for the perturbed variables are the eigenfunctions of the form:

$$\vec{\zeta}(r,\theta,\phi,t) = \sum_k a_k\vec{\zeta}(r)Y_l^m(\theta,\phi)e^{(i\omega_k t+\Phi_k)}, \tag{1.9}$$

where $\vec{\zeta}$ represents the perturbed variable and r, θ, ϕ and t are the radial, colatitude, longitude and time variables respectively. The complex exponential represents the harmonic behaviour of the perturbation with angular frequency ω_k, amplitude a_k and phase Φ_k, where k denotes the mode index. Radial and angular solutions can be separated as $\vec{\zeta}(r)$ (separable

in their radial and/or tangential components) and $Y_l^m(\theta, \phi)$ respectively. The latter, namely a spherical harmonic, can also be separated as:

$$Y_l^m(\theta, \phi) = P_l^m(\cos \theta)e^{im\phi};$$ (1.10)

where P_l^m is the Legendre function and l and m are quantum numbers which are going to be explained next.

1.1.3   Pulsation modes

The general equation of oscillations 1.9, characterizes each oscillation (of frequency ω_k) as a pulsation mode with index k described by the quantum numbers l, m and n. The index l is the angular degree of the mode, it accounts for the number of node lines in the surface of the star. The index m is the azimuthal order of the mode, $|m|$ accounts for the number of node lines in the surface to be longitudinal lines but m can take any value in the range from $-l$ to l, consequently for each degree l there are $2l+1$ modes. The index n is the radial order, it accounts for the number of radial nodes inside a star, which by definition specifies the overtone of the mode.

Radial and non-radial modes

Since l and m are involved in the angular solution of Eq. 1.9, the particular case of $l = 0$ describes the radial modes. In this situation, the star expands (cooling) and contracts (heating) as a whole if it is pulsating in the fundamental radial mode, or in the particular shell for any overtone n. Concentric shells expand and contract in anti-phase.

The general case, when $l \geq 1$, Eq. 1.9 refers to a non-radial mode (Fig. 1.1)(see Unno et al. (1989) for the full development of the equations). The simplest non-radial pulsation is the asymmetrical dipole pulsation ($l = 1$). In this pulsation mode the upper section of the sphere is contracting while the other is expanding, leaving the center of mass of the star unchanged. Non-radial modes become difficult to detect from the quadruple mode (when
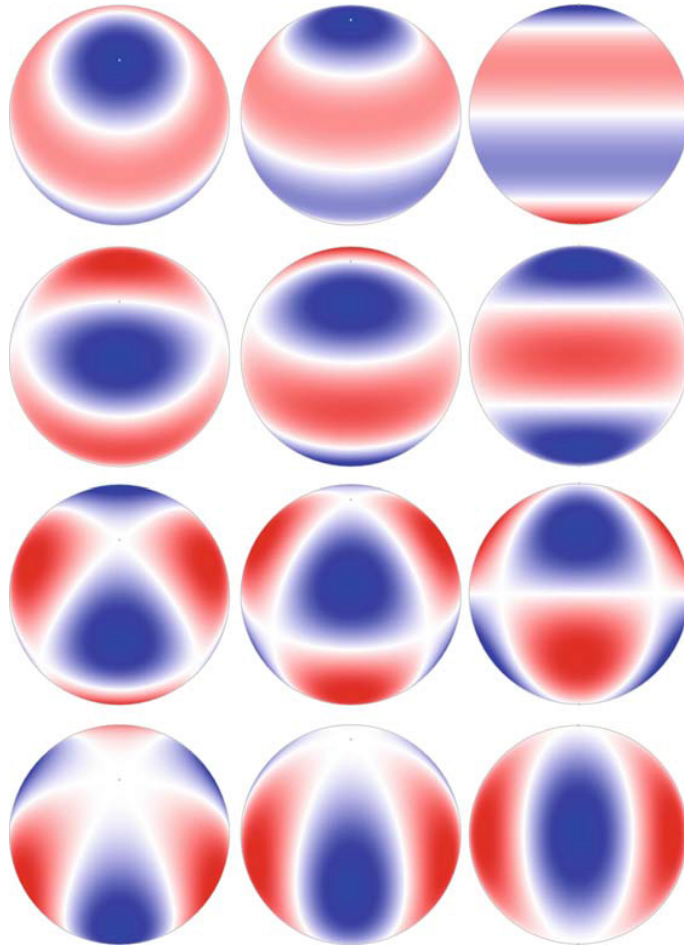
Figure 1.1 Radial and non-radial pulsation modes examples. The columns show the modes from different viewing angles; the left column is for an inclination of the pulsation pole of 30°, the middle column is for 60°, and the right column is for 90°. The white bands represent the positions of the surface nodes; red and blue represent sections of the star that are moving in (out) and/or heating (cooling) at any given time, then vice versa. The top row shows the (l = 3,m = 0) mode, where the nodes lie at latitudes ±51°and 0°. The second row shows the (l = 3,m = ±1) mode, with two nodes that are lines of latitude and one that is a line of longitude. The third row is the (l = 3,m = ±2) mode, and the bottom row shows the (l = 3,m = ±3) mode. Rotation distinguishes the sign of m. Source: (Aerts et al., 2010)

$l = 3$) to higher degree numbers due to effects of partial canceling. When the degree of the mode is high means that many node lines run across the stellar surface, dividing it in many swelling and contracting sections. The partial cancelling effects refer to flux cancellations that take place when a hotter section (brighter) counteracts with a cooler section (dimmer)
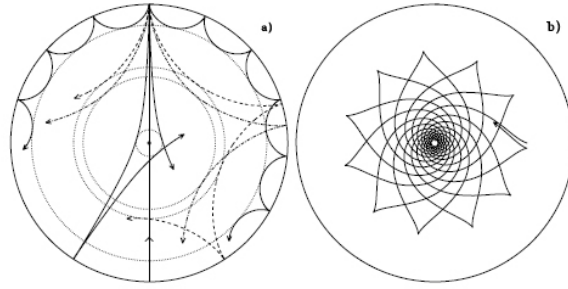
Figure 1.2 Pressure (a) and gravity (b) modes ray path examples. Shown in panel (a) are rays corresponding to modes of frequency 3000 μHz and degrees (in order of increasing penetration depth) l = 75, 25, 20 and 2; the line passing through the centre schematically illustrates the behaviour of a radial mode. The g-mode ray path (panel b) corresponds to a mode of frequency 190 μHz and degree 5 and is trapped in the interior. In this example, it does not propagate in the convective outer part. This figure illustrates that the g-modes are sensitive to the conditions in the very core of the star. Source:(Cunha et al., 2007)

when measuring the integrated light of the whole stellar disk.

Deviations from the spherical symmetry cause the non-radial mode to split, breaking the azimuthal degree degeneracy. This means that the star is pulsating in a multiplet of frequencies, one for each m, separated at a distance proportional to the mechanism that originates the spherical deviation (e.g. the rotation of the star or the presence of a magnetic field).

Pressure and gravity modes

Considering plausible approximations, the motion equation 1.6 can be simplified resulting in a waveform equation, so that plain waves can be solutions. Two possibilities, in terms of the restoring force considered can explain the high and low frequencies of a star. Pressure modes (or p-modes) are the plain waves travelling inside the star due to the pressure restoring force. Whereas, gravity modes (or g-modes) have the gravity as the restoring force.

Both p-modes and g-modes interact in the stellar interiors at different depths. They reach certain returning r depths values on which the wave energy is reflected. For p-modes,

the returning points and the frequencies are directly proportional to the order of the mode n: the higher the order the higher the frequency and the radius value of the returning shell (see Fig. 1.2a). Consequently, p-modes of low order travel the vast majority of stellar radius. On the other hand, order values of g-modes are inversely proportional to the frequency: the higher the order the lower the frequency. These gravity modes have returning points which are near the nuclei (see Fig. 1.2b). Therein lies the importance of their detection, them travelling so close to the stellar core potentially allows to infer the core properties.

1.1.4 Excitation mechanisms

Developing the idea of a star working as a heat engine, one of the parameters Eddington had to model was the opacity. Although he struggled to overcome the opacity discrepancy from assuming the wrong elements present in the star, with discoveries of Saha (1920), Payne (1925) and Strömgren (1932), he could solve the issue. But in this quest, he sustained the hypothesis that if opacity increases increasing the temperature, the star could become unstable against its natural pulsations. In this scenario the retention of energy creates a pressure force outwards, thus decreasing the opacity and so allowing the radiation to escape. This dilated layer can no longer support the outer layers of the star so it contracts again, thus, increasing opacity and temperature, starting a dynamic of periodic nature. Zhevakin (1953) proved that this occurs in the Hydrogen ionization zone through linearised equations. Today known as the κ-*mechanism*, this thermodynamical exchange of energy into mechanical energy is common to occur in the majority of pulsating stars. Whether it is stars with high opacity zones, such as helium or hydrogen ionization zones, or stars that suffer from an increased opacity of iron, this is the mechanism they have in common that sustains their pulsations (Fig. 1.3).

Another mechanism found to be driving pulsations in stars is the *stochastic excitation mechanism*. It is active in the convective shells of solar-like stars where the noise energy
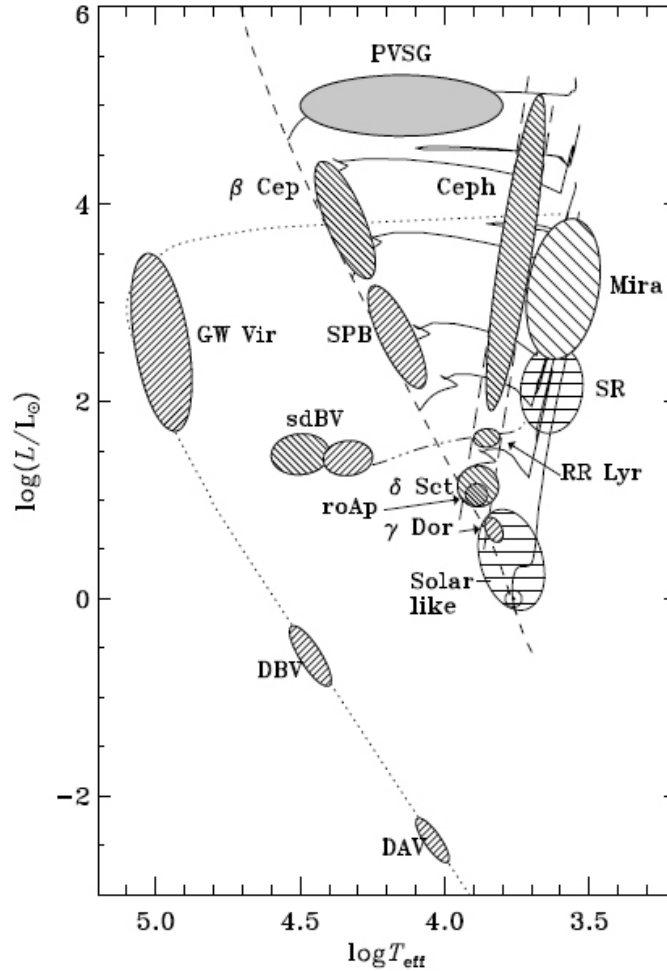
Figure 1.3 H-R diagram of different variable stars and their driven mechanism. Graph taken from (Aerts et al., 2010)

from convection is enough for the outer layer to resonate in some of their natural acoustic modes. Since it is directly related with convective turbulence, it is, as the name indicates, a randomly excitation process.

A recently known mechanism, considered to be responsible for the low frequencies in γ Dor stars, is the *convective blocking mechanism* (Dupret et al., 2005, Guzik et al., 2000, Pesnell, 1987). It refers to the radiative flux blocking that may occur in the frontier of the radiative core and a convective layer, causing a retention of energy similar to the one caused by the increment in opacity acting in the κ-mechanism.

Not all pulsations are explained by these mechanisms. Other possibilities have been explored, e.g. ϵ-mechanism, where the rate of matter production ϵ might induce instability of oscillations modes. However, for the purpose of understanding the analysis in this research thesis, this basic introduction of the most common and proved driven mechanisms is enough.

1.2 Delta Scuti stars

There are many different types of pulsating stars which are classified by the mechanism that drives their pulsations, by the type of modes that are unstable or by peculiarities in their chemical abundances. Fig. 1.3 shows the positions of this classification in the H-R diagram. A particular group of great relevance for asteroseismology are the Delta Scuti pulsating stars (δ Sct).

The δ Sct are metal rich stars (Population I) with spectral types from A2 to F2. Their temperature varies in the range of $6300 \leq T \leq 8900\ K$ and their masses from $1.5 \leq M \leq 2.5\ M_\odot$. Regarding its pulsations, they are mainly driven by the κ mechanism (see Fig. 1.3) and are what are called multi-periodic pulsators, meaning that they can resonate in radial and non-radial modes from 3 d^{-1} up to 80 d^{-1} frequency region (p-modes) (Aerts et al., 2010, Balona and Dziembowski, 2011, Grigahcène et al., 2010, Uytterhoeven et al., 2011). The multi-periodicity is such that it is often difficult to identify the oscillation modes clearly. Generally, they follow Stellingwerf (1979) period relations for radial modes:

$$0.756 \leq \frac{P_1}{P_0} \leq 0.787$$
$$0.611 \leq \frac{P_2}{P_0} \leq 0.632 \tag{1.11}$$
$$0.500 \leq \frac{P_3}{P_0} \leq 0.525$$

where the exact value depends on the stellar mass and composition.

The amplitude range of δ Sct stars can go from 10^{-3} up to 10^{-1} mag. The ones with higher amplitudes, from minimum to maximum in the light curve exceeding ~ 0.3 mag (see

Balona, 2016, McNamara, 1997), are called High Amplitude δ Sct (HADS) stars. They are not very common, only 0.8% of the stars in the δ Sct instability strip are HADS (Lee et al., 2008), the rest are common Low Amplitude δ Sct (LADS) stars. Generally, HADS stars pulsate in radial modes and are mostly slow rotators ($v \sin i < 30$ km s^{-1}) . Additionally, HADS stars have been assumed to be in an intermediate state of evolution between δ Sct stars and classical Cepheids (Poleski et al., 2010). Although, many studies show that there are exceptions for these characteristics, making them physically not very different from a normal LADS highlighting the arbitrariness of the HADS stars definition. For example, some HADS stars have been found to be pulsating in non-radial modes (Garrido and Rodriguez, 1996, Mathias et al., 1997, Poretti, 2003), Balona et al. (2012) found a fast rotating HADS, and finally Balona (2016) convincingly proved that HADS do not seem to be an extension of Cepheids to lower masses.

The knowledge of stellar structure and evolution can greatly benefit from the astero-seismic study of these stars. δ Sct stars mass range involves the estimated limits for stars having radiative cores and convective envelopes($M \leq 1$ $M_{\odot}$) to stars with convective cores and radiative envelopes ($M \geq 2$ $M_{\odot}$). Knowing that they are multi-periodic stars, many modes can pierce into different depths of their stellar interior, enabling to characterize the different regions of this interesting transitional evolutionary state.

Historically, variability studies in δ Sct stars began with Eggen (1956), who suggested that they should be grouped separated from the β Ceph stars and become a new group of variables with their particular properties. In the 70s, extensive research of δ Sct stars enable to characterize them. For example, in Baglin et al. (1973) the first definition of δ Sct variable is formally given. After this well-defined class of variable star was established, important discrepancies with the models started to be obvious. Also, what was very puzzling is how different δ Sct stars, with similar stellar parameters showed so different frequency distributions (see Fig. 1.4) .The first suspicions about the origin of this difference were regarding the quality of the observations. Small duty cycles of the observations available
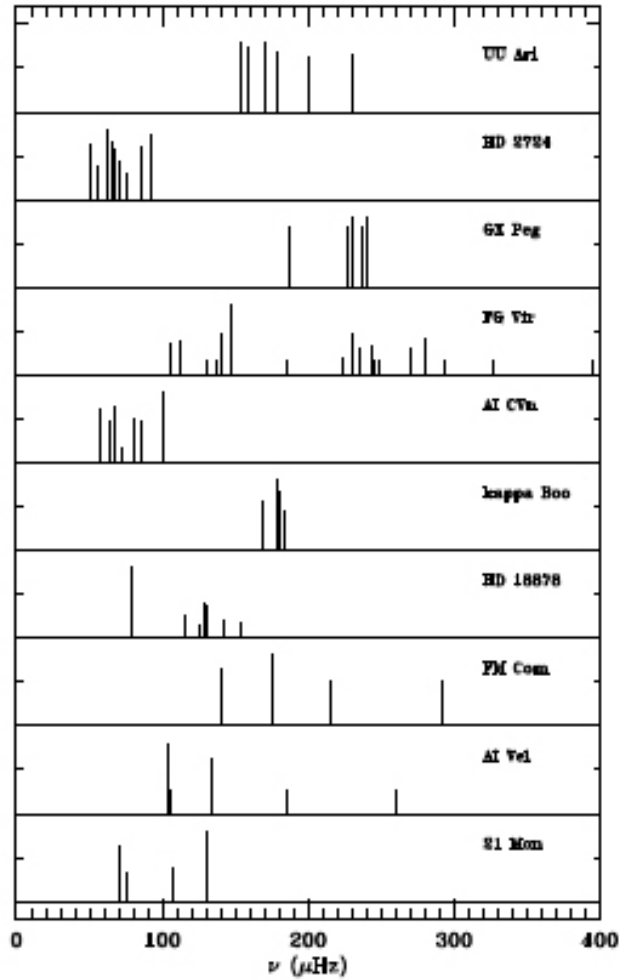
Figure 1.4 Schematic oscillation spectra of a number of δ Sct stars. Very different frequency distributions for the same type of variables of similar parameters. Source: Christensen-Dalsgaard (1997)

could be biasing the signal interpretation and the mode identification in these stars.

In a collaborative effort to increment the duty cycle of δ Sct observations, Michel Breger founded the δ Sct network in 1983. Coordinating three ground-based observatories, San Pedro Mártir observatory in Baja California Mexico, Sierra Nevada Observatory in Granada Spain and Xian Lang in China, observations of consecutive cycles were achieved. Data taken by this network allowed the creation of the popular δ Sct catalogue (Rodríguez et al., 2000), and enabled full asteroseismic analyses to δ Sct variables (e.g. Breger et al., 1999). However,

the discrepancies with the models were still present and by that time, the technology was advanced enough to start thinking of the possibility of space observations.

1.2.1   Ultra-precise photometry for Delta Sct stars

The birth of the space era for asteroseismic analyses with Corot and Kepler missions brought amazing findings for the δ Sct stars (Balona and Dziembowski, 2011, Michel et al., 2017) . For example, it was found that most of the δ Sct stars are hybrids (Balona, 2014, Balona et al., 2015), meaning that they have low frequencies associated to g-modes of pulsation as well as the expected p-modes, already detected by ground-based observations. Another interesting finding, thanks to very large surveys of δ Sct stars, ware the precise estimations of the red and blue edge of the instability strip. After determining the instability region for these variables, it was intriguing to find that 68% of the stars in these particular zone do not pulsate (Balona, 2018, Balona and Dziembowski, 2011). All these arose questions of the actual knowledge of the driven mechanisms, damping effects and mode selection in this stars.

Additionally, the low noise level of space measurements enabled the detection of frequencies following regular patterns. These frequencies were associated to non-linear effects, which are very common in stars with pulsations driven by the κ mechanism.

1.3   Non-linear effects

In Section 1.1.2 we have seen that the perturbed hydrodynamic equations are linearised, meaning that they are truncated to the first order, discarding interactions between variables and second order terms. This was justified by assuming the reasonable approximation of small oscillation amplitudes in comparison with the stellar inherent characteristics (e.g. its radius). However, features of the observed light curves could not be represented by models in the linear regime. For example, high amplitudes and phase lags in observations of Cepheids

and RR-Lyrae lead to think that linearity was underestimating the physics working within some pulsating stars.
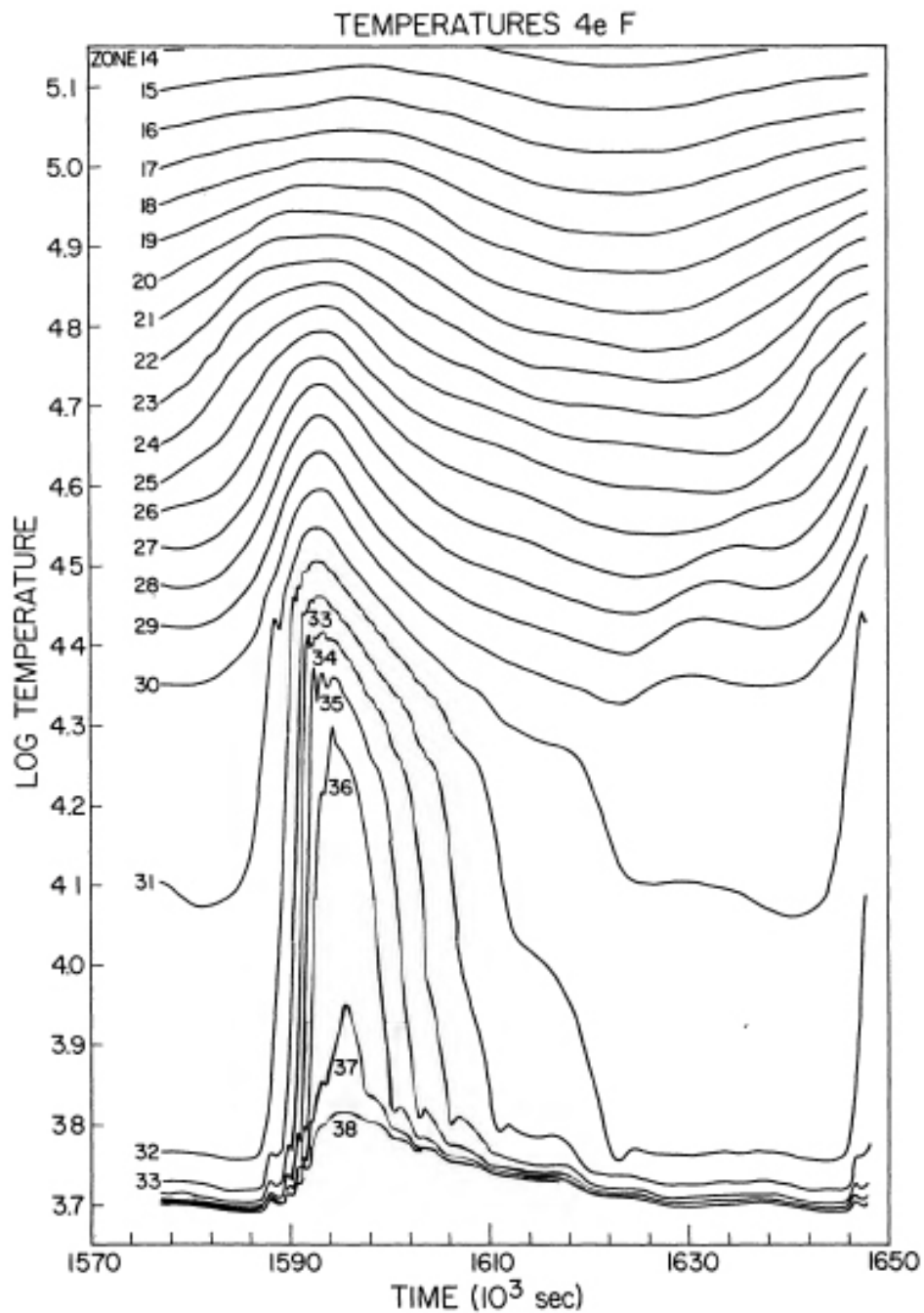
Figure 1.5 Non-linear temperatures variations in different depths. Source: Christy (1967)

Non-linear effects could explain the amplitudes and phase lags between the luminosity

curve and the velocity curves representative of RR-Lyrae and Cepheids stars (Christy, 1962, 1964, 1966, 1967). Non-linear models were also developed for white dwarfs, successfully explaining their light curves in therms of a non-linear responses of the envelope to high amplitude changes in temperature (see Fig. 1.5). (Brassard et al., 1995, Brickhill, 1992, Christy, 1967, Montgomery, 2005, Wu, 2001).

Yet, for δ Sct stars, Stellingwerf (1980) pointed out that between the mass range of these variables, the non-linear equations undertake an unexpected turn. The models predicted a continuous and exponential growth of amplitudes, even passing the escape velocity, ending up in an incredible amount of mass loss. This was called by Stellingwerf *The Main Sequence Catastrophe*, since the observations did not provide evidence of a great amount of mass loss for these stars in the main sequence.

A great deal of effort has been made to solve the main-sequence catastrophe of the non-linear effects for δ Sct stars. Stronger damping effects, non-linear mode selection or some amplitude saturation mechanism must be acting somehow within the pulsating star. For example, the resonant mode coupling (Buchler et al., 1997, Dziembowski, 1982, Van Hoolst, 1994), was proposed as a possible mechanism that could explain, to some extent, the observed amplitudes. At this point, due to the lack of precise data to prove these mode coupling hypothesis, discussions in this matter stopped for a while. Recent analyses of the ultra-precise photometric data taken by space satellites have reignited the non-linear effects subject. For example, the light curves of g-mode pulsators (such as γDor, SPB and SX Phoenix stars), have been explained in terms of non-linear effects (Kurtz et al., 2015). In particular for δ Sct stars, given that non-linear effects could explain their not yet understood pulsational content, the non-linear effect discussion is in its apogee (Balona, 2012, 2016, Balona et al., 2012, Bowman, 2017, Breger and Montgomery, 2014).

In summary, non-linear models are far from being complete. Until this date they have been developed only for radial modes, with expensive calculations and mainly for RR-lyrae, Cepheids and White dwarfs. The non-linear models for δ Sct are extensions of the models

for these subgroups of completely different variable stars, and with no very encouranging results (Balona, 2012, Stellingwerf, 1980). Particularly in Stellingwerf (1980), mode amplitude predictions of stars are too high. The amplitudes vary with the viscosity parameter, however such dependency is not backed up by any known physics. In addition, Balona (2012) proved that assumptions in the white dwarfs non-linear models were not applicable to main-sequences stars (geometrical effects, i.e. variation in radius and surface normal, are not negligible in main-sequence stars in contrast to the case of white dwarfs, where due to their high density the lack of these variations are a valid approximation.), so discarding the applicability of these models to a star of the δ Sct type. Consequently, there is a lack of knowledge in the models, on one side in the damping mechanisms: we do not know much about interaction between modes (e.g. coupling), or the physics of them passing through a convective zone. On the other hand, we also do not know much about the selection of pulsating modes (e.g. the existence of δ Sct hybrids and non pulsating stars in the instability strip). Answering these open questions is just one part of the motivation of this research thesis.

1.4 Motivation and objective of the research thesis

Non-linear effects must be taken into account to explain observations when the perturbed variable undertakes large amplitudes. Deviations from linearity occur for example in the hydrogen ionization zone of a pulsating star, where the κ-mechanism is proved to be responsible for driving oscillations. In fact, pulsating stars in which the oscillations are mainly heat-driven (RR-Lyrae, Cepheids, White dwarfs, β Cepheids, SPB stars) exhibit high non-linear effects signatures in their light curves (although they can also be seen in γ Dor stars , where the excitation mechanism is the convective flux blocking). Unfortunately, non-linear models are far from complete.

In the heat-driven group of variable stars, the δ Sct are of special interest. They are

in the mass range where the transition between radiative to convective envelopes happens, without a doubt an evolutive state worth of studying. Moreover, they show very complex and dense pulsational content. This is a very important characteristic in an asteroseismic context because many oscillation modes travelling at many different depths across the star translates to more detailed information of the internal profile of the star.

Stellingwerfs' *Main Sequence Catastrophe* explained in section 1.3, showed that non-linear modeling could explain δ Sct variables, but important knowledge is missing from the models for them to be complete. The main objective of this research thesis is to try to characterise non-linear effects of δ Sct pulsating stars observationally. The motivation is the lack of non-linear models for δ Sct stars. Altogether, the aim is that at some point in the future, this study would allow to build effective non-linear models for main-sequence pulsators that could lead to understand their mode selection or damping mechanisms, their convective zones (e.g. mixing length, overshooting), and overall the structure and evolution of the stars.

In empirical research such as this, special emphasis should be devoted to the correct application of the analytical tools for data interpretation. In our case, understanding the mathematical foundations of the time series analysis techniques is critical to interpret photometric data. That is why, in the next chapter, the main concepts on the subject are presented.

Chapter Two

Photometric Time Series Analysis
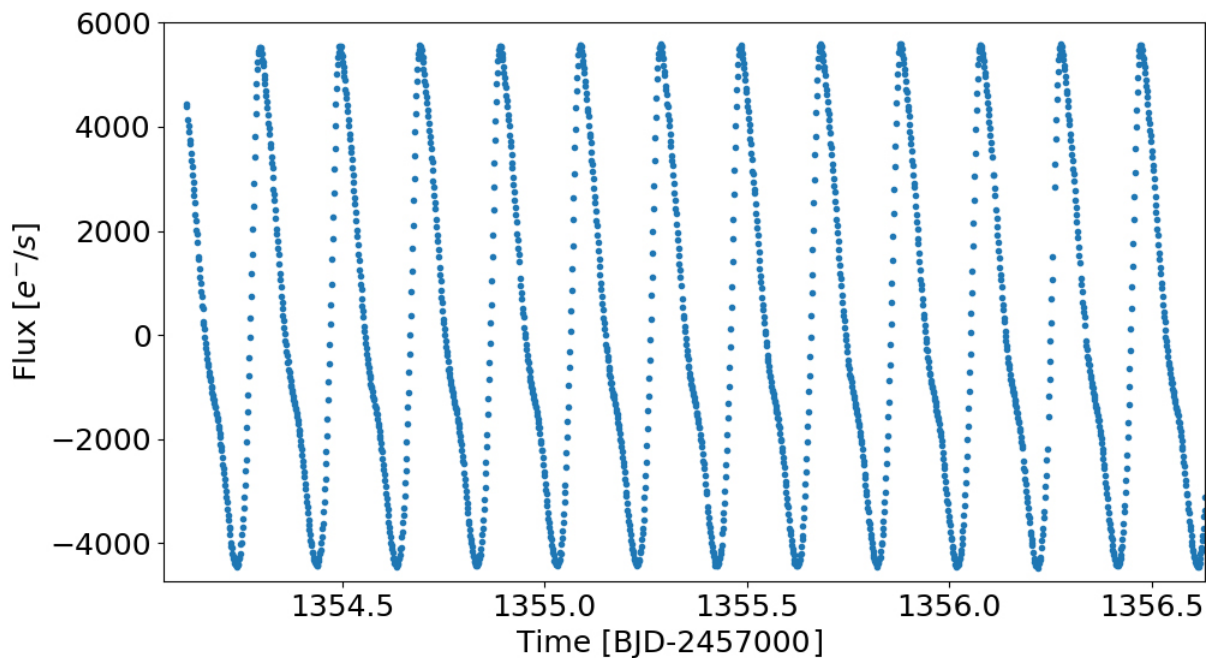
Figure 2.1 First 2,4 days of the time series or light curve of the mono periodic δ Sct star TIC 9632550 observed with the TESS space satellite

A chronologically arranged sequence of measurements of any observable is what is called a *time series*. When the observable is the number of photons coming from the light of a sky source that are captured by a photometer (during a certain exposure interval), it constitutes a photometric time series called *light curve*. Particularly, if the sky source is a pulsating star, its light curve captures the periodic light variability of the star (see Fig. 2.1).

A time series can be characterised in the frequency space by Fourier analysis, which is based on the assumption that any function can be represented as a sum of sine and cosine functions. Sometimes, it is useful to understand a function in terms of the frequencies of these harmonic components, for example in voice recognition analyses, electrocardiogram analyses, or in the case that concerns us, asteroseismic analyses. Considering that asteroseismic modelling begins with identifying properly the pulsation modes frequency of a variable star, it is relevant to review the Fourier tools and its principles. In this chapter, important concepts to take into account when carrying out a discrete Fourier analysis of photometric time series are presented in some depth.

2.1 Discrete Fourier Analysis

The discrete Fourier analysis is the suited formalism for analysing data such as stellar light curves. Light curves are finite and discrete data from where the frequency content, corresponding to the intrinsic variability of the star, is expected to be extracted. To transform a finite discrete function from the time space to the frequency space, one makes use of the finite *Discrete Fourier Transform* (DFT) defined as:

$$F_N(\nu) = \sum_{k=1}^{N} f(t_k) e^{i2\pi\nu t_k};\qquad(2.1)$$

where ν is the discrete range of frequencies to be evaluated (whose size and discretization are explained in Sections 2.1 and 2.5, respectively), N is the number of integrated light measurements and the $f(t_k)$ is the light curve data point at time t_k. Generally, $f(t_k)$ will be treated as a periodic or harmonic signal of the form:

$$f(t_k) = \sum_{j=1}^{n} A_j \sin(2\pi f_j t_k + \phi_j);\qquad(2.2)$$

where n is the number of components, A_j is the amplitude of the signal j^{th} component with

frequency f_j and phase ϕ_j.

Notice that $F_N(\nu)$ is a complex function. By computing the square amplitude of $F_N(\nu)$, the complex components are eliminated. This is called a *Power Spectral Density* (PSD) estimation (or simply, the power spectrum) based on the DFT equation 2.1:

$$P(\nu) \equiv |F_N(\nu)|^2 = \frac{1}{N} \left| \sum_{k=1}^{N} f(t_k) e^{i2\pi\nu t_k} \right|^2 ; \tag{2.3}$$

where the $\frac{1}{N}$ is a normalization constant, chosen like this so that in the special case of equally-spaced data, the size of the peak recovers the corresponding Fourier component amplitude, A_j (Deeming, 1975). Now, $P(\nu)$ is a real-valued even function for a real signal. In this way, the higher the value of $P_N(\nu)$, the higher the contribution to the signal of the harmonic component with ν as a frequency. This is known as the *classical periodogram*.

A very common algorithm to compute a DFT is the Fast Fourier Transform (FFT) algorithm which, as its name implies, considerably reduces the computational time of the calculations. Two conditions have to be met so it can be applied. First, the points of the series must be equally-spaced and second, the total number of point N must be a power of 2. However, this second condition is no longer a necessary condition in more recent modifications to the FFT algorithm (Cooley and Tukey, 1965).

Nyquist Frequency

The Nyquist frequency is the highest frequency value that can be studied. This follows from the Nyquist-Shannon sampling theorem that states that a complete reconstruction of a periodic signal with period P can be done only if the sampling interval is, at much, half of it. This can be expressed analytically in terms of frequency as:

$$F_{Ny} = \frac{1}{2\Delta t}; \tag{2.4}$$

where Δt is the sampling rate or cadence.

Generally, the δ Sct frequency range of pulsation is expected to be between $3d^{-1}$ to $80d^{-1}$ (Aerts et al., 2010, Balona and Dziembowski, 2011, Grigahcène et al., 2010, Uytterhoeven et al., 2011). According to Eq. 2.4, in order to sample the δ Sct stars pulsations, Δt must be of at least $0.01d$. Every instrument has chosen this value carefully. For example, δ Sct stars observed by CoRot have been sampled in two cadence modes: the Short Cadence (SC), where $\Delta t \approx 32s$, and the Nominal Cadence (NC), where $\Delta t \approx 512s$. Kepler measurements are also taken in two modalities, the SC and Long Cadence (LC) modes but the Δt are $\approx 58.5s$ and $\approx 29.45m$, respectively. TESS observations of δ Sct stars are given in a unique mode of 2 min cadence (or $\approx 120s$). Consequently, the δ Sct light curves used in this study are the ones in SC mode of the CoRoT and Kepler data, and the $120s$ cadence of TESS, since they exceedingly cover the frequency range of interest.

Frequency Resolution

The separation between frequencies, determined by the observation time spam ΔT, is what is called the frequency resolution:

$$\Delta \nu = \frac{1}{\Delta T} \tag{2.5}$$

The expression 2.5 is often referred to as the *Rayleigh resolution*. As the main input data for asteroseismic modeling are the natural oscillating modes of the star, it is really important to resolve every frequency so they can be clearly distinguished from one another. In other words, the proper situation, where the modes are well separated, is given when the following condition is met:

$$|\omega_i - \omega_j|\Delta T \gg 1; \tag{2.6}$$

for all pairs of $i \neq j$.

Notice that the Rayleigh resolution can be easily mistaken with the precision of the frequency. When two or more frequencies are in the same interval of Rayleigh size, because the frequencies are very close together or because the length of the observation is not enough

to resolve them, then the Rayleigh resolution is the frequency uncertainty. Sometimes, it could be even larger than the Rayleigh resolution ($\Delta\nu = \frac{12}{\Delta T}$, see Christensen-Dalsgaard, 1997).

However, precision can go further if in the Rayleigh interval there is only one frequency component. Dense power spectra is a common characteristic of δ Sct star power spectra, yet the space measurements are long enough even to resolve very close rotational frequency splittings.

Spectral windows

When dealing with real data, unfortunately one must take into account interferences that arise due to the inevitable finite length of the observation and the sampling. An important conclusion in this regard, stated by Deeming (1975), is that "[...] the observed Fourier transform, $F_N(\nu)$, is the *convolution* of the true Fourier transform $F(\nu)$ with a *spectral window $\delta_N(\nu)$*". This can be expressed analytically by:

$$F_N(\nu) = F(\nu) * \delta_N(\nu) \equiv \int_{-\infty}^{\infty} F(\nu - \nu')\delta_N(\nu')d\nu'; \qquad (2.7)$$

where the $*$ symbol corresponds to the convolution operation, and $\delta_N(\nu)$ takes the form of:

$$\delta_N(\nu) = \sum_{k=1}^{N} e^{i2\pi\nu t_k} \qquad (2.8)$$

The effect of a convolution is shown in Fig. 2.2. A simple continuous periodic function $Y(t)$ (upper left) has an exact DFT shown in the upper right panel. If this continuous function $Y(t)$ is sampled with the window function of the mid left panel, the resulting DFT of the sampled function (bottom left) will be the one shown in lower right panel. Therefore, in order to disentangle the real Fourier transform (upper right) one must know the spectral window, this is, the Fourier transform of the observation function or window function (mid right panel).
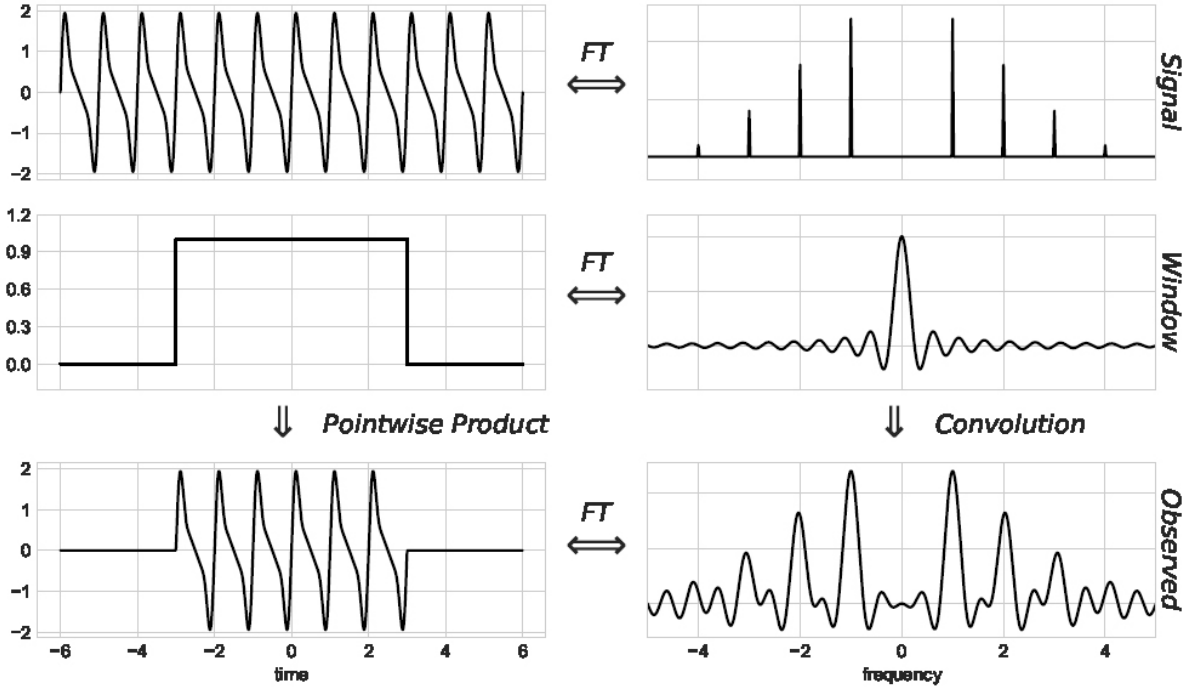
Figure 2.2 Convolution effect over the continuous function $Y(t) = 1.2sin(2\pi t) + 0.8sin(4\pi t) + 0.4sin(6\pi t) + 0.1sin(8\pi t)$. Source: VanderPlas (2018)

Window functions can have very diverse forms depending on how the data is gathered. One characteristic window functions are the ones generated by ground-base observations. They usually are a discrete number of photon counting (done by a photometer) of the integrated light from a stellar disk, separated by periodic gaps of one day approximately, owing to the day-night cycle. When computing a DFT to this type of window functions, one obtains a spectral window with a periodic component of one cycle per day which will be modulating the entire DFT of the stars light curve.

Besides windows from ground-base observations, there are the ones generated by space observations. These windows improve the precision of the data by not only removing undesired atmospheric distortions, but by removing the one cycle per day periodic contribution of the ground-based observations. The data used in this research thesis is gathered by space satellites such as CoRoT, Kepler or TESS. In Fig. 2.3, window functions of each of these
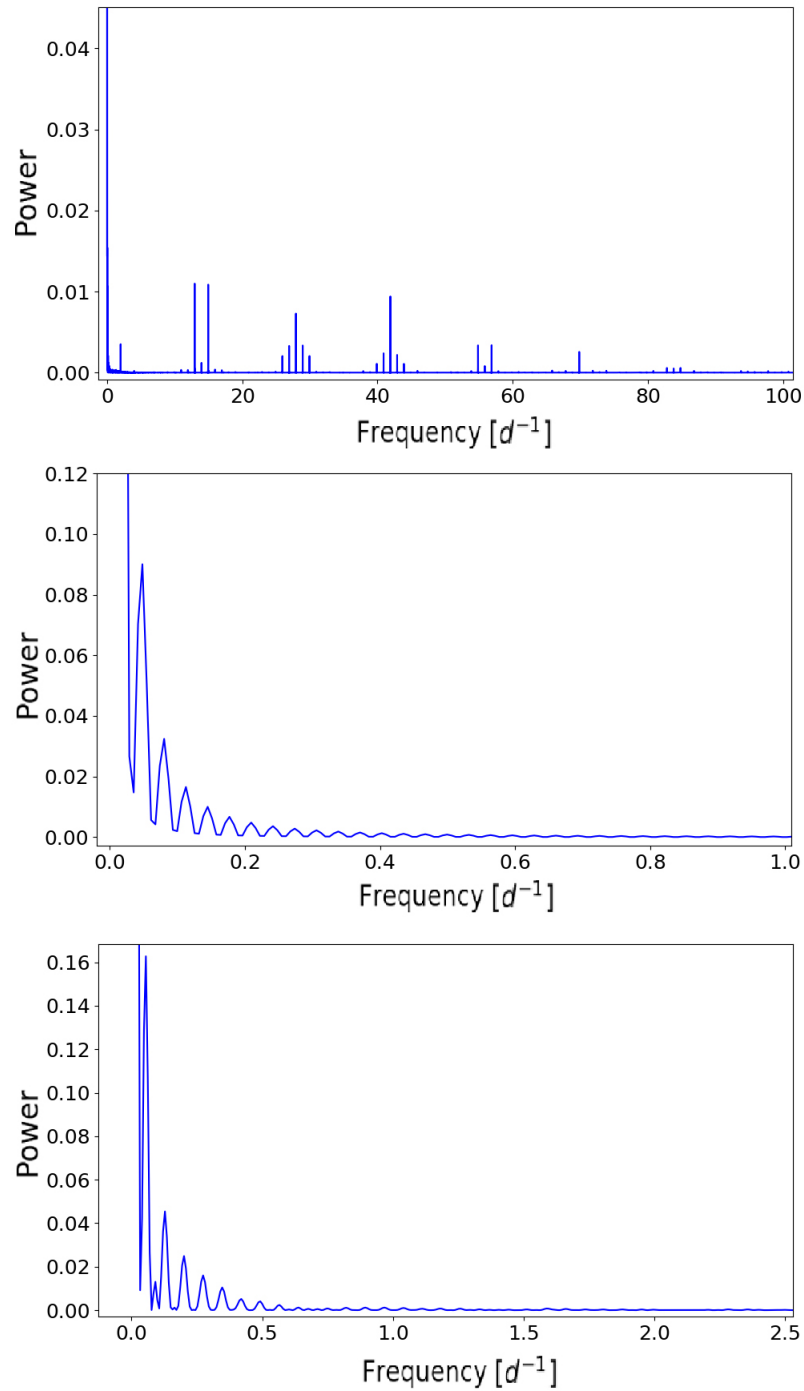
Figure 2.3 Examples of real window functions. CoRot window function of a ≈ 79 days long SC observation (upper panel). Kepler window function of quarter 4 (Q4), ≈ 31 days long SC observation (mid panel). TESS window function of a ≈ 27 days long SC observation (bottom panel).

instruments are shown.

Corot gaps every 0.072 days are due to the pass of the instrument over the South Atlantic Anomaly (SAA), which influences the instrument's electronics invalidating the measurements gathered during that period of time. Big gaps are uncommon in Kepler light curves, although must of the instrumental artefacts are due to a drift in time and consequently unevenly spaced measurements (see 'undisciplined time' in Van Cleve et al., 2016), generating an important source of picks in the spectral window, that distorts the light curve's DFT. TESS window functions of sector 1 and 2, shows a gap every $\approx$ 13 days due to the moment when the satellite orients the antennas to send the data to Earth. It Occurs one time in each orbit of the satellite, which is in a 2:1 resonance with the Moon. Moreover, a disturbance in the signal in the form of irregular gaps is common for the second part of the light curve (after the gap due to data downlink to Earth).

On the other hand, another consequence of the finite duration of the observation is the **leakage effect**. This effect can occur when the signal to which the DFT is going to be computed, does not have an integer number of cycles. This affects how the power spectrum looks like, because the energy of the frequency is not focused in one single bin, so it is distributed in near apparent Fourier contributions called sidelobes.

2.1.1 Overcoming the DFTs interference from the spectral windows

The Lomb-Scargle periodogram

The Lomb-Scargle (LS) periodogram is an algorithm that tackles the very common issue of uneven sampling when analysing astronomic time series. Unevenly-spaced data entails an unstructured spectral window, whose convolution with the Fourier transform of the continuous signal introduces interference in the DFT, jeopardizing the frequency analysis. Concepts of classical Fourier analysis, such as the Nyquist frequency or the classical periodogram, do not hold for the nonuniform sampling case. In the former, owing to the ambiguous value of

Δt, and in the latter, owing to the discrepancy between the classical periodogram solution for the unevenly sampled data from the chi-square distributed solution, corresponding to the uniform case.

Scargle (1982) introduces a correction to the classical periodogram 2.3, allowing it to conserve the statistical properties for the uniform case:

$$P(\nu) = \frac{1}{2} \left[\frac{\left(\sum_n f(t_k) \cos(2\pi f[t_n - \tau]) \right)^2}{\sum_n f(t_k) \cos^2(2\pi f[t_n - \tau])} + \frac{\left(\sum_n f(t_k) \sin(2\pi f[t_n - \tau]) \right)^2}{\sum_n f(t_k) \sin^2(2\pi f[t_n - \tau])} \right] \qquad (2.9)$$

where τ is a function of the frequency f, ensuring time-shift invariance (see VanderPlas, 2018):

$$\tau = \frac{1}{4\pi f} tan^{-1} \left(\frac{\left(\sum_n sin(4\pi f t_n) \right)}{\left(\sum_n cos(4\pi f t_n) \right)} \right) \qquad (2.10)$$

It should be noted that Lomb-Scargle periodogram is the same as filling the gaps with zeros and computing a FFT, therefore the influence of the gaps remain in the resulting periodogram. Conversely, the MIARMA interpolation method does break the gaps-signal correlation.

MIARMA interpolation

Another solution to the unevenly-spaced sampling problem is to interpolate the gaps of the time series. The interpolation algorithm will influence directly the shape of the light curve, and consequently the resulting frequency spectra. When trying to explain the light curve in term of a sum of harmonic components, it is possible that the gap-filling differs significantly from the signal. In this case, not only the harmonic components owing to the intrinsic variability of the star are enough, but more components are required in the sum to completely explain the signal. In this sense, the interpolation algorithm chosen to fill in the gaps is critical for an asteroseismic analysis.

In this research, gaps are interpolated by the MIARMA interpolation algorithm (Method of Interpolation by Auto Regressive and Moving Average) (Pascual-Granado et al., 2015b),

which aims to preserve the frequency content of the star. It uses the Moving Average Auto Regressive models (ARMA models) to predict the data inside the gaps, without making assumptions on the analyzed signal. As a consequence of this flexibility, statistical criteria can be applied to choose a model in which minimal-loss of information can be guaranteed. Moreover, periodograms of MIARMA interpolated light curves have proven to be suppressing the effects of the spectral window to its minimum, in contrast to linear interpolation or by simply leaving the gaps intact (Pascual-Granado et al., 2018). Altogether, the fact that the MIARMA gap-filling algorithm aims to preserve the original frequency content of the time series, besides minimizing the effects of the spectral window, makes it the more suited interpolation method for an asteroseismic analysis.

Direct Deconvolution

Defining X as a continuous function describing the light variation of a pulsating star, then, the product $X \cdot W$ is the observed light variation denoted by,

$$f_w(X) = X \cdot W \tag{2.11}$$

where W is the window function, which can be extended to the concept of an effective window if we define I_e to represent any instrumental response as a function of time, yielding the definition of the effective window W_e,

$$W_e = W \cdot I_e \tag{2.12}$$

In such a way, this definition gives us a clear independence between the window and the function X. Obviously, the effects of the window expected to be removed are those that do not come from the observing box (i.e. Rayleigh resolution) and the sampling (i.e. Nyquist frequency).

Generally, the samples are not evenly spaced, so the Fourier Transform for unevenly spaced data is applied, here denoted by $FT_{LS}[\cdot]$, which is based on the same framework as

that behind the LS periodogram, but yields an estimate Fourier transform, the absolute-square of which is identical to the periodogram (see Scargle, 1989, for details). This function is an estimation of the Fourier Transform

$$FT_{LS}[f_w(X)] = FT_{LS}[X \cdot W]$$
$$= FT_{LS}[X] * FT_{LS}[W], \tag{2.13}$$

where dot means product and asterisk convolution. Note that X does not depend on the observational window.

Taking the Fast Fourier Transform of Eq. 2.13 denoted by $FFT\{\cdot\}$,

$$FFT\{FT_{LS}[f_w(X)]\} = FFT\{FT_{LS}[X] * FT_{LS}[W]\}$$
$$= FFT\{FT_{LS}[X]\} \cdot FFT\{FT_{LS}[W]\} \tag{2.14}$$

Now its possible to obtain a ratio because the $FFT\{FT_{LS}[W]\}$ is a complex function of the LS Fourier Transform of the window, which is now evenly sampled in frequency following prescriptions established in Scargle (1989). Then,

$$\frac{FFT\{FT_{LS}[f_w(X)]\}}{FFT\{FT_{LS}[W]\}} = FFT\{FT_{LS}[X]\} \tag{2.15}$$

Finally, taking the Inverse Fast Fourier Transform,$FFT^{-1}\langle\cdot\rangle$, we will obtain the 'true' Fourier Transform of the signal without any procedure attempting to remove the effects of the window (see e.g. Scargle et al., 2017).

$$FFT^{-1}\langle\frac{FFT\{FT_{LS}[f_w(X)]\}}{FFT\{FT_{LS}[W]\}}\rangle = FFT^{-1}\langle FFT\{FT_{LS}[X]\}\rangle$$
$$= FFT\{FT_{LS}[X]\}; \tag{2.16}$$

which is, by construction, clearly independent of the window.
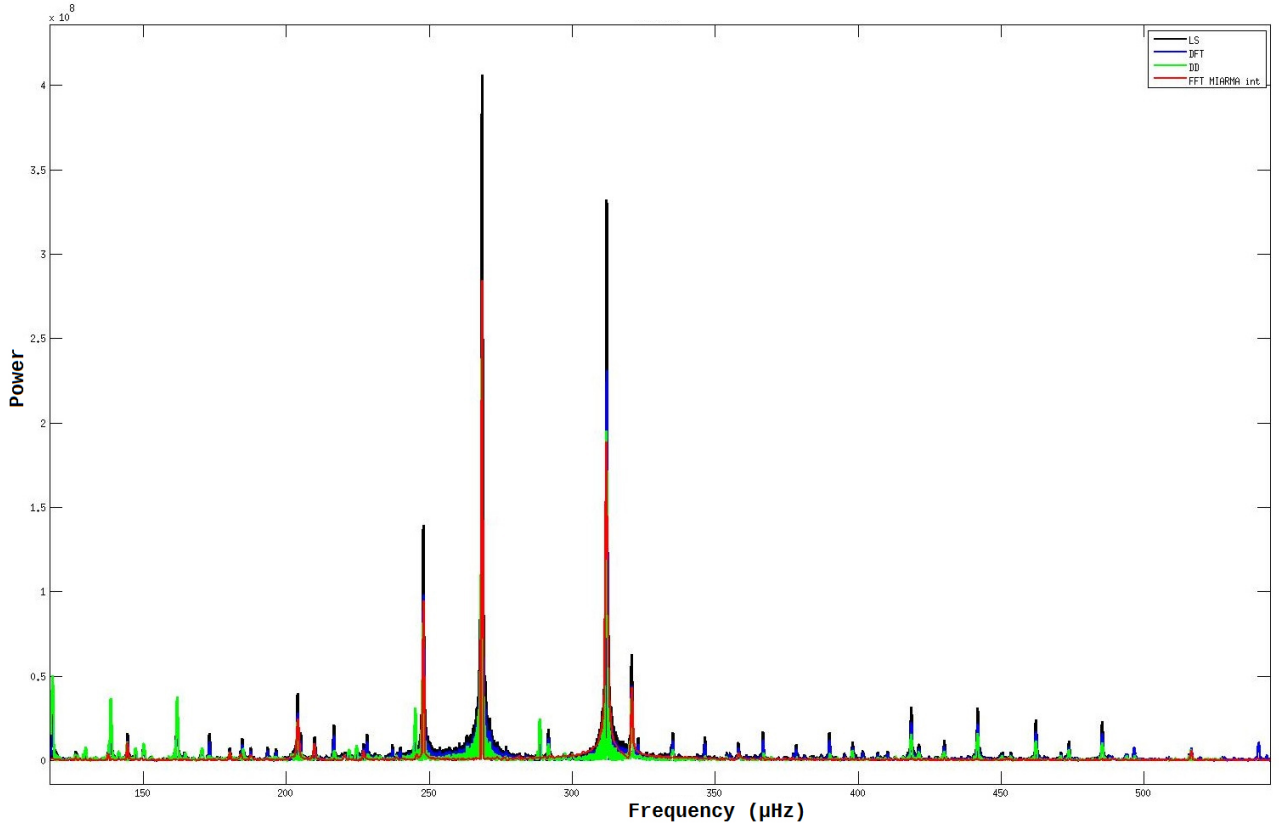
Figure 2.4 Representative result of the application of the direct deconvolution (DD) to the HD 174966 δ Sct star. The power contribution at 161.713 μHz, corresponding to the orbital frequency of the satellite, is not removed by the DD.

The above formalism, namely the Direct Deconvolution (DD) formalism, aims to minimize the contribution of the observational window in order to obtain only information from the physical system in question. Fig. 2.4 shows the LS periodogram (black), the DFT (blue), the FFT of the light curve interpolated with the MIARMA algorithm (red) and the DD (green), for the δ Sct star observed by CoRoT, HD174966. The DD power spectra shows frequencies that result from the convolution of the signal coming from the star with the observation window, for example: the maximum at 161.713 μHz corresponding to the orbital frequency of the CoRoT satellite and its pass over the SAA (Auvergne et al., 2009). Comparing to the FFT of the light curve interpolated with the MIARMA (Pascual-Granado et al., 2015a) algorithm, it is clear that the 161.713 μHz maximum (and its harmonics), is

completely removed.

The DD was applied to a sample of 15 δ Sct stars observed by CoRoT. The behavior exemplified in Fig. 2.4 is repeated for all of them: the DD does not remove the contribution from the observation window as expected. It could be of interest for further studies to demonstrate that the term $FFT\{FT_{LS}[W]\}$, of Eq. 2.1.1 is never zero. Such demonstration could enable to correctly isolate (into one side of the equation) the term $FFT\{FT_{LS}[X]\}$, which would allow to finally obtain the DD expression with mathematical rigor. In this sense, a LASSO regularization was performed but no conclusive results were obtained. Therefore, the preferred method in this monograph to overcome the periodicities due to the observational window, is to apply the MIARMA algorithm of interpolation (except for when the gaps are small enough or not periodic, in those cases a LS is preferred).

2.1.2 Prewhitening

Once the computed periodogram is correctly representing the frequency content of the star (either by the LS approximation or with the MIARMA interpolation algorithm) the next step in the analysis is to specify the frequency values of those components that generate the signal. This is commonly done by a prewhitening procedure.

The prewhitening procedure is based on the assumption that the light curve $f(t)$ is a composition of an harmonic part and an added Gaussian white noise $\epsilon(t)$ in the following form:

$$f(t) = \sum_{k=1}^{n} A_k \sin(2\pi f_k t + \phi_k) + \epsilon(t); \qquad (2.17)$$

where n is the number of components. Under this hypothesis, if n sine waves (each with its ν_k frequency) are fitted to the light curve by the least squares method, ist expected for the residual light curve to be the Gaussian white noise function $\epsilon(t)$.

The prewhitening algorithm first fits a sine wave with the frequency amplitude and phase

of the highest contribution of power in the periodogram. Next, the highest contribution in the periodogram of the residual light curve is fitted. This step is repeated until the residual light curve shows only noise. By the end, the algorithm yields a list of frequencies, amplitudes and phases corresponding to each sinusoidal component of the signal. This parameters can be optimized computing a non-linear least squares, guaranteeing that the frequencies, amplitude and phases correspond to the parameters of the minimized solution (minimal variance of the residuals).
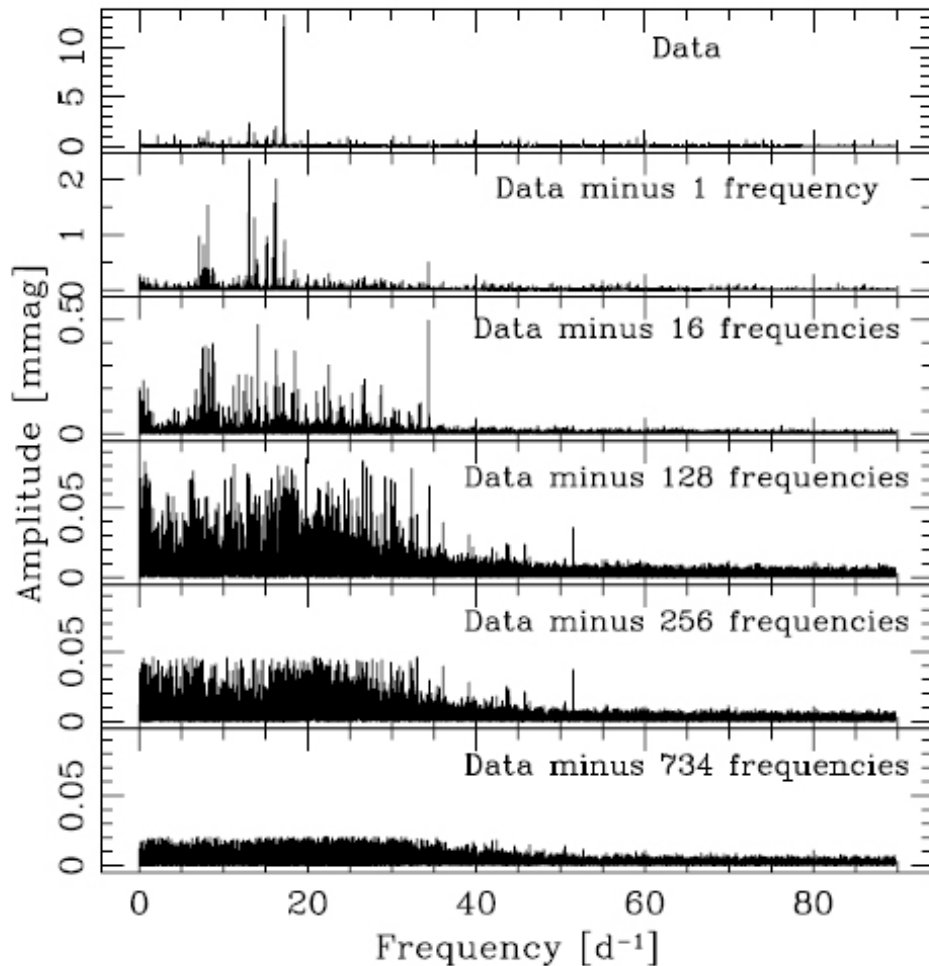
Figure 2.5 Example of the *Plateau* or *grass* of frequencies formed after N number fits for the HD 50870 star. Source: Mantegazza et al. (2012)

Unfortunately, the expectation of reaching a residual light curve uncorrelated with the

original signal after a sub sequence of sine waves fittings is not always fulfilled. Research in this topic (Mantegazza et al., 2012, Poretti et al., 2009) have shown that, after a considerable amount of fits, the residual light curve is still correlated with the signal and spurious information in the low frequency range is added, forming a *Plateau* (see Fig. 2.5).

In any case, despite the lack of stopping criteria owing to the never-reached white noise residual light curve, the prewhitening algorithm remains the most common tool to determine the list of statistically significant frequencies. Along with a non-linear least-squares parameter optimization, the prewhitening cascade is still practical if an ad hoc, but reasonable, stopping criteria is adopted. For example, a very often criteria used by the asteroseismology community is to consider a peak significant if the signal to noise ratio (S/R) of the peak is ≥ 4 in an amplitude spectrum (Breger et al., 1993), or ≥ 12.57 in a power spectrum (Reegen, 2007).

2.2   Time series analysis of Delta Sct light curves

In stellar physics, the use of light curves and power spectra to determine properties of variable stars and their evolution is quite common, but these spectra can sometimes be extremely difficult to interpret. Fourier analysis applied to light curves does not result in accurate frequency identification. This can be due to various reasons such as the following:

1. Finite duration of the time series (e.g. the leakage effect).

2. Gaps (window function)

3. Damping of oscillations.

4. Combinations between modes.

5. Noise from the observation process.

These, among other reasons, are introducing alterations in the power spectra. In this way, there is a confusion between the system's own frequencies and those that are not, called spurious, which could lead to an incorrect identification with the theoretical frequencies.

The power spectra of δ Sct stars are not yet understood using standard physics. Until now, it has not been possible to identify most of the oscillation modes, and therefore the interior structure of the convective nucleus and the rotation profile are not known in detail. They are often dense and complex, and do not match current available models (García Hernández et al., 2013, Mantegazza et al., 2012, Poretti et al., 2009). This thesis will address the problem of interpretation of the power spectra of the light curves of pulsating stars of the δ Sct type. Specifically, it will focus in point 4 of the above list, on the study of the combinations between excited modes, namely non-linearities, which have their origin in the non-linear effects present in some of their light curves. Such concept of non-linear effects is presented developed in the next chapter, along with a theoretical explanation of how non-linearities can be present in δ Scts' non-linear light curves.

Chapter Three

Non-linear effects in Delta Scuti stars.

Non-linear effects are consequences of physical processes that can be explained by second or higher orders of the perturbed variables of the stellar structure equations, namely the non-linear models. As mentioned in Section 1.1.4, non-linear models were able to describe the non-sinusoidal shapes of some pulsating star light curves. Most of the studies of non-linear effects through non-linear modeling were made for DA and DB variable stars (Brassard et al., 1995, Brickhill, 1992, Montgomery, 2005, Wu, 2001). In this studies, such particular changes in luminosity had physical explanations related to mechanisms that follow non-linear dependencies, such as the T^4 dependence in the Stefan–Boltzmann law for the emergent flux, or the non-linear response of the stellar interior to the oscillation wave occurring in the thin outer convective layer. The interaction between the oscillation and the variation of the depth of the convective zone in the outer layer of a pulsating star (Brickhill, 1992, Wu, 2001), or the non-linear flux response of the stellar medium induced by surface geometrical and temperature distortions (Brassard et al., 1995) are going to be grouped in this monograph into the *non-linear distortion processes* (NLDP). These theories were extrapolated to the rest of the pulsating stars where a convective envelope is believed to be present.

Balona (2012) found that some parts of non-linear modeling for white dwarfs are not suited for intermediate-mass pulsating stars, such as δ Sct stars. According to him, the assumption of no geometric variations (instant adjustment of the surface convective layers)
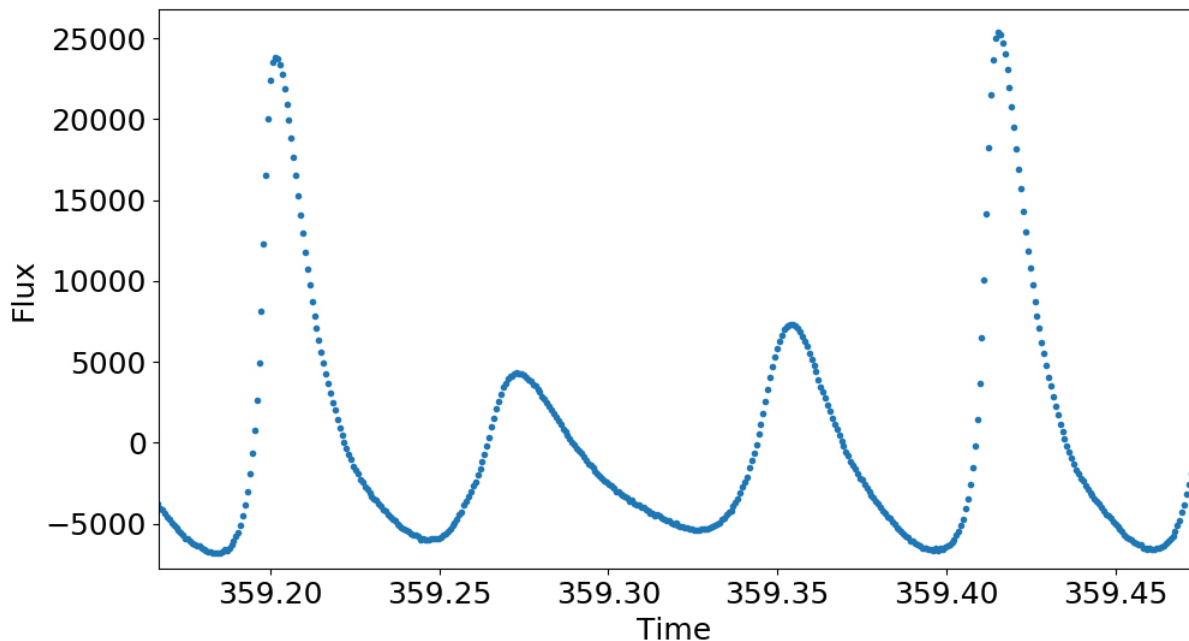
Figure 3.1 Extract of the GSC 00144-03031 light curve observed by CoRoT. Steep ascends and slow descends move away from the characteristic sinusoidal shape.

assumed for DA and DB stars can not be adopted for these variable stars. Nevertheless, the above mentioned NLDP are still adopted as the possible explanation for the non-linear effects seen in δ Sct variables. However, non-linear variations of the radius of the star (geometric displacement) must be taken into account. It is worth to mention that Brickhill (1992) non-linear models of white dwarfs discard the possibility of non-linear effects being generated in the radiative zone of the star. Nonetheless, the group of δ Sct variables may contain stars with enough mass to suffer the transition from a convective envelope to a radiative one, so non-linearities coming from the radiative interior can not be ruled out in future attempts of non-linear modeling of δ Sct stars.

Along with the non-linear effects from the NLDP, there are non-linear effects coming from the amplitude limiting mechanisms (that could be time dependent. See Bowman, 2017), as well explained by second order theories. Recalling the study of the non-linear theory for δ Sct stars done in Stellingwerf (1980), amplitude predictions have considerably exceeded the

observed ones (see Section 1.1.4). For this reason, assumptions over unknown damping or mode selection mechanisms operating in these type of variables have been the motivation of many recent studies. For example, the mode coupling theory developed by Dziembowski (1982) proves parametric and direct resonance as possible amplitude limiting mechanisms. Many authors have claimed that this type of non-linear effect is acting in some δ Sct stars (Bowman et al., 2016, Breger and Montgomery, 2014, Buchler et al., 1997). It is important to note, however, that this non-linear effect is not distorting the light curve. Mode coupling footprint in a light curve is just the addition of another sinusoidal component in the Fourier sense, the resonantly excited mode.

NLDP are responsible for distorting the light curve (see e.g. Fig. 3.1). Distorted light curves induce harmonics to the Fourier power spectra. How harmonics and cross-terms can appear in a power spectra is shown mathematically in the next section. However, it is important to remark that this thesis is an observational or empirical study and that the non-linear theory given in this chapter is not only abbreviated but general.

3.1 General non-linear theory for pulsating stars.

The non-linearised equation of oscillations, for the displacement vector ξ and considering weakly non-linear pulsations, can be expressed by the following equation (see Kurtz et al., 2015):

$$\frac{\delta^2 \xi}{\delta t^2} + L(\xi) + N^{(2)}(\xi, \xi) + N^{(3)}(\xi, \xi, \xi) + ... = 0; \tag{3.1}$$

where the $L(\xi)$ and $N^{(k)}(k = 2, 3, ...)$ are the linear and the non-linear operators of order k, respectively. The solution of Eq. 3.1 up to the first order operator is already given in Eq. 1.9.

When including second-order terms of Eq. 3.1 the differential equation to be solved is:

$$\frac{\delta^2 \xi^{(2)}}{\delta t^2} + L(\xi^{(2)}) = -N^{(2)}(\xi^{(1)}, \xi^{(1)}); \tag{3.2}$$

which is the equation of a forced oscillation, being $N^{(2)}(\xi^{(1)}, \xi^{(1)})$ the force inducing the oscillation. Eq. 3.2 is an inhomogeneous differential equation, therefore its solution is the sum of the general solution (Eq. 1.9) plus the particular solution. Including the general solution in Eq. 3.2, the final inhomogeneous differential equation to be solved for a second-order non-linear oscillation is:

$$\frac{\delta^2 \xi^{(2)}}{\delta t^2} + L(\xi^{(2)}) = - \sum_{nlm,n'l'm'} N^{(2)}(a_{nlm}\vec{\Xi}_{nlm}, a_{n'l'm'}\vec{\Xi}_{n'l'm'})e^{i\{(w_{nlm} \pm w_{n'l'm'})t + (\Phi_{nlm} \pm \Phi_{n'l'm'})\}};$$
(3.3)

where the general solution for two modes of index $k \equiv (n, m, l)$ and $k' \equiv (n', l', m')$ are:

$$\xi_k^{(1)} = \sum_{nlm} \vec{\Xi}_{nlm}(r)Y_l^m(\theta, \phi)e^{(i\omega_{nlm}t + \Phi_{nlm})},$$
(3.4)

$$\xi_{k'}^{(1)} = \sum_{n'l'm'} \vec{\Xi}_{n'l'm'}(r)Y_{l'}^{m'}(\theta, \phi)e^{(i\omega_{n'l'm'}t + \Phi_{n'l'm'})}$$
(3.5)

and the radial and horizontal displacement components of $\vec{\Xi}$ are:

$$\vec{\Xi}_{nlm} = \xi_{nl}(r)Y_l^m e_r + H_{nl}(r)\left[\frac{\delta Y_l^m}{\delta\theta}e_\theta + \frac{1}{sin\theta}\frac{\delta Y_l^m}{\delta\phi}e_\phi\right],$$
(3.6)

$$\vec{\Xi}_{n'l'm'} = \xi_{n'l'}(r)Y_{l'}^{m'} e_r + H_{n'l'}(r)\left[\frac{\delta Y_{l'}^{m'}}{\delta\theta}e_\theta + \frac{1}{sin\theta}\frac{\delta Y_{l'}^{m'}}{\delta\phi}e_\phi\right]$$
(3.7)

The particular solution to Eq. 3.3 will have cross-terms of frequencies $w_{nlm} + w_{n'l'm'}$ and $w_{nlm} - w_{n'l'm'}$, explaining the combination frequencies. The particular case of $w_{nlm} = w_{n'l'm'}$ originates the second harmonic $2w_{nlm}$ and so on for higher orders of the non-linear operator.

The development of the perturbed stellar structure equations up to the second order perturbation above presented, have shown how cross-terms frequencies from independent modes interaction can be explained when the variables are not truncated to the first order of perturbation. But, are these the cross-terms showed in the power spectra?. To try to answer this question, many studies focused in reproducing the non-linear light curves so the non-linear terms in the power spectra could be completely explained.

3.2 Modeling non-linear light curves

In Balona (2012), the expression for the luminous flux variations over time in the direction of an observer in the co-rotating frame is given by the following expression:

$$\frac{\Delta F}{F} = \frac{\epsilon_i}{2\pi}\Re\{(V_1 + V_2)Y_{l_i}^{m_i}(\Theta, \Phi)Y_{l_j}^{m_j}(\Theta, \Phi)e^{i((\omega_i+\omega_j)t+x_i+x_j)}\} \tag{3.8}$$

where the points on the surface of the star are described by the angular coordinates (Θ, Φ), (ω_i and ω_j) are the angular frequencies of two modes with arbitrary phases (x_i and x_j) and their spherical harmonics ((l_i, m_i) and (l_j, m_j), respectively). V_1 is an expression that comprehends the variations in the flux coming from geometry changes (i.e radius and surface normal) and V_2 from temperature and surface gravity changes.

Note that the relative flux variation expression can not be compared with the observations. The observed measures are integration of flux over the complete stellar disc, whereas the equations are expressing the flux in a surface point. In theory, the observed light variation is described by $\frac{\Delta L}{L}$, which is obtained by integrating $\frac{\Delta F}{F}$ over the visible hemisphere. Additionally, one must take into account the limb darkening effect, as well as the way the instrument takes the measurements.

In white dwarf non-linear theory (assuming that geometric effects are negligible), the relative flux variation expression could be simplified and therefore integrated (numerically according to Brickhill (1992), or analytically according to Montgomery (2005), Wu (2001)) obtaining the $\frac{\Delta L}{L}$, so it can be compared with the observations. Conversely, this was not possible for intermediate-mass stars (Balona, 2012), where the variations of radius and surface normal have to be taken into account.

A possible path to take, in order to shed some light into the non-linear behaviour of intermediate-mass pulsating stars, is to characterize the observed non-linear light curve by its Fourier decomposition parameters (Simon and Lee, 1981). Their correspondence with physical processes can be of later work. Generally, such characterization for combination frequencies is described in the literature by the non-linear distortion model or simple model.

In this dissertation, the Volterra-based model is introduced as an alternative way of characterizing non-linear light curves.

3.3   Modeling the Fourier parameters

3.3.1   The non-linear distortion model (or simple model)

Non-linearities are combination frequencies arising in the star power spectrum due to non-linear processes taking place inside the pulsating star, whose footprints are captured in their light curves. These harmonics and cross-terms express interaction between the oscillating modes of the physical system. The simplest interaction between modes can be explained by the non-linear distortion model (or simple model). The luminosity signal of a double mode pulsating star can be explained in terms of a product of two sinusoidal waves Y_1 and Y_2

$$Y_1 = A_1 \cos(2\pi\nu_1 t + \phi_1) \tag{3.9}$$

$$Y_2 = A_2 \cos(2\pi\nu_2 t + \phi_2); \tag{3.10}$$

where ν_1 and ν_2 are the independent frequencies (also called parent frequencies). They interact with each other originating a signal $Y_c(t)$ of cross-terms at $\nu_{\pm c}$ called combination frequencies (or children frequencies)

$$
\begin{aligned}
Y_c(t) &\propto Y_1(t)Y_2(t) \\
&\propto A_1 A_2 \cos(2\pi\nu_1 t + \phi_1)\cos(2\pi\nu_2 t + \phi_2) \\
&\equiv A_c \cos(2\pi\nu_{+c}t + \phi_{+c}) + A_c \cos(2\pi\nu_{-c}t + \phi_{-c});
\end{aligned}
\tag{3.11}
$$

where

$$\nu_{\pm c} = \nu_1 \pm \nu_2; \tag{3.12}$$

$$\phi_{\pm c} = \phi_1 \pm \phi_2; \tag{3.13}$$

$$A_c = \frac{A_1 A_2}{2}; \tag{3.14}$$

are the frequency, phase and amplitude relations of the combinations at $t = 0$, respectively.

In this model, children are expected to mimic (to correlate with) their parents phase and amplitude. Unfortunately, this model does not explain many of the observed amplitude distributions of combination frequencies in δ Sct stars. It is very frequent to find amplitudes of combination frequencies much larger than the predicted by the simple model (Breger and Montgomery, 2014), even surpassing their parents amplitudes (Kurtz et al., 2015).

3.3.2 Resonant mode coupling model

If any resonance condition is met, for example

$$\omega_c \approx \omega_1 + \omega_2 \qquad (3.15)$$

or

$$\omega_c \approx 2\omega_1; \qquad (3.16)$$

then the parent frequencies (ω_1 and ω_2) and their children are locked in energy, enabling the possible interchange of energy between them (Buchler et al., 1997, Dziembowski, 1982, Nowakowski, 2005). This means that any variation of the parent modes can be affecting the children in the same amount. The energy of the independent mode is distributed in all the coupled family.

In terms of Fourier parameters, frequency and phases under a resonant mode coupling situation will follow the same relation as the non-linear mixing model (Eqs. 3.12 and 3.13). However, the amplitudes relation for couple modes obeys a more sophisticated expression (Dziembowski, 1982):

$$A_c = \mu_c A_1 A_2; \qquad (3.17)$$

where μ_c is the coupling coefficient described by the following form:

$$\mu_c = \frac{H}{2\sigma_c \gamma_c I_c}; \qquad (3.18)$$

where the H coefficient determines the strength of the coupling and the σ_c, γ_c and I_c are the dimensionless frequency, damping rate and inertia of the coupled child, respectively.

This formulation could explain the amplitude enhancement observed sometimes for children frequencies, inexplicable by the simple model. According to Dziembowski and Krolikowska (1985), the most likely resonance mechanism occurring in δ Sct stars is the parametric resonance. Two g-modes (parents) can couple with an unstable p-mode (child). The coupling of these modes would cause interchange of energy in anti-correlation with the parent modes. Examples of this are given in Barceló Forteza et al. (2015), Bowman and Kurtz (2014), Bowman et al. (2016), Breger et al. (2012), Breger and Montgomery (2014) where identifications of families of couple modes in δ Sct stars were made. Their method is based on the assumption that amplitudes of the members of a coupled family are similar, therefore, larger values of μ_c are expected. For example, in KIC 8054146, the order of magnitude of μ_c was of 10^3 for parents with an amplitude $\approx 10^{-1}$ mmag (Breger and Montgomery, 2014). Their models for the amplitude of the coupled child match very precisely with the observations. However, it is important to note that to test their models the modes have to have large-scale amplitude modulation, therefore, application of their method can be cumbersome since variation in time between all the modes has to be studied to check the expected interchange of energy.

3.3.3 The Volterra expansion model

In the context of system and signal analysis, the Volterra expansion (or Volterra series) is a general non-linear model that can describe the output of a non-linear system in terms of an infinite sequence of functions, namely, the *generalized transfer functions*.

Considering the pulsating star to be the non-linear system in question, and if the input to such system is a single real-valued sine wave with frequency ω_0 and amplitude A_0, the

output can be expressed as (see Priestley, 1988, p.29)

$$Y(t) = A_0 \cdot \Gamma_1(\omega_0) \cdot e^{i \cdot \omega_0 \cdot t + \phi_0} + A_0^2 \cdot \Gamma_2(\omega_0, \omega_0) \cdot e^{2 \cdot i \cdot \omega_0 \cdot t + 2 \cdot \phi_0}$$

$$+ A_0^3 \cdot \Gamma_3(\omega_0, \omega_0, \omega_0) \cdot e^{3 \cdot i \cdot \omega_0 \cdot t + 3 \cdot \phi_0} + \dots$$

(3.19)

where the Γ_O functions are the generalised transfer complex functions. Sub-index O denotes the non-linear order of interactions, i.e. Γ_1 represents the system response for each independent frequency, Γ_2 represents the system response for first order interactions, and so on. With the purpose of obtaining a physical model that explains non-linear effects, the generalised transfer functions must be fully characterized.

Although Y(t) is not linear between the input/output spectra, it is linear between Y(t) and the Γ_O functions (Scargle, 2020), so a standard least-squares procedure quantify not only the parameters of the input components, but also the contribution from the generalised transfer functions. For example, since the Γ_O functions are complex functions, they can be expressed by

$$\Gamma_o(\omega_i) = |\Gamma_o(\omega_i)| e^{i arg\{\Gamma_o(\omega_i)\}}$$

(3.20)

Therefore, Eq.3.19 can be rearranged as:

$$Y(t) = \tilde{A}_1 \cdot e^{i\omega_0 \cdot t + \tilde{\phi}_1} + \tilde{A}_2 \cdot e^{2 \cdot i \cdot \omega_0 \cdot t + \tilde{\phi}_2} +$$

$$\tilde{A}_3 \cdot e^{3 \cdot i \cdot \omega_0 \cdot t + \tilde{\phi}_3} + \dots$$

(3.21)

where,

$$\tilde{A}_1 = A_0 \cdot |\Gamma_1(\omega_0)|,$$

$$\tilde{A}_2 = A_0^2 \cdot |\Gamma_2(\omega_0, \omega_0)|,$$

(3.22)

$$\tilde{A}_3 = A_0^3 \cdot |\Gamma_3(\omega_0, \omega_0, \omega_0)|$$

and

$$\tilde{\phi}_1 = \phi_0 + arg\{\Gamma_1(\omega_0)\},$$

$$\tilde{\phi}_2 = 2 \cdot \phi_0 + arg\{\Gamma_2(\omega_0, \omega_0)\},$$

(3.23)

$$\tilde{\phi}_3 = 3 \cdot \phi_0 + arg\{\Gamma_3(\omega_0, \omega_0, \omega_0)\}$$

Examining the case when the input is composed of two real-valued sine waves at frequencies ω_0 and ω_1, the output of a non-linear system modelled by a Volterra series is:

$$Y(t) = A_0 \cdot \Gamma_1(\omega_0) \cdot e^{i \cdot \omega_0 \cdot t + \phi_0} + A_1 \cdot \Gamma_1(\omega_1) \cdot e^{i \cdot \omega_1 \cdot t + \phi_1}$$

$$+ A_0^2 \cdot \Gamma_2(\omega_0, \omega_0) \cdot e^{2 \cdot i \cdot \omega_0 \cdot t + 2 \cdot \phi_0} + A_1^2 \cdot \Gamma_2(\omega_1, \omega_1) \cdot e^{2 \cdot i \cdot \omega_1 \cdot t + 2 \cdot \phi_1}$$

$$+ A_0 \cdot A_1 \cdot \Gamma_2(\omega_0, \pm\omega_1) \cdot e^{i \cdot (\omega_0 \pm \omega_1) \cdot t + (\phi_0 \pm \phi_1)}$$

$$+ A_1 \cdot A_0 \cdot \Gamma_2(\omega_1, \pm\omega_0) \cdot e^{i \cdot (\omega_1 \pm \omega_0) \cdot t + (\phi_1 \pm \phi_0)} + \dots$$

(3.24)

Eq.3.24 can be rearranged as:

$$Y(t) = \tilde{A}_1 \cdot e^{i \cdot \omega_0 \cdot t + \tilde{\phi}_1} + \tilde{A}_2 \cdot e^{i \cdot \omega_1 \cdot t + \tilde{\phi}_2} +$$

$$\tilde{A}_3 \cdot e^{2 \cdot i \cdot \omega_0 \cdot t + \tilde{\phi}_3} + \tilde{A}_4 \cdot e^{2 \cdot i \cdot \omega_1 \cdot t + \tilde{\phi}_4} +$$

$$\tilde{A}_5 \cdot e^{i \cdot (\omega_0 \pm \omega_1) \cdot t \pm \tilde{\phi}_5} + \dots$$

(3.25)

where,

$$\tilde{A}_1 = A_0 |\Gamma_1(\omega_0)|,$$

$$\tilde{A}_2 = A_1 |\Gamma_1(\omega_1)|,$$

$$\tilde{A}_3 = A_0^2 |\Gamma_2(\omega_0, \omega_0)|,$$

$$\tilde{A}_4 = A_1^2 |\Gamma_2(\omega_1, \omega_1)|,$$

(3.26)

$$\tilde{A}_5 = A_0 A_1 |\Gamma_2(\omega_0, \omega_1)|,$$

$$\text{or } \tilde{A}_5 = A_1 A_0 |\Gamma_2(\omega_1, \omega_0)|^1$$

and

$$\tilde{\phi}_1 = \phi_0 + arg\{\Gamma_1(\omega_0)\},$$

$$\tilde{\phi}_2 = \phi_1 + arg\{\Gamma_1(\omega_1)\},$$

$$\tilde{\phi}_3 = 2 \cdot \phi_0 + arg\{\Gamma_2(\omega_0, \omega_0)\}, \tag{3.27}$$

$$\tilde{\phi}_4 = 2 \cdot \phi_1 + arg\{\Gamma_2(\omega_1, \omega_1)\},$$

$$\tilde{\phi}_5 = \phi_0 \pm \phi_1 + arg\{\Gamma_2(\omega_0, \pm\omega_1)\},$$

$$or\ \tilde{\phi}_5 = \phi_1 \pm \phi_0 + arg\{\Gamma_2(\omega_1, \pm\omega_0)\}^1$$

A Fourier Transform of Eq.3.25 results in a power spectrum with peaks at the parent frequencies ω_0 and ω_1, as well as on the frequencies of the non-linear terms or children frequencies. This is a well-known phenomenon in system and signal analysis called *inter-modulation distortion*. In the case of one parent frequency it is called *frequency multiplication* or *harmonic distortion*.

The Volterra expansion model was first proposed by Garrido and Rodriguez (1996) to be suited to model non-linear light curves. The non-sinusoidal shapes of the light curves can be reproduced by treating the variable star as a non-linear but stationary system, where the origin of the pulsation is interpreted as the application of a known input (a basic harmonic signal) to the system. In the next chapters, non-linear terms in δ Sct stars power spectra are going to be empirically characterized under the general non-linear model given by the Volterra series. In chapter 5, results of a first approach to an empirical characterization of the Γ_O functions are presented.

---

[1]since no condition of symmetry is yet imposed.

Chapter Four

Non-linearities in Delta Sct stars. I The frequency relation

Combination frequencies in the power spectrum of a variable star due to NLDP, or from a resonantly excited nature, are called non-linearities. To start to characterize them observationally, it is imperative to determine their position in the power spectrum, i.e. their frequency value. So far, discerning unambiguously whether a maximum in the power spectrum is due to an excited radial or non-radial mode of the pulsating star, or the result of a combination produced by the interaction between these modes has not been possible.

In this study, the variable star behaviour as a non-linear system is taken as a hypothesis, so that all the underlying theory of signals and systems (explained in Section 3.3.3) could be applied. Therefore, in order to identify combinations as non-linearities, the frequency, amplitude and phase relations must be hold. The frequency relation is considered first as it is totally determined, and is exactly the same for the Volterra model as for the simple model.

In this chapter, a self-consistent method to identify the frequencies of the power spectrum that comply with the parent-child relationship is presented in Section 4.2, along with its application to various δ Sct stars (Sections 4.3.1-4.3.3). This method is capable of yielding great precision in the frequencies as well as to exhaustively find the parents that 'best' explain

the signal in terms of their non-linear components, although it does not clarify which are the parents and which are the children. To begin with its description, it is important to review current methods available to identify families of parents and children.

4.1 Identifying combination frequencies: state of the art

4.1.1 Frequency near a combination frequency value

An heuristic approach, commonly used as initial inspection to solve the problem of combination frequencies identification, is to simply examine a list of frequencies (f_i) resulting from a prewhitening cascade (see Sec. 2.1.2) and select as combination frequencies those that differ a small quantity (δ_f) from an exact combination frequency value (f_c)

$$|f_i - f_c| \leq \delta_f, \tag{4.1}$$

where $i = 1, 2, 3, ..., K$, and K is the number of prewhitened frequencies. The f_c values are calculated choosing as parents any of the frequencies from the list. Often, the chosen δ_f is the Rayleigh frequency resolution (Degroote et al., 2009, Murphy et al., 2013, Pápics, 2012, Saio et al., 2018, Zwintz et al., 2020). Nevertheless, the value of this parameter is arbitrary and can be chosen differently (e.g. García Hernández et al., 2013).

The inconsistency of the reasoning behind this method is that when the frequency does not match the value of the combination exactly, the residuals after the fit will still be correlated with the combination frequency. Evidently, that could lead to uncleaned power spectra from the contribution of combination frequencies but more importantly, it could lead to wrongly identify an oscillation mode as a combination frequency. Moreover, the premise of choosing the Rayleigh frequency resolution as δ_f enclose that it is taken as if it were the uncertainty in the frequency, however it could be a very coarse limit election when frequencies are resolved, since uncertainty can go further the Rayleigh frequency resolution in such cases.

4.1.2 COMBINE

COMBINE is a software package that performs iterative analyses to identify combination frequencies. It was developed by Reegen (2011), and basically consists in a more sophisticated version of the method explained in Section 4.1.1. It adds tools to measure the *Reliability* of a combination that obeys Eq. 4.1.1, and an automatized mechanism which iteratively finds linear combinations of any of the previously identified as significant frequencies. Despite of the efforts to provide robustness to the method, it can not guarantee that the residual light curve will be free of the contribution of combination frequencies. This is because frequencies identified as combinations are not the exact combination values.

4.1.3 Fitting exact combination values

Selecting the exact combination frequencies to fit them to the variable star light curve could guarantee that the residual light curve of such fit is uncorrelated to the combination frequencies initially contributing to the stellar light curve variability. This was the identification method in Balona (2016) and in Kurtz et al. (2015). Both studies take into account that non-linearities must be found exactly in their combination frequency value (since they are mathematical footprints of non-linear effects), but parents are determined by a non-exhaustive non-linear least-squares method (*Period 04*), so the children originated by those parents may be slightly different from the real ones.

Period 04 is a software package dedicated to perform time series analyses (Lenz and Breger, 2004). The Fourier decomposition tool allows to decompose the signal in sine waves with frequency, amplitude and phases parameters which can be optimized by a non-linear least-squares fit. This optimization option is the functionality behind the buttons "calculate" (to optimize only amplitudes and phases) and "calculate all" (to optimize frequencies, amplitudes and phases). However, the optimization procedure that the algorithm follows is not described in the software manual whatsoever. In fact, when conducting a Fourier

analysis and wanting to compute the non-linear least-squares, clicking the "calculate" (or "calculate all") button several times leads to different values of the parameters and smaller values of the residual light curve variance, but no explanation is found to how many times the user of the package should press this button and what is it really doing. Such *black box* in the non-linear least-squares determination does not make it possible to guarantee that the yielded parameters are their best optimization, or that the search for these optimization is conducted exhaustively. Besides, although by using *Period 04* is possible to fit the exact combination values of any chosen parents, this input must be entered manually, so the user must know in advance the combination frequencies present in the power spectrum (which can often go unnoticed), not to mention that it can become a laborious task when many combination frequencies are present.

4.2   The Best Parent Method

The Best Parent Method (BPM), consists in an algorithm that recursively searches for the parent frequencies that describe the most of the variable star non-linear signal in terms of its non-linearities, or combination frequencies. This is accomplished by computing different non-linear least-squares fits for different possible parent frequencies and the children generated by them. In these fits, Eqs.3.21 and 3.25 are the chosen approximation functions modelling the non-linearities (in light curves of mono-periodic and double-mode variable stars, respectively).

The residual light curve of each fit should be uncorrelated with the parents and the statistically significant combination frequencies fitted. Then, the variance of the residual light curve (in comparison with the variance of the original light curve) quantifies to which extent the parents and children fitted explain the signal: the lower the variance value the better the fit. Therefore, the minimum variance value of all the fits, will indicate the independent frequencies that best describe the signal, i.e. the 'best' parent frequencies.

Formally, it is possible to define V (namely, the variance function) as a continuous function conformed by the variance values of fittings relating different parent frequencies (and their children) to a given light curve. The aim of the method is to find a local minimum in V. Note that V is only a function of the parent frequencies (i.e. $V = V(\omega_i)$). There are several procedures for finding the minimum in a non-linear least-squares fitting (Bevington and Robinson, 2003), but in the method here presented we follow an empirical approach which consists in exploring the n-dimensional independent frequencies surface exhaustively.

The code for the algorithm implementation is written in Python, and now constitutes an importable Python library called *combi_filter.py*.

4.2.1 Algorithm flow

For a global understanding, a representation of the design of the algorithm is presented in Fig.4.2.1. However, the linear flow of the algorithm is described in the following steps:

- **Number of parents**

  The number of parents (or independent frequencies) is asked. In the code this variable is named n_p.

- **Building the families to test**

  Several possible parents, differing in a small step (ϵ) from each other, around a first coarse parent guess (ν_i), are chosen. Concretely, if $n\_p = 1$, then the possible parents are:

$$\nu_i \pm k \cdot \epsilon; \tag{4.2}$$

  where k is an integer number from zero to the number of sets of the exploration variable, n_exp, which can be chosen by the user of the library (see panel (a) from Fig. 4.2.1). The small step (ϵ) is also a variable in the code.
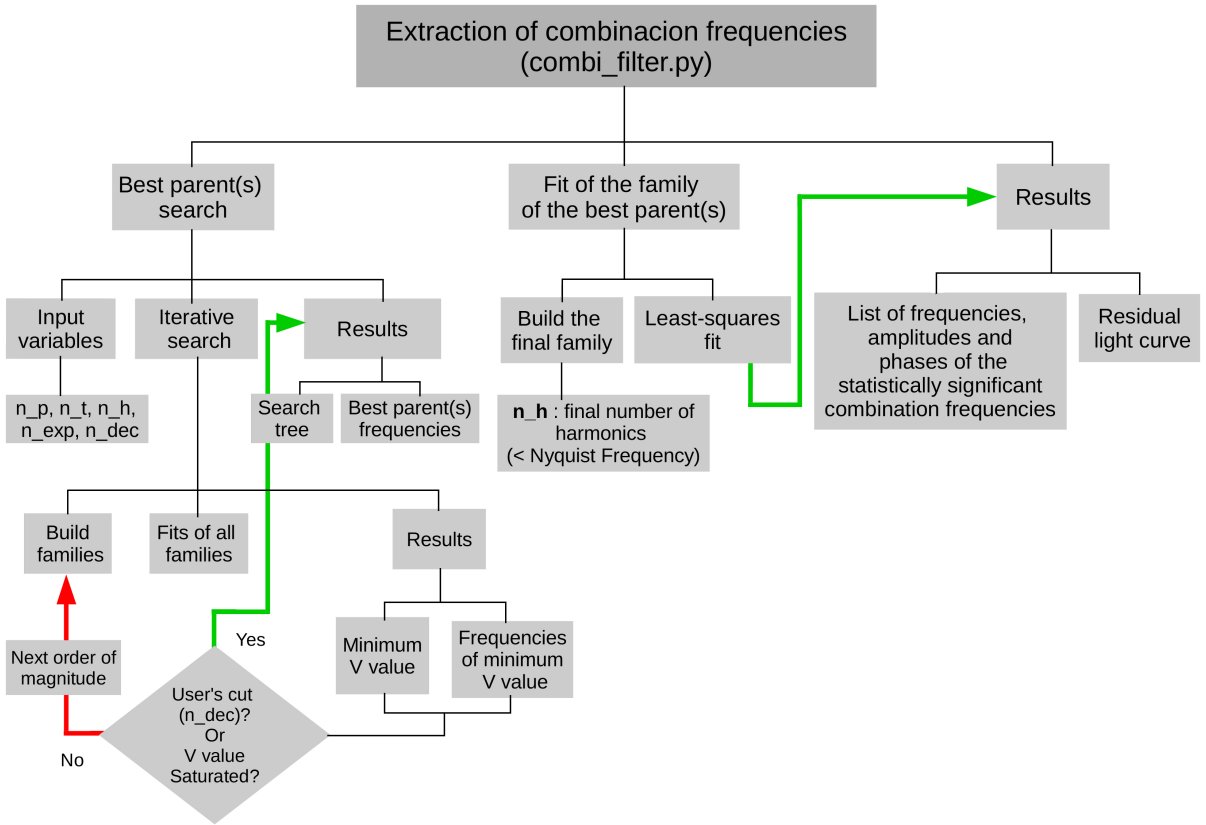
Figure 4.1 Design of the algorithm for the extraction of combination frequencies.

When $n\_p \geq 2$, then the user can choose the number of terms composing each combination with variable n_t. This variable refers to the number of addends in the frequency relation between parents and children:

$$\omega_k = |\pm n \cdot \omega_i \pm m \cdot \omega_j \pm ...| \tag{4.3}$$

where m and n are integer numbers and their absolute sum is the order of the combination,

$$O = |\pm n| + |\pm m| \tag{4.4}$$

For each parent to be tested, their children are calculated. In this moment, the user will be asked for the number of harmonics (the n and m in Eq. 4.3). In the algorithm,
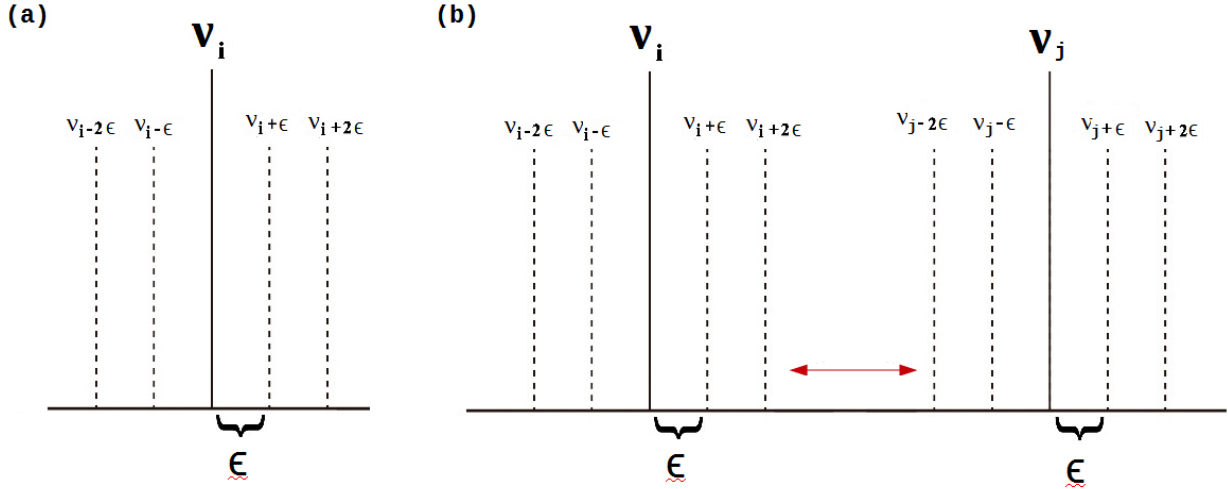
Figure 4.2 Schematic representation of best parent search with $n\_exp = 2$. Panel (a) for one parent frequency ω_i and panel (b) for two parent frequencies ω_i and ω_j. The search does not allow overlapping of the possible parents (red arrow)

these are represented by the variable name n_h.

- **Iterative Search**

In this step the iterative computations of the least-squares fitting starts. For each family, only the combination frequencies surviving a statistical test of significance (e.g. Student's t or Snedecor's-F) are fitted to the light curve. In this research thesis, a Student's t criterion of significance with a level of confidence of 99.9% is used. An array of variance values for the residual light curve of each fit results from this procedure. The minimum value of this array points out to the 'best' parent(s) of the first iteration.

Now that the parent(s) that minimise the V function is (are) found, this result is used as seed for the next iteration, where the search is conducted with a smaller ϵ step. This recursive process is repeated until the ϵ have the same number of decimals set in a variable set by the user n_dec. At the end of this loop the aim of the search is achieved, that is, to sift out which possible parent(s) yielded the minimum variance value.

- **The final extraction**

  This last step is when the user's intention is to obtain the power spectrum free of combination frequencies. To obtain it, a last fitting of a series of sinusoids to the original light curve is computed. This time, the frequencies of the fitted sinusoids are of the 'best' parent(s) found and the children. Again, the value of the n and m in Eq. 4.3 is asked for this final extraction. The residual light curve of such fit is expected to be uncorrelated with the non-linear terms and the 'best' parents, so, a FFT to that residual light curve will yield the wanted clean power spectrum.

4.2.2   Criteria adopted for the input parameters

The search of the 'best' parent(s) can be computationally expensive in terms of time consumption. Therefore, although the algorithm was developed to use any wanted value for each variable, in this research certain limiting criteria over the input parameters were chosen caring for efficiency, without jeopardizing the exhaustive property of the search. In Table (4.1), the algorithm variables are listed along with their description and the values used in the analysis made in this research.

Concretely, the criteria adopted in this work for n_p is that no more than two parents are chosen. In the particular case of $n\_p = 2$, only combinations of two terms are explored ($n\_t = 2$). Then, all the possible parents around the initial ones are calculated according to Eq. 4.2, where $n\_exp = 4$ steps around the initial guess are explored (the algorithm does not allow overlapping when choosing n_exp if $n\_p \geq 2$. See panel (b) from Fig. 4.2.1). Therefore, all potential pairs (when $n\_t = 2$) of possible parents are the parents to be tested.

The criteria adopted for n_t allow to avoid increasing the probabilities for false combination frequencies identifications since any frequency value can be represented as a linear combination of other frequencies (Balona, 2012, Pápics, 2012). Additionally,

Variable name	Description	Values used in this research.
n_p	Number of parents	1 (mono-periodic stars) or 2 (double-mode stars)
ϵ	Array of values of the small step of separation between possible parents for each iteration	$(0.1, 0.01, 0.001, \cdots)$
n_exp	Integer number of steps of ϵ value to explore around the initial guess	4
n_t	Number of terms: addends in the combination expression	2
n_h	Number of harmonics: highest integer number of the harmonics to explore	The corresponding n and m in Eq. 4.3 so the harmonic value do not exceed the Nyquist frequency
n_dec	Number of decimals to explore or the uncertainty to reach. Corresponds to the number of iterations of the search.	5 (See Section 4.4)

Table 4.1 Input parameters in the BPM algorithm.

choosing $n\_p = 2$ as maximum value diminishes the computational time considerably since exploring all possible combinations between more than 2 parents represents many more combinations to test as follows:

$$Number\_of\_pairs = \frac{d!}{r!(d-r)!},$$
(4.5)

where d is the number of possible parents to choose from and r is how many to select from them. So, if $n\_p = 2$ ($r = 2$) and $n\_exp = 4$, then $d = 10$ and so 100 pairs of possible best parents have to be tested in each iteration, whereas if $n\_p = 3$ ($r = 3$), then 1000 pairs of parents have to be tested.

Moreover, in this dissertation, for an exhaustive search, the first ϵ is set to 0.1 and will be decreasing in order of magnitude in each interaction (second iteration with the next lower magnitude order: 0.01, and so on). In the iterative search, a minimum will be reached in an unknown number of steps, but in this algorithm the user can choose to truncate the search to a certain final precision with the variable n_dec. An example of this can be seen at Section 4.3.1 in Table 4.2, where the minim is really reached in the 14^h iteration, however, the value taken as the final result is the one of the 5th iteration. For all the other analyses in this work n_dec is also set to 5, and the reasoning behind it is explained in Section 4.4.

The criteria in this work to select the n_h parameter is that the highest combination (harmonic or sum) does not exceed the Nyquist frequency. When dealing with more than one parent frequency, it was convenient to choose smaller values for the n_h parameter in the iterative search for it to be faster. This is based on the fact that very often the combinations contributing the most to the light curve variability of the star have low orders ($O < 5$). However, in the final extraction phase of the procedure, the one that yield the residual light curve for posterior studies, the criteria of not going beyond the Nyquist frequency is adopted. It is important also to highlight that the applicability of this method is not just for evenly spaced data. When dealing with

unequally spaced data, the set of combinations to calculate and fit can be accordingly chosen up to any convenient frequency, since Nyquist frequency is undetermined in these cases (Δt is not unique. See Section 2.1).

4.3   Application of the BPM

To test the performance of the method, three δ Sct stars, of different pulsational contents, were chosen: first, a mono-periodic δ Sct variable, in order to verify the process of finding the 'best' parent; next, a double-mode pulsator; and finally, a multi-periodic δ Sct star, where more complex non-linearities can be present and where their extraction could be critical to the frequency analysis. Relevant information describing the light-curves is listed in Table A.1.

4.3.1   Mono-periodic variables:

In the case of a single parent frequency (e.g. a Cepheid or a high amplitude mono-periodic variable), the highest peak in the power spectrum is selected as a first approximation to the parent frequency with a coarse precision. Then, $V(\omega)$ is sampled with a progressively smaller step until the minimum is reached. In this way, the minimum V value yields a much more precise frequency. Often, the frequency error is smaller than the Rayleigh resolution (see Section 2.1). The frequency value is compatible with that obtained by the O-C (Observed minus Calculated) method (Sterken, 2005), which is basically how the times of arrival of the pulses are determined in the Pulsar Timing analysis technique, known for yielding extraordinary precision when calculating the period of a pulsar (Lorimer and Kramer, 2004). All this was proved in Lares-Martiz et al. (2020), where the mono-periodic δ Sct star TIC 9632550 observed by The Transiting Exoplanet Survey Satellite (TESS, Ricker et al., 2014) was analysed in order to test the performance of the BPM.

In Lares-Martiz et al. (2020), it is shown how the BPM applied to a light curve of a mono-periodic pulsating star results in a local minimum of the V function, which determines
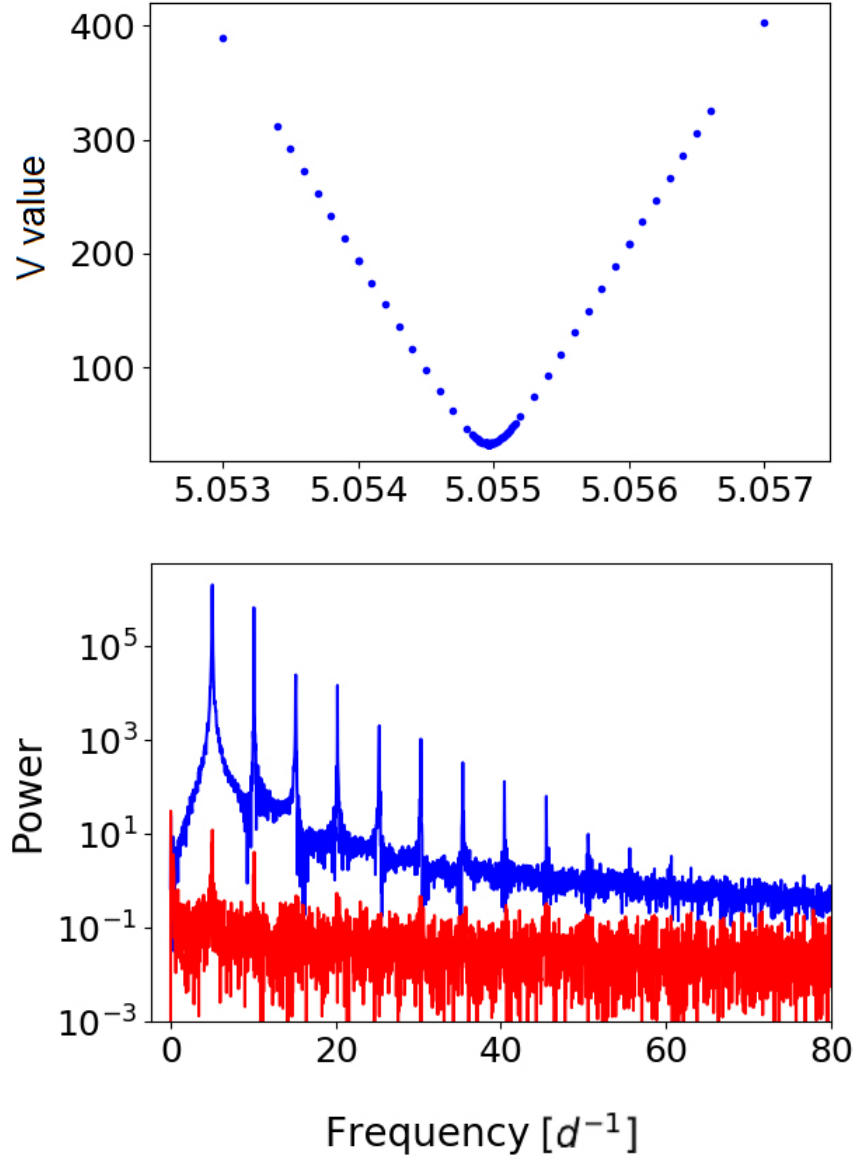
Figure 4.3 Application of the BPM to the light-curve of TIC 9632550. Upper panel: fundamental period found as a local minimum at 5.054963644 d^{-1}. Lower panel: in blue, the FFT of the original light-curve; in red, the FFT of the residuals after fitting the fundamental frequency and 13 statistically significant harmonics. Units of power are $[(e^-/s)^2]$. Source: Lares-Martiz et al. (2020)

Table 4.2 The 'best' parent search tree for the mono-periodic δ Sct star TIC 9632550. The first column quantifies the number of statistically significant frequencies, or children, detected with the parent frequency specified in the third column, in d^{-1} (zeros are omitted for the sake of clarity). The second column is the variance after fitting the parent and combination frequencies (in this case, only harmonics of the highest one).

No. of statistically significant frequencies	V value	Frequency[d^{-1}]
1	3155.844405793707201	5.0
5	948.937738175725485	5.05
14	33.629889361388315	5.055
14	33.629889361388315	5.055
14	**32.871889584474623**	**5.05496**
14	32.862102488776905	5.054964
14	32.862102488776905	5.054964
14	32.862101660828912	5.05496404
14	32.862101656257245	5.054964037
14	32.862101656225789	5.0549640372
14	32.862101656224368	5.05496403722
14	32.862101656224311	5.054964037229
14	32.862101656223409	5.0549640372274
14	32.862101656222627	5.05496403722726
14	32.862101656222627	5.05496403722726
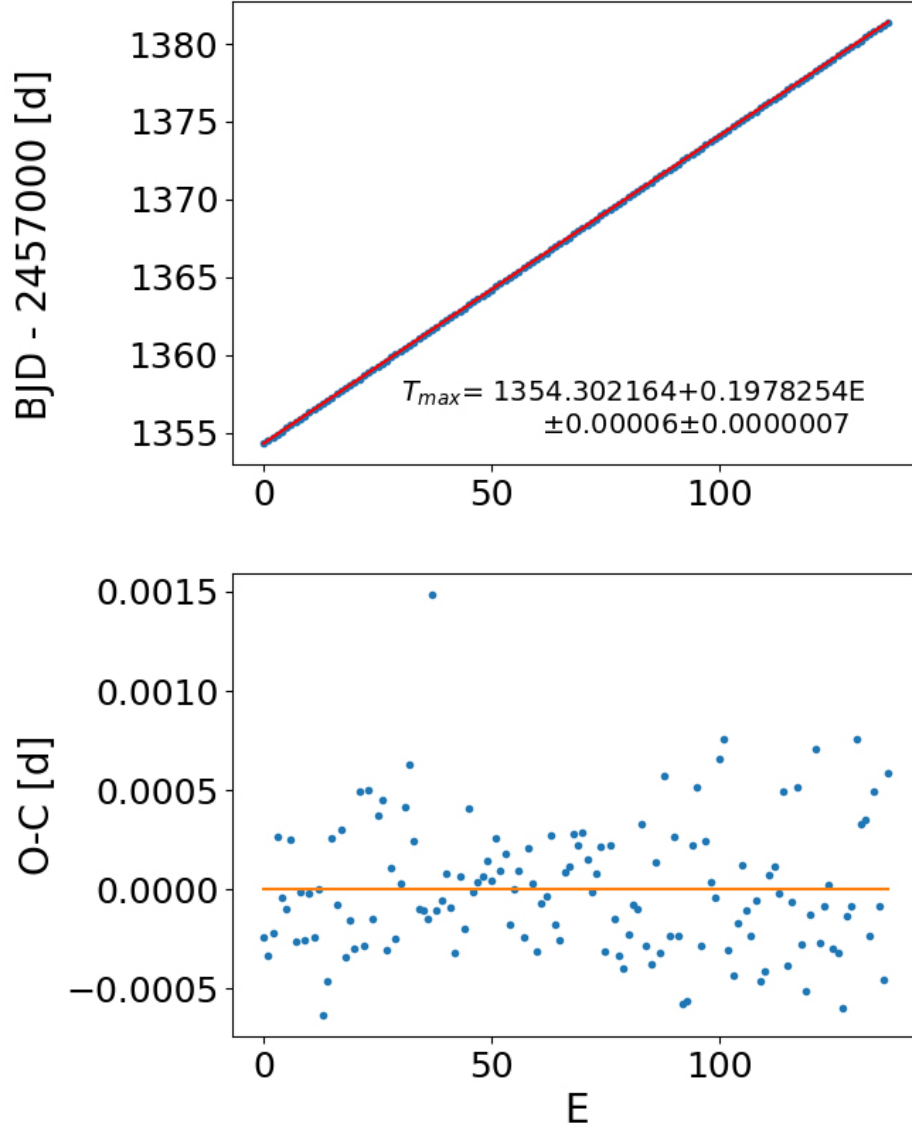
Figure 4.4 Application of the O-C method to the light-curve of TIC 9632550. Upper panel: in blue, the times of the light maximum, corresponding to the maximum value of a parabola fitted to each cycle; in red: the regression line $T_{max} = T_0 + PE$, where P is the trial period, T_0 is the zero epoch, and E is an integer number of cycles elapsed since the zero epoch. The fundamental frequency ($\omega_0 = 1/P$) calculated by the O-C method is $\omega_0 = (5.05496 \pm 0.00002)$ d^{-1}. Lower panel: residuals of the regression. Source: Lares-Martiz et al. (2020)

Table 4.3 Results of the combination frequencies extraction process for the mono-periodic δ Sct star TIC 9632550. The first column shows the 'best'parent from the search tree in cycles per day. The second column specifies the number of statistically significant frequencies, or children, extracted. The %CF (third column) quantifies the percentage of the initial power attributable to the combination frequencies and their parents.

	TIC 9632550		
Tag	'best' parent [d^{-1}]	Combinations extracted	%CF
f0	5.05496	13 Harmonics	98.98

the fundamental period.(see Fig. 4.3, upper panel). The iterative process of searching for the 'best' parent explained in Section 4.2, refines the frequency until the variance value (V) does not change. In this particular case, it happened in the 14th iteration (see Table 4.2). However, the value at the 5th interaction is the one chosen to be the best parent (see discussion subsection 4.4 for a full explanation). This result for the fundamental frequency is compatible with the one obtained by the O-C procedure (see Fig. 4.4):

$$\omega_0 = (5.05496 \pm 0.00002) \text{ d}^{-1}.$$

The results of the final extraction procedure are graphically represented in the lower panel of Figure 4.3 and quantitatively expressed by the high percentage of the original power explained by these non-linear effects and their parents (expressed as %CF in Table 4.3). These results shows that after the parent and its children are extracted, the power spectrum is almost cleaned from all signal contribution. Still, there are three peaks remaining in the residual power spectrum: the first one corresponds to the first frequency bin and it is the residual of a second order polynomial fitting, performed in order to remove any trend in the light curve; the second peak, appearing next to the fundamental frequency, and the third one, which is next to the first harmonic, are possibly explained by an amplitude modulation of the fundamental frequency. An alternative explanation of these two peaks, appearing at about the same frequencies as the fitted ones, might be the fractal property studied by

Table 4.4 Results of the combination frequencies extraction process for the double-mode HADS star KIC 5950759. The first column shows the 'best' parents from the search tree in cycles per day. The second column specifies the number of statistically significant frequencies, or children, extracted. The %CF (third column) quantifies the percentage of initial power attributable to the combination frequencies and their parents.

	KIC 5950759		
Tag	'best' parents [d^{-1}]	Combinations extracted	%CF
f0	14.22136	177 in total:	97.48
f1	18.33722	17 harmonics	
		92 sums	
		and 68 differences	

De Franciscis et al. (2018), which is impossible to reproduce by using a Fourier representation. In any case, the logarithmic scale shows 5 orders of magnitude difference between the original and the residual power, which is in very good agreement with our expectation of uncorrelated residuals.

4.3.2 Double-mode variables:

In the case of two parent frequencies, for example double-mode Cepheids, HADS stars or RR Lyrae, the procedure for finding the 'best' parents is also effective. There is a slight tendency for HADS stars to have higher number of non-linearities (Balona, 2016). This is why in Lares-Martiz et al. (2020) the KIC 5950759, a HADS star observed by the Kepler satellite (Gilliland et al., 2010), was chosen to test the BPM. The original power spectrum (blue in Figure 4.5) shows a very regular structure where the first two highest peaks follow the fundamental period and first overtone ratio expected to occur for δ Sct stars (see Stellingwerf, 1979).

In a recent study for this star by Yang et al. (2018), the parent frequencies for the SC
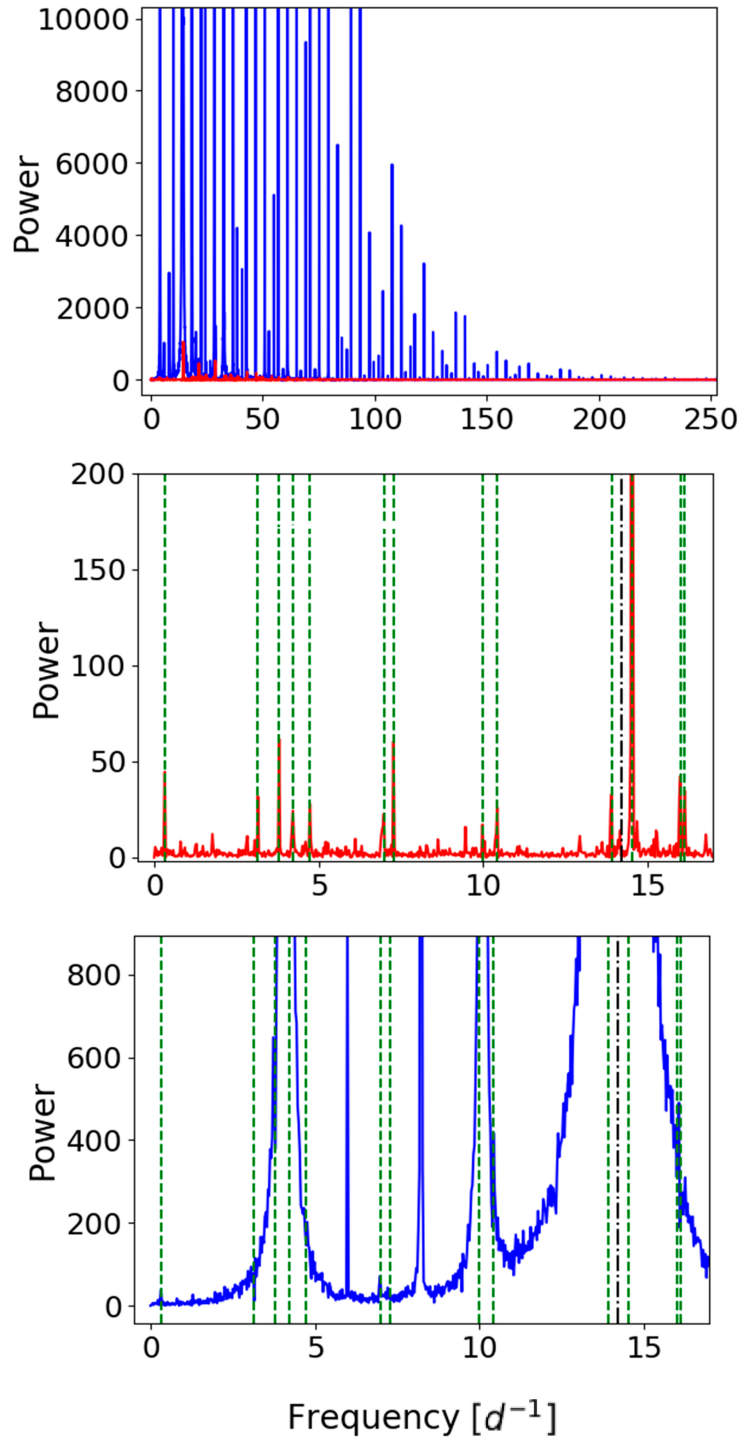
Figure 4.5 Application of the BPM to the light-curve of KIC 5950759. Blue: FFT of the original light-curve. Red: FFT of the residuals after fitting the 'best' parents and the combinations generated by them. Green dashed: new frequencies detected in the residuals of the fitting. Black dash–dotted: 'best' parent frequencies. Notice in the middle panel the significant peak corresponding to $\omega_m \approx 0.32\ \mathrm{d}^{-1}$. Also notice that the separation between the dashed green lines around the black dash–dotted line is equal to ω_m. Units of power are $[(e^-/s)^2]$. Source: Lares-Martiz et al. (2020)

data were:

$$\omega_0 = (14.221367 \pm 0.000015) \ d^{-1}$$

$$\omega_1 = (18.337228 \pm 0.000023) \ d^{-1}$$

Which are compatible with the 'best' parents computed by the BPM (see Table 4.4). In Yang et al. (2018), frequency errors were calculated according to a heuristically derived formula for the upper limit of the frequency uncertainty in Kallinger et al. (2008). The precision reached with the 'best' parents search is also empirically justified in Section 4.4.

When dealing with very high power of the initial components, the significance level is set too high, leading to an incomplete combination frequency extraction when computing the final extraction procedure. In such a scenario, the extraction from the residual light curve has to be completed in several steps, three in this particular case. In the first step, 71 combinations were significant (black in Fig.4.6), in the second 99 (green in Fig.4.6), and finally 7 (red in Fig.4.6). Notice how the black FFT still have many significant combination frequencies (in the range of 160 and 300 d^{-1}), which justify the extraction continuation. The green FFT is almost completely covered, since it is practically the same as the red (only 7 frequencies of small amplitudes different).

As a consequence of these fittings, a new frequency structure (that was previously hidden) emerges in its power spectrum (see middle panel of Fig. 4.5). Notice that the frequency $\omega_m \approx 0.32$ d^{-1}, that is modulating the entire spectrum, is now significant according to the Reegen (2007) criteria of signal/noise > 12.57 in the power domain. As firstly discussed by Bowman (2017), the new frequency structure seen for the KIC 5950759 deserves further studies regarding its origin, since it could be possibly indicating the existence of other independent modes. Yang et al. (2018) explored several physical explanations, proposing as the most likely to identify ω_m as the rotation of the star, meaning that the dashed lines around ω_0 in the middle panel of Figure 4.5 corresponds to the modulation of the main pulsation modes with rotation frequency. Other possible explanations for the fine structures appearing
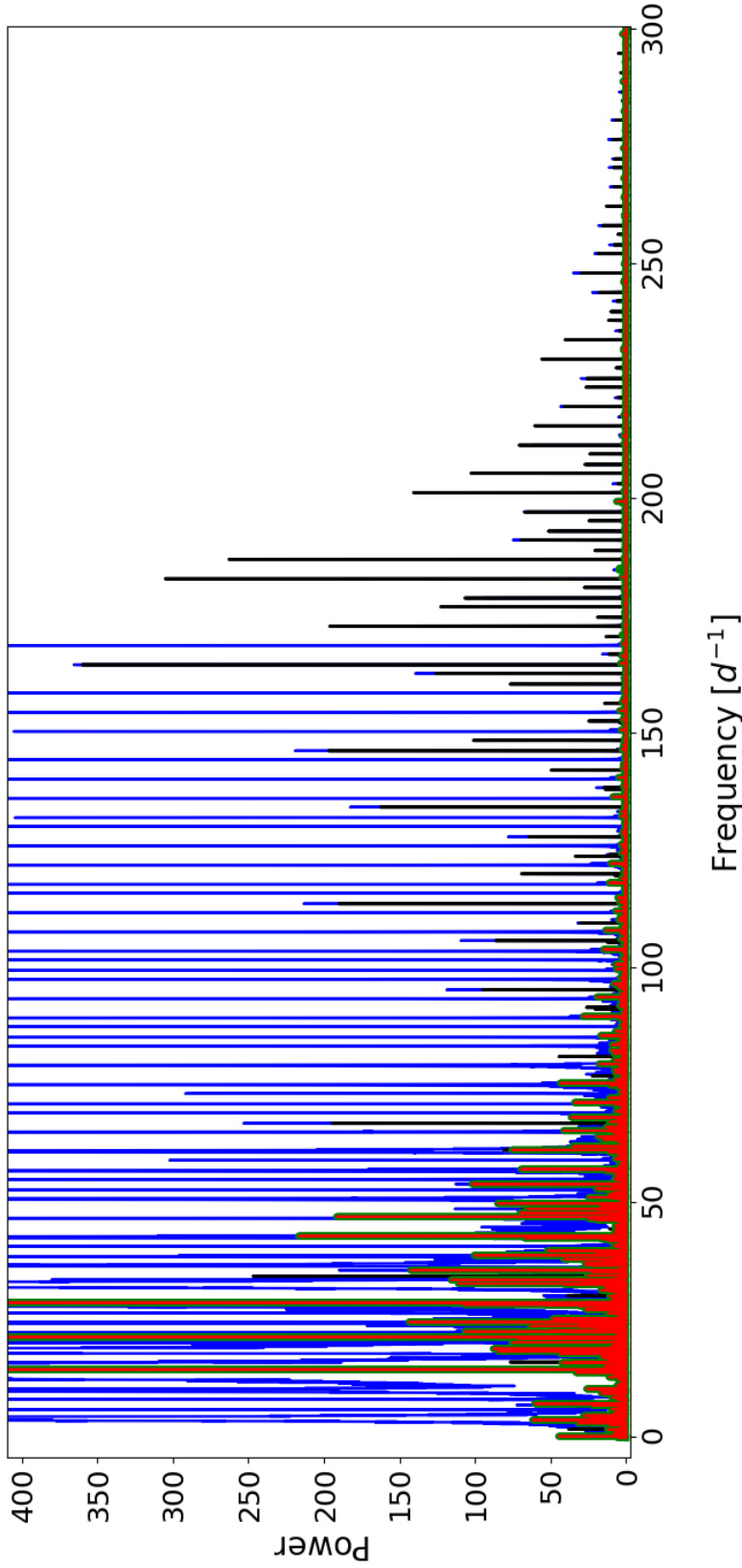
Figure 4.6 Extraction of non-linearities by groups for KIC 5950759. The power spectra of the residuals after fitting each group of frequencies are colour-coded:blue corresponds to the original light-curve, black to the residuals after fitting the first group of frequencies (71 children), green to the residual light-curve obtained after fitting the second group of frequencies (99 children), and red to the residual light-curve after fitting the last group of frequencies (7 children). Units of power are $[(e^-/s)^2]$. Source: Lares-Martiz et al. (2020)

around the main frequencies, might be carefully evaluated taking into account the work of Zong et al. (2018), where different frequency and/or amplitude modulation patterns were identified in the power spectra of an ensemble of pulsating hot B subdwarf (sdB) and white dwarf stars observed by the Kepler satellite.

In any case, the results shown in Figure 4.5 stress the need of a correct extraction of the combination frequencies. It was shown that it is possible to unveil frequency structures that previously did not exceed the detection threshold. In this particular case, the detection of ω_m frequency was possible using SC data, whereas in Yang et al. (2018), using LC data, a super-Nyquist and alias analysis were necessary in order to identify it.

4.3.3 Multi-periodic variables:

When analysing non-linear light curves of multiperiodic stars such as low amplitude δ Sct (LADS) stars, γ Dor, etc., the application of the BPM could be done for more than two parents. In such cases, exploring the frequency space of the V function recursively to find its minimum value can be computationally expensive, but the implications of applying the BPM can be crucial for an asteroseismic analysis, as showed in the previous section. In Lares-Martiz et al. (2020), the BPM method was tested to the light curve of HD 174966, a LADS (or simply δ Sct star) observed by the CoRoT satellite (Auvergne et al., 2009). This star was studied in García Hernández et al. (2013), who found that the 5th highest peak in the amplitude spectrum was very near to the estimated fundamental radial mode $(17.3 \pm 2.5 \text{ d}^{-1})$.

In multi-periodic variables, the independent frequencies are not easy to identify. The first five peaks of highest power are chosen as independent frequencies, to seek possible frequency relations, of the form of Eq. 4.3. This way of choosing independent frequencies is arbitrary, but it will reveal the signal components following the non-linearities frequency relation Eq. 4.3, even if the chosen independent frequency is actually a combination.
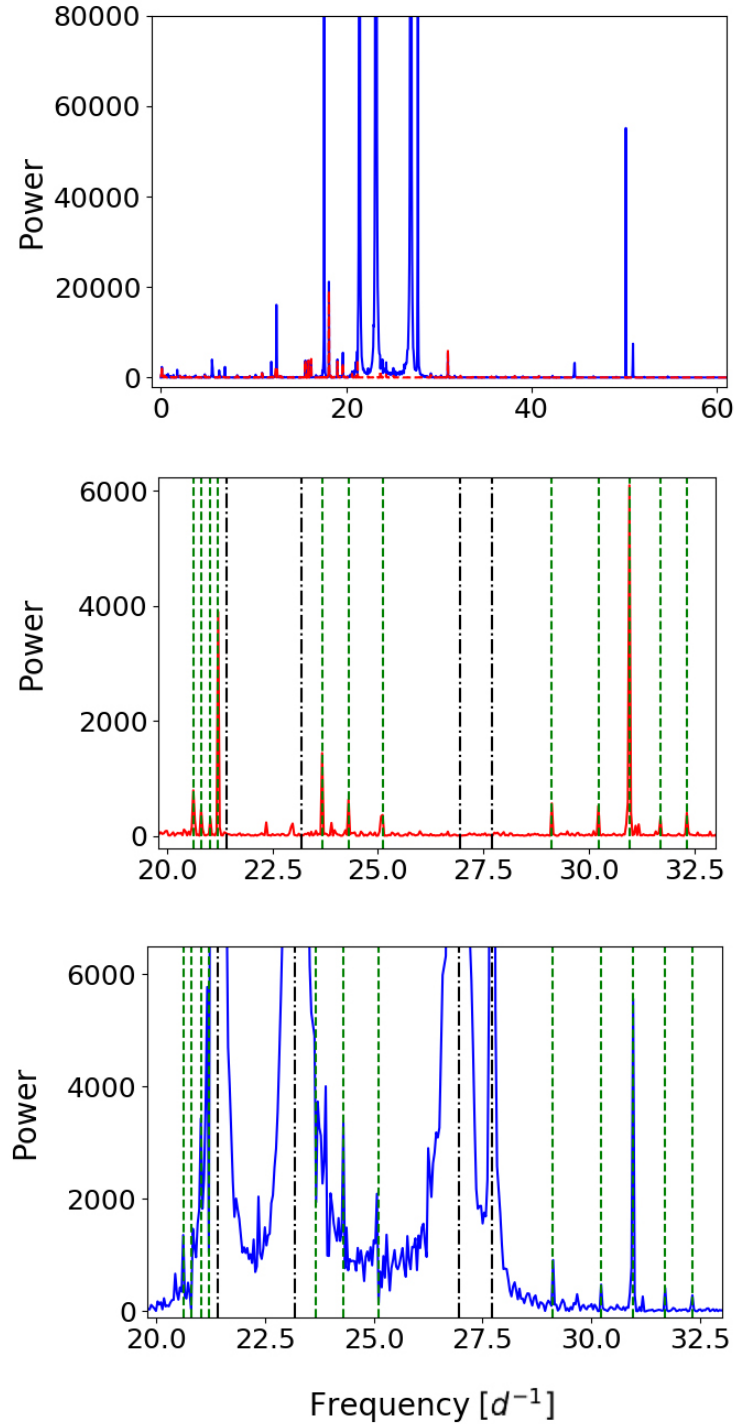
Figure 4.7 Application of the BPM to the light-curve of HD 174966. Blue: FFT of the original light-curve. Red: FFT of the residuals after fitting the 'best' parents and the series of combinations originating from them. Green dashed: new frequencies detected after the fit. Black dash–dotted: 'best' parent frequencies. Units of power are $[(e^-/s)^2]$. Source: Lares-Martiz et al. (2020)

Table 4.5 The 'Best' parents for every possible couple of the first five highest power peaks in the HD 174966 power spectrum

Couple Tag	Couple Frequencies [d^{-1}]
(f0, f1)	(17.62288, 23.19479)
(f0, f2)	(17.62298, 21.42079)
(f0, f3)	(17.62280, 26.95853)
(f0, f4)	(17.62291, 27.71456)
(f1, f2)	(23.19477, 21.42097)
(f1, f3)	(23.19479, 26.95851)
(f1, f4)	(23.19477, 27.71503)
(f2, f3)	(21.42078, 26.95853)
(f2, f4)	(21.42078, 27.71463)
(f3, f4)	(26.95851 , 27.71487)

Instead of searching the combinations of the full set of five independent frequencies, the search is divided in couples in order to reduce the computational cost of the BPM solution. In Table 4.5, the results of the BPM for every possible couple with the precision adopted in this work (see 4.4) show small differences. In this case, we select as the 'best' parents for the 5 highest amplitude peaks the median of all the found values.

In the final extraction procedure (see Fig. 4.7 for the resulting combination frequency free power spectrum) it was found that particularly in this star, 118 combinations were statistically significant (see Table 4.6). Notice that the number of subtractions is higher than the number of sum combinations. This may raise concerns about the validity of these identifications in the lower frequency range.

The majority of the subtraction combinations correspond to high order combinations (see Table B.3), but harmonics ($n \cdot \omega_i$ or $m \cdot \omega_j$) with such high n and m, are not statistically significant (only $2f3$ is detected). Alternatively, these significant differences could simply

Table 4.6 Results of the combination frequencies extraction process for the multimode δ Sct star HD 174966. The first column shows the 'best' parents in d^{-1}, which are derived from the median value in Table 4.5. The second column specifies the number of statistically significant frequencies, or children, extracted. The %CF (third column) quantifies the percentage of the initial power resulting from the combination frequencies and their parents.

HD 174966			
Tag	'best' parents [d^{-1}]	Combinations extracted	%CF
f0	17.622895	122 in total:	93.02
f1	23.194755	1 harmonic	
f2	21.420785	13 sums	
f3	26.958552	108 differences	
f4	27.714750		

be false identifications, due to the fact that at higher n and m more combinations are tested, increasing the probability of a match, as well as the possibility of choosing as parent frequencies a combination frequency. In this work, we do not exclude any match because the interest relies upon finding the set of combination frequencies that could explain the most of the signal as non-linearities. Furthermore, Kurtz et al. (2015) state that the amplitude of a child frequency could be higher than their parents' amplitudes, which could explain the missing high-order harmonics issue.

Further discriminating criteria (apart from the frequency value) are required for an unambiguous identification, so as to avoid false identifications due to high values of n and m. Nevertheless, this example shows that in no case the extraction procedure (here presented as the BPM method) is introducing new frequencies. Moreover, even when it is not clear that the arbitrarily chosen parent frequencies are actual oscillation modes of the star (which is often the case when dealing with multiperiodic stars), the set of significant combinations resulting from the algorithm can still be useful to test whether extracting them has simplified

the power spectrum in agreement with a solution from a linear stellar oscillation mode (see Fig.4.7. Notice that, some of the green dashed lines are equally spaced, possibly identifiable with non-radial frequency structures or rotational splittings). This could be showing again that extracting combination frequencies in a least-squares sense, as a first step before undertaking the frequency analysis, can expose pulsation modes or frequency spacing patterns that would otherwise be hidden.

4.4 Uncertainties in frequencies

The method described in this manuscript mainly relies in how well the BPM determines the 'best' parents. Progressively increasing the precision in frequency (when searching the minimum of the V function) involves getting closer to the floating point number precision, which implies that numerical errors are an important source of uncertainty. Finding when these numerical effects are hampering the 'best' parents computations provides us with an estimate of the upper limit in the uncertainty of the frequencies. We find this limit by building a synthetic light curve with this analytical expression:

$$S(t) = \sum_{k=1}^{n} A_k \cos(2\pi k\omega t + \phi_k), \quad k, n \in \mathbb{N} \tag{4.6}$$

where the input Fourier parameters are obtained by initially applying the method to real data, meaning that ω is the 'best' parent frequency for a mono-periodic variable up to n harmonics. Notice that there is no added noise and the synthetic light curve has the same number of data points as the observations. In this way, the minimum of the V function for the synthetic light curve, theoretically expected to be zero, will reveal the error in machine calculations. Results of this test, using the components extracted from the mono-periodic δ Sct star TIC 9632550 to build the synthetic light curve, are listed in Table 4.7. The 'best' parent is reached with the V value of order $\approx 6 \cdot 10^{-10}$. Consequently, V values smaller than this number are compromised by the numerical errors intrinsic to machine calculations.

Table 4.7 The 'best' parent search tree for the synthetic light-curve built from TIC 9632550 data. The first column quantifies the number of statistically significant frequencies, or children, detected with the parent frequency specified in the third column, in d^{-1} (zeros omitted for the sake of clarity). The second column is the variance after the fit of the parent and combination frequencies (in this case, only harmonics of the highest one).

N of fitted frequencies	V value	Frequency [d^{-1}]
1	3156.591456884018044	5.0
5	948.685924387723073	5.05
14	7.165213986246192	5.055
14	7.165213986246192	5.055
14	0.804372110830800	5.05496
14	0.007417117763935	5.054964
14	0.007417117763935	5.054964
14	0.000552438323944	5.05496404
14	0.000045278362580	5.054964037
14	0.000005430569507	5.0549640372
14	0.000000546520136	5.05496403723
14	0.000000051236668	5.054964037227
14	0.000000008582531	5.0549640372273
14	**0.000000000602951**	**5.05496403722726**

Table 4.8 Results of the fundamental frequency determination by the 'best' parent search and O-C method for the four partitions of the light-curve of the mono-periodic δ Sct star TIC 9632550. Each section is ≈7 d long.

Section	'Best' parent [d^{-1}]	O-C Frequency [d^{-1}]
S1	5.05491643	5.0548 ± 0.0001
S2	5.05490929	5.0550 ± 0.0001
S3	5.05501342	5.0549 ± 0.0002
S4	5.05501167	5.0548 ± 0.0002

Table 4.9 Results of the fundamental frequency determination by the BPM regarding the number of cycles in the light-curve of the mono-periodic δ Sct star TIC 9632550.

Number of cycles	'Best' parent [d^{-1}]
138.4	5.0549640
138	5.0549637
137.5	5.0549631
137.2	5.0549627
132.4	5.0549595

In addition, another test was built dividing the real light curve of TIC 9632550 in four sections to find the 'best' parent in each of this partitions. In spite of the reduced frequency resolution, due to the smaller time interval of the light curve, the parent frequency found for each partition is similar, and also compatible with the O-C method up to the 4th decimal (see Table 4.8). This test confirms the robustness of the BPM search.

In order to test if the effect of leakage (see Section 2.1) had something to do with the small variation in the 4th decimal (i.e. ≈ 0.000004 d period variations), the BPM was applied to the mono-periodic light curve with exactly an integer number of cycles and with a half-integer number of cycles (along with other number of cycles). Results of this test (see Table 4.9) highlighted the influence of the number of cycles on the determination of the period. Future

work could explore this issue to give a precise lower limit to the frequency uncertainty. In this regard, a conservative approach is adopted in this dissertation, expressing results with the precision that the O-C method achieves.

As a last remark, the duration of the observation T is a relevant parameter for estimating the frequency uncertainty when dealing with two close frequencies (closer than $1/T$ to each other). In that case, the Rayleigh frequency resolution becomes a good estimator. But, precision can go further the Rayleigh frequency resolution if there is only one frequency component inside the Rayleigh interval (see Section 2.1). This was just proved for each $\approx$7 days long sections of the light curve of the mono-periodic δ Sct star, TIC 9632550. The numerical precision reached was $\pm 1 \cdot 10^{-8}$ and is not "as if we were observing $\approx$274000 years". Rayleigh resolution remains the same: $\approx$1/7 days, that is, $\approx$0.14 d^{-1}.

4.5 Chapter Summary

- The BPM consists essentially in a 'standard' approach of fitting sinusoids to the light-curve, but under the framework given in Section 3.3.3. The advantage of this empirical minimisation is that it assures an exhaustive search for the 'best' parents, which can not be accomplished by any other algorithm of non-linear least-squares available at the moment.

- Commonly, combination frequencies are identified when significant frequencies from a prewhitening cascade are near an exact combination value. Fitting combination frequencies identified in such way (to extract them from the power spectrum) can introduce spurious frequencies in the signal, hampering the analysis. The BPM does not add information to the residual light curve, since it fits the exact combination values simultaneously. The method guarantees that any variance that remains after calculating the power spectrum of the residual light curve, is not caused by the parent mode frequencies and their associated children frequencies.

- Although in this work we focus the application on δ Sct stars, this method could be applied to any type of variable star, where non-linearities are expected to be present in their power spectrum.

- For mono-periodic stars, it achieves precision in frequencies approximately equal to those achieved by the O-C method.

- For double-mode and multi-periodic stars, it allows frequency structures to emerge from what was previously considered as noise. The structures are not seen without doing the correct combination frequencies extraction.

- For multi-periodic stars, the identification of non-linear terms is still ambiguous. Obeying only the equation of the relationship in frequencies between parents and children, does not guarantee that the combination is a non-linearity from a non-linear distortion process. There is still the possibility that it is an independent mode that coincides with the position in frequency of a combination purely by chance. It might also be coinciding with a component of a rotational splitting or any other. For this reason, more constraints are required and therefore, the phase and amplitude relationships are reviewed in the next chapter.

Chapter Five

Non-linearities in Delta Sct stars. II
Phases and Amplitude relations

In the last chapter it was clear that there is ambiguity in identifying non-linearities considering only their frequency relation with the parent modes. Significant power at the exact frequency value of a combination between the parent modes could still be confused, for example, with a rotational splitting (Bowman, 2017), or even be a coincidence with an independent mode. Extra criteria for discerning the nature of the combination frequency is needed. In this chapter, a study of the phases and amplitude relations that non-linearities must obey is presented.

The approach in Simon and Lee (1981) was to characterize non-linear light curves of mono-periodic Cepheid's with two parameters they called the phase difference and the amplitude ratio, which they obtained by Fourier decomposition (see Section 2.1.2). This was also explored by Antonello et al. (1986) for the characterization of mono-periodic HADS and δ Sct's non-linear light curves, whereas Balona (2012) explored it for multi-periodic HADS and δ Sct. Similarly to all these previous studies, in this thesis the characterization approach is through a Fourier decomposition of the non-linear light curve, but under the mathematical expressions derived from Eq. 3.19 and the BPM presented in Section 4.2. This is a continuation of the Garrido and Rodriguez (1996) exploration where, for the first time, the

Volterra series is proposed for modeling non-linearities in a pulsating star.

In the formalism given in Section 3.3.3, the phases (Eqs.3.23 and 3.27) and amplitudes (Eqs. 3.24 and 3.26) relations can be generalized in the following forms respectively:

- Phases:

$$arg\{\Gamma_o\} = \Delta\phi = \phi_{obs} - \phi_{calc} \qquad (5.1)$$

$$= \phi_{obs} - (\pm n\phi_i \pm m\phi_j) \qquad (5.2)$$

- Amplitudes:

$$|\Gamma_o| = A_r = \frac{A_{obs}}{A_i^n A_j^m} \qquad (5.3)$$

where the A_{obs} and ϕ_{obs} are the amplitudes and the initial phases, parameters resulting from the least-squares fit of sinusoids whose frequencies are the significant combination frequencies (i.e. children of the best parents frequencies found by the BPM). In the same way, $A_{i,j}$ and $\phi_{i,j}$ are the parameters resulting from the least-squares fit of sinusoids whose frequencies are the best parent frequencies. From these expressions it is obvious that the amplitudes and phases of non-linearities are expected to be correlated with the amplitudes and phases of their parents.

The complex generalized transfer functions Γ_O, where O is the order of the combination (see Eq. 4.4), contain the non-linear physics that may be involved within the star. Therefore, it is of great interest to somehow characterize them. In Chapter 3 it was already mentioned that two forms of non-linearities are present in δ Sct stars: the non-linearities due to the NLDP and non-linearities in the form of resonant mode coupling. Many efforts have been made to be able to differentiate the nature of a combination frequency (Bowman et al., 2016, Breger and Lenz, 2008, Breger and Montgomery, 2014, Degroote et al., 2009, Zong et al., 2016). There is a special interest in the characterization of non-linearities of NLDP nature, because these are just harmonics and cross-terms (additions and subtractions) of

the independent modes of oscillation owed to the mathematical interaction between modes, meaning that they are not solutions of the perturbed linear stellar structure equations and in this sense, it is imperative to remove them from the variable star power spectrum.

In this chapter, it is shown that an empirical characterization of the Γ_O functions is possible when the the combination frequencies are effects of the non-linear distortion processes. This is done by assuming that the combination frequencies observed in HADS stars power spectra are non-linearities of this nature, which is a reasonable assumption and is sustained by 5 arguments:

- There are too many combination frequencies to be eigenmodes themselves.

- They usually are slow rotators, and the fine structure (i.e. spacings between modes) due to slow rotation can easily be explained with linear superposition of the splitting multiplet of the independent modes. The fine structure that double-mode HADS stars display is more intricate, so very unlikely to be confused with rotational splittings.

- The double-mode HADS normally pulsate in radial modes, meaning that the high amplitude modes follow the $0.765 < \frac{f_0}{f_1} < 0.781$ frequency relation for the fundamental en first overtone modes, the exact value depending on the stellar mass and composition (Suárez et al., 2007). This assures that the children frequencies are cross-terms of clear independent modes as parents.

- It is expected that high amplitude parents have many detectable combination frequencies because of the large pulsation amplitudes of the parent modes.

- Interchange of energy between modes due to mode coupling induce amplitude modulation of the modes. The majority of the known HADS do not show amplitude variability, supporting the assumption of their combination frequencies being consequences of NLDP.

The assumption that significant combination frequencies in HADS are due to the NLDP is not new (Bowman, 2017, Bowman et al., 2016). Nonetheless, this is not proven to be a fact. In the next section, this is going to be explored applying the general form of phases and amplitudes (Eqs. 5.1 and 5.3, respectively) to the combination frequencies in HADS stars. Special features found in the results are expected to be associated with the NLDP.

5.1   Phase relation of HADS combination frequencies

In order to show the results of the general reasoning explained in this chapter introduction, a single star is presented as case of study. The chosen case of study star is the HADS KIC 5950759 observed by Kepler space satellite. It is a *book style* HADS where the first two highest amplitude Fourier components follow the Stellingwerf (1979) period relation for the fundamental mode and first overtone and it is not a fast rotator. Moreover, high quality and precise photometric data is available, revealing many detectable (i.e. statistically significant) combination frequencies.

The general form for the arguments of the Γ_O functions (Eq. 5.1) can be understood as the difference between the observed phase (phase from the Fourier decomposition, see Section 2.1.2) and the expected phase (i.e. the one predicted by the simple model, see Section 3.3.1). Observed and expected phases are plotted for KIC 5950759 in the upper panel of Figure 5.1. The delay between the observed phase and the expected one seems to be decreasing with the order of the combination O. According to Eq. 5.1, each delay corresponds to the argument of the Γ_O function of order O ($arg\{\Gamma_O\}$) and the aim here is to characterise them. Representations of $arg\{\Gamma_O\}$ versus the frequency of each combination will be referred to as the *relative phases plots* ($\Delta\phi$) from now on. Bottom panel of Figure 5.1 shows the relative phases plot (up to order 4) for the case study star, where the independent frequencies have, by definition, relative phases equal to zero.

In Garrido and Rodriguez (1996), the relative phases for HADS stars were studied for
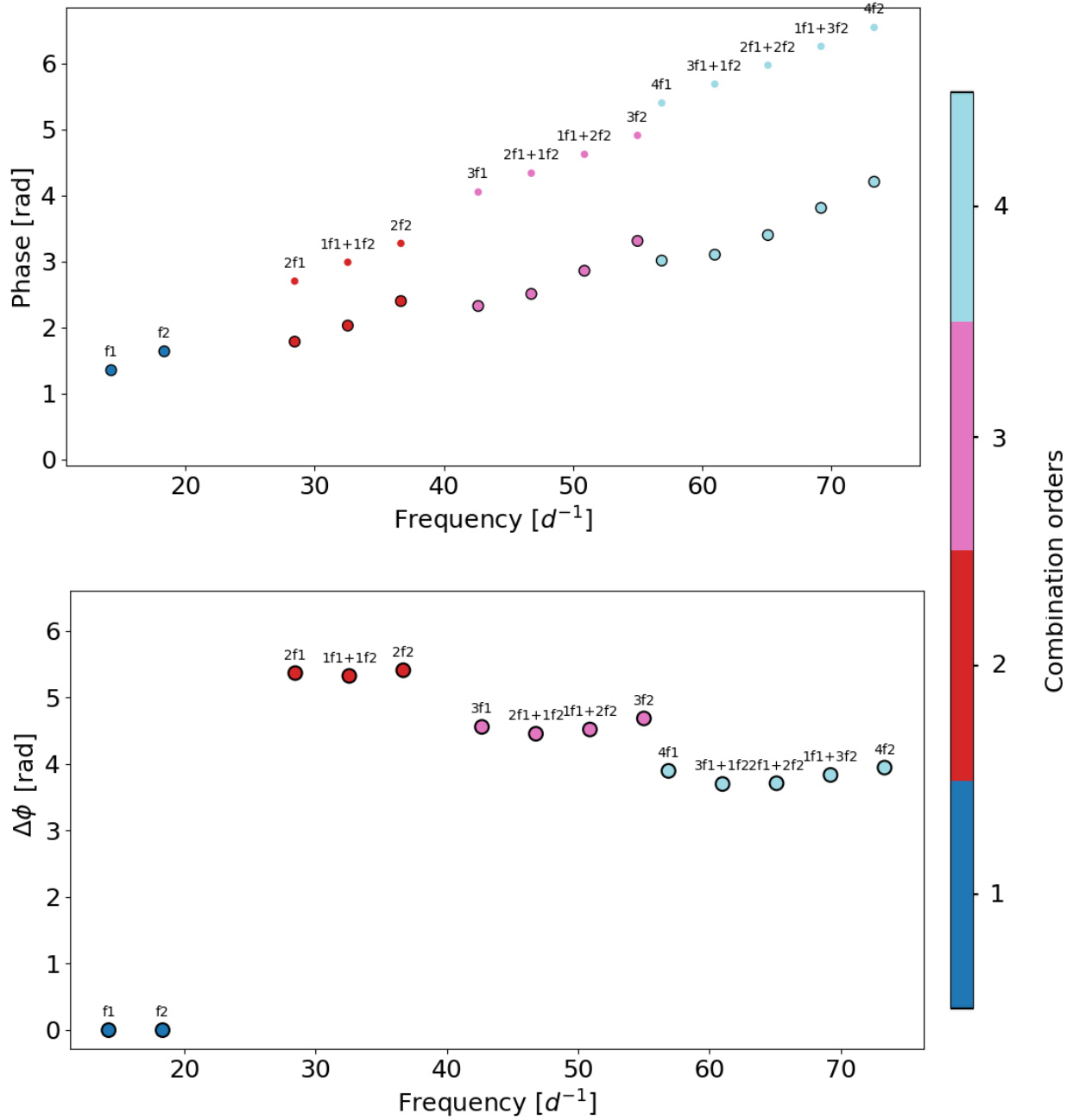
Figure 5.1 First 4 combination orders of the case study star KIC 5950759. Upper panel: Observed (circles) and calculated (dots) phases of the statistically significant combination frequencies (only sums and harmonics). Parents (f1 and f2) follow the Stellingwerf (1979) period relation of fundamental en first overtone. Botton Panel: Relative phases plot.

ground-based observations, so not many combination frequencies were fitted. Nevertheless, those observations allowed Garrido to inspect at least up to the second combination frequency order and to notice that the relative phases were almost constant, supporting the hypothesis he made over the Γ_O functions. The hypothesis consisted in stating that at least for δ Sct stars, one can safely assume that the generalized transfer functions are independent of the frequency, thus imposing the symmetry condition over the generalized transfer functions:

$$\Gamma_2(\omega_0, \omega_0) = \Gamma_2(\omega_1, \omega_1) = \Gamma_2(\omega_0, \omega_1) = \Gamma_2(\omega_1, \omega_0) = \Gamma_2; \tag{5.4}$$

where one must take into account that a complex function is the same as other if they have the same modulus and their phases are the same plus 2π, so

$$|\Gamma_2(\omega_0, \omega_0)| = |\Gamma_2(\omega_1, \omega_1)| = |\Gamma_2(\omega_0, \omega_1)| = |\Gamma_2(\omega_1, \omega_0)| = |\Gamma_2| \tag{5.5}$$

and

$$arg\{\Gamma_2(\omega_0, \omega_0)\} = arg\{\Gamma_2(\omega_1, \omega_1)\} = arg\{\Gamma_2(\omega_0, \omega_1)\} = arg\{\Gamma_2(\omega_1, \omega_0)\} = arg\{\Gamma_2\} \tag{5.6}$$

which, one might think, is holding up to order 4 when seeing the bottom panel of Figure 5.1. However, this hypothesis is not fulfilled when examining a more complete relative phases plot, provided by the new available ultra-precise photometric data.

The 177 statistically significant combination frequencies (see Table 4.4) found by the BPM using the ultra precise photometric data of the KIC 5950759 allow to build a rich relative phases plot (see the relative phases of 92 sums and 17 harmonics plotted in Fig. 5.2). Subtraction combinations are not discussed in this monograph because their relative phase plots do not show a clear pattern like the harmonics and sums. This is possibly due to the fact that subtraction does not hold the commutative property, the phase would be different in terms of the order of the factors in the subtraction, implying that somehow the Γ_O functions may not be symmetric. It could also be due to an unknown dependence of the Γ_O functions on the frequency. Regardless of the subtraction problem, the analysis for harmonics and sums continued considering the interesting patterns obtained.
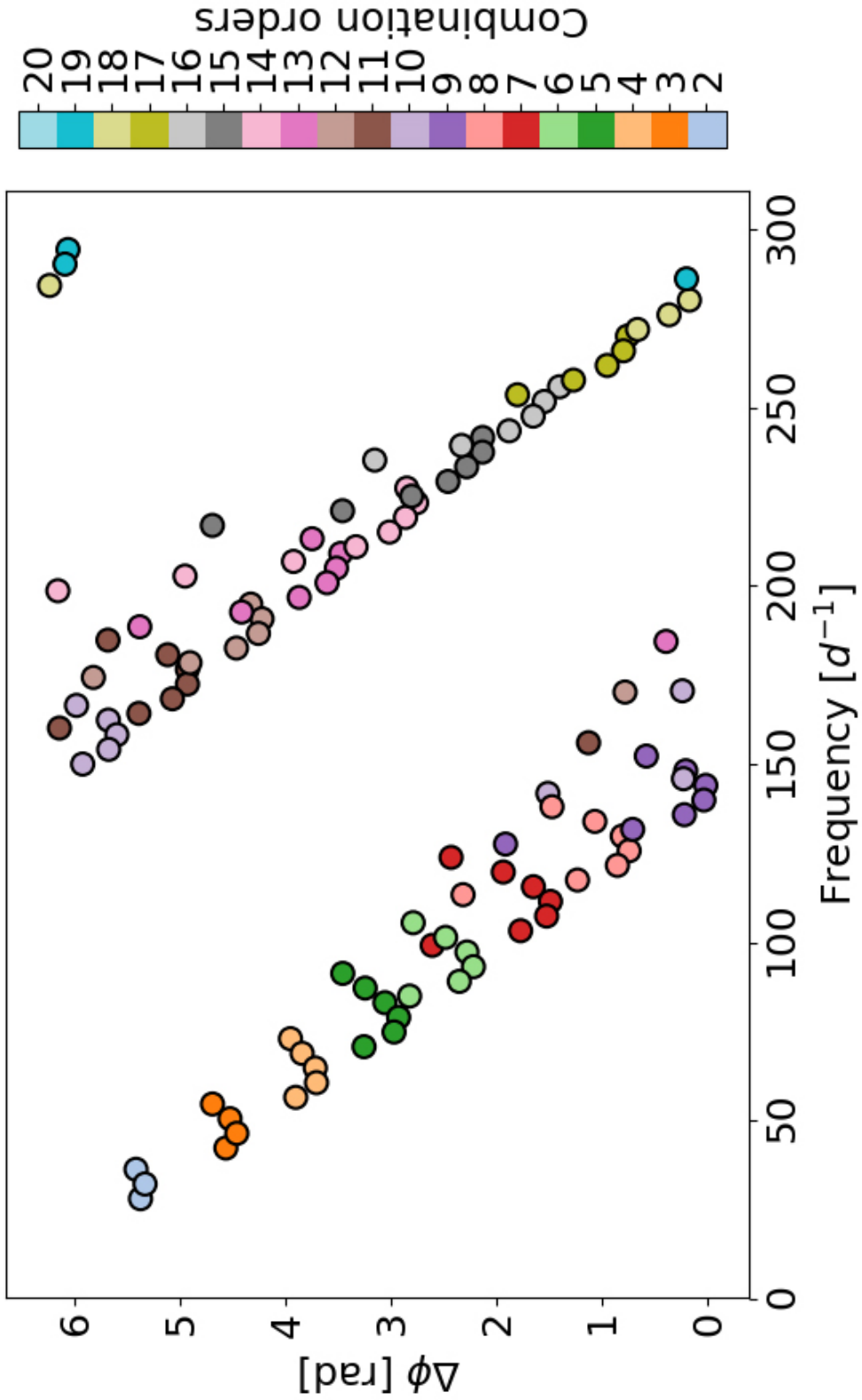
Figure 5.2 Relative phases plot of all the statistically significant sums and harmonics of the case study star KIC 5950759. The maximum combination order detected is of $O = 20$ (Order defined in Eq. 4.4)

Note that in Fig. 5.2 the Y-axis, representing the difference between observed and expected phase is between $0 - 2\pi$ radians. Every phase exceeding 2π (or below 0 radians) is corrected to be between this range. In this way, one can think of the first set of points (from combination order 2 to ≈ 9) as the first Riemann surface or the first phasor cycle, the second set of points of higher frequency (from combination order 10 to ≈ 18) as the second Riemann surface or second phasor cycle, and so on. Moreover, the cyclic property of the Y-axis explains that the order $O = 1$ (corresponding to the parents) represents no discontinuity in the plot since *zero* is the same as 2π. To avoid confusion in this regard, circles of the parent frequencies ($O = 1$) are going to be removed from the following plots.

A clear parabolic pattern for each combination order is noticed. This is the first study to expose this pattern of relative phases. Although Balona worked with ultra-precise photometric data when studying the correlation between relative phases and frequency, only low order combinations were fitted, then perceiving linear patterns (see Fig.1 and 3 in Balona, 2012).

A zoom of Fig. 5.2, to represent the first 5 combination orders with labels over each combination, is shown in Fig. 5.3. The relative phases are in consecutive order, harmonics being the left and right ends of the parabola branches. The $6f2$ harmonic is not detectable, the same happens with higher combination orders. The $f2$ frequency belongs to the parent with the lowest amplitude, so it is expected not to detect many of its harmonics. That is why the parabolas of $O > 5$ are incomplete (detecting only the parabola left branch).

Physically, how can this pattern of relative phases be explained?. Kurtz et al. (2015) proposed that the phases of combination frequencies and harmonics are determined by the balance between driving and damping mechanisms in each individual star. The driving of the independent frequencies (e.g. the κ mechanism and the convective blocking for intermediate-mass pulsating stars) and the damping of the harmonics (by heat loss) may show phase differences different to zero in the presence of changes in the thermal properties of the star. If the difference of phases is zero, then the maximum of the combination frequency is the
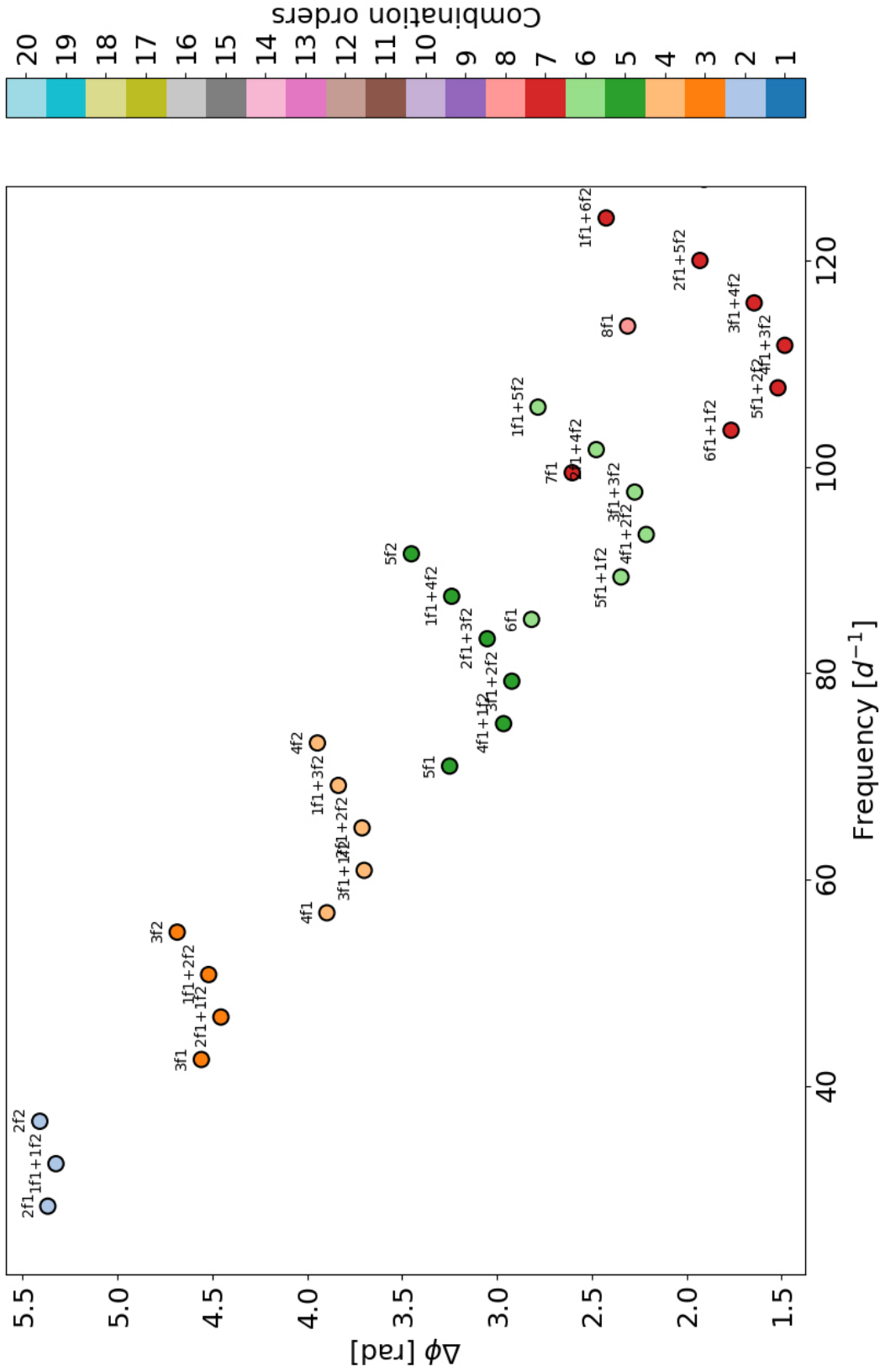
Figure 5.3 Relative phases plot of all the statistically significant sums and harmonics of the case study star KIC 5950759. The maximum combination order detected is of $O = 20$ (Order defined in Eq. 4.4)

same as that of their parents and, so, reinforcing its maximum. This (along with other factors like amplitudes) determines the upward shape of the light curve. Conversely, if its π delayed, then it determines the downward shapes of the light curves. Intermediate values of relative phases attenuate these effects in the shapes. Kurtz et al. (2015) study was focused in g-mode pulsators (γ Dor, SPB en Be stars), but can be extrapolated to p-mode pulsators. Kurtz's approach might explain the extremely symmetric light curve of the case study HADS star KIC 5950759. The relative phases pattern is very regular and cancels the effects from one another. The regular spacing between orders may be pointing to regular changes in the thermal properties of the outer (or superficial) layers of the star, in this way characterizing combination frequencies of NLDP. Additionally, it must be taken into account that non-linear effects in δ Sct stars, meaning the variations in geometry (i.e. radius and surface normal) and variations in temperature and surface gravity, are in general out of phase, so every relative phase also accounts for this phase difference (Balona, 2012).

From Figure 5.3 it can be said that Garrido's relationship is more or less fulfilled for the first orders but is no longer acceptable for higher orders ($\approx O > 4$). Moreover, for each combination order O of the statistically significant combination frequency, the relative phase can take a range of values corresponding to that combination order O. Roughly speaking, the argument of each generalised transfer function can take a range of possible values, constituting for each combination order a band of possible values. For example, arguments of the generalised transfer function of order 2 can take values inside the $6.28 \geq arg\{\Gamma_2\} < 5.28$ interval. $5.28 \geq arg\{\Gamma_3\} < 4.28$ for order 3, taking into account that the bands become thicker for higher O values and allowing overlapping between bands. A more sophisticated characterization is needed to cope with the overlapping that starts to be evident around $O = 5$. This is a matter of future work (e.g. only values over fitted parabolas), but for the sake of initial characterization, this is enough. The question is, does this hold for other HADS stars?

As the aim is to characterise the relative phases for combination frequencies from NLDP,

Table 5.1 Time series information from each space satellite. T is the length of the observation in days and δ_t is the cadence or sampling rate in seconds. For the TESS and Kepler light curves, we used the instrumental effects free light curve resulting from the Pre-Search data Conditioning (PDC) pipeline, accessible in the Mikulski Archive for Space Telescopes (MAST: https://archive.stsci.edu/). Stars with a peculiar relative phases pattern are marked with the letter p ahead of the name. Modes column tells if the star is mono-periodic (Mp) or a double-mode pulsator(Dm).

Star name	Modes	T [d]	δ_t [s]	Obs. Sequence
KIC 5950759	Dm	31.04	58.85	Quarter 4
GSC 00144-03031	Dm	76.67	31.99	Run LRa04
TIC 51991595	Mp	13.04	120.00	Sector 2
TIC 139845816	Mp	13.23	120.00	Sector 1
TIC 144309524	Mp	13.04	120.00	Sector 2
TIC 183532876	Mp	13.04	120.00	Sector 2
TIC 224285325	Dm	13.04	120.00	Sector 2
TIC 231632224	Mp	13.23	120.00	Sector 1
TIC 355547586	Dm	13.23	120.00	Sector 1
TIC 355687188	Dm	13.04	120.00	Sector 2
TIC 358502706	Dm	13.23	119.99	Sector 1
p TIC 9632550	Mp	13.04	120.00	Sector 2
p TIC 126659093	Mp	13.23	120.00	Sector 1
p TIC 260654645	Dm	13.04	120.00	Sector 2
p TIC 261089835	Mp	13.23	120.00	Sector 1
p TIC 431589510	Mp	13.04	120.00	Sector 2
p KIC 9408694	Dm	27.07	58.85	Quarter 6a
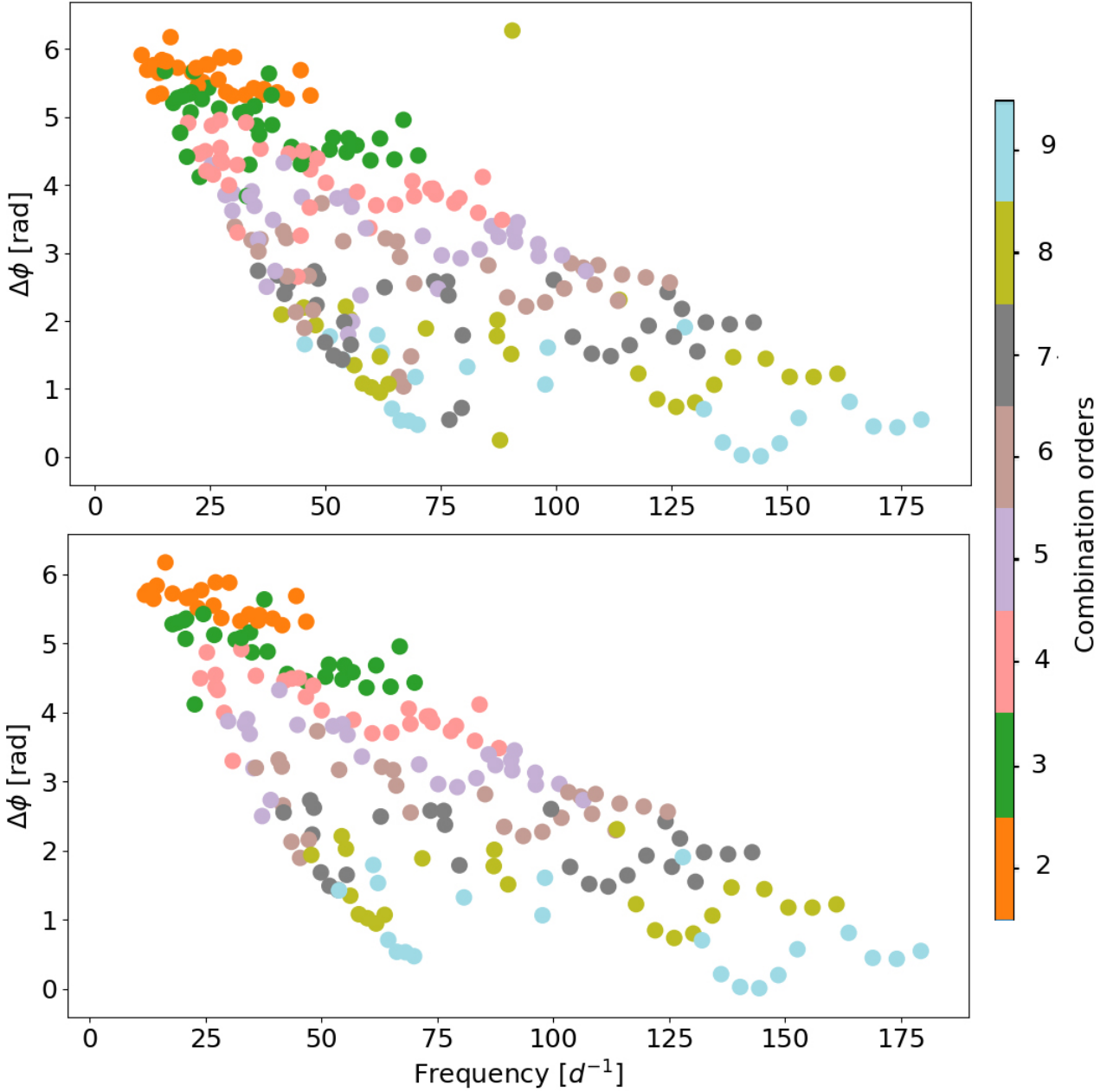
Figure 5.4 Relative phase plot of 17 HADS stars (top panel). In the bottom panel, 6 peculiar HADS stars have been removed.

the relative phases plot is computed for a set of stars where the combination frequencies are most likely to be non-linearities of such nature, meaning the HADS stars. The relative phases plot for a sample of 17 HADS stars is represented in the top panel of Fig. 5.4. For the sake of simplicity, only the first phasor cycle is represented. From the HADS sample, 14

were observed by TESS, 2 by Kepler and 1 from CoRoT (see Table 5.1 for the light curve parameters). It seems that the pattern holds similarly for all the HADS, except for a few peculiar patterns (see bottom panel of Fig. 5.4) which are going to be carefully examined.
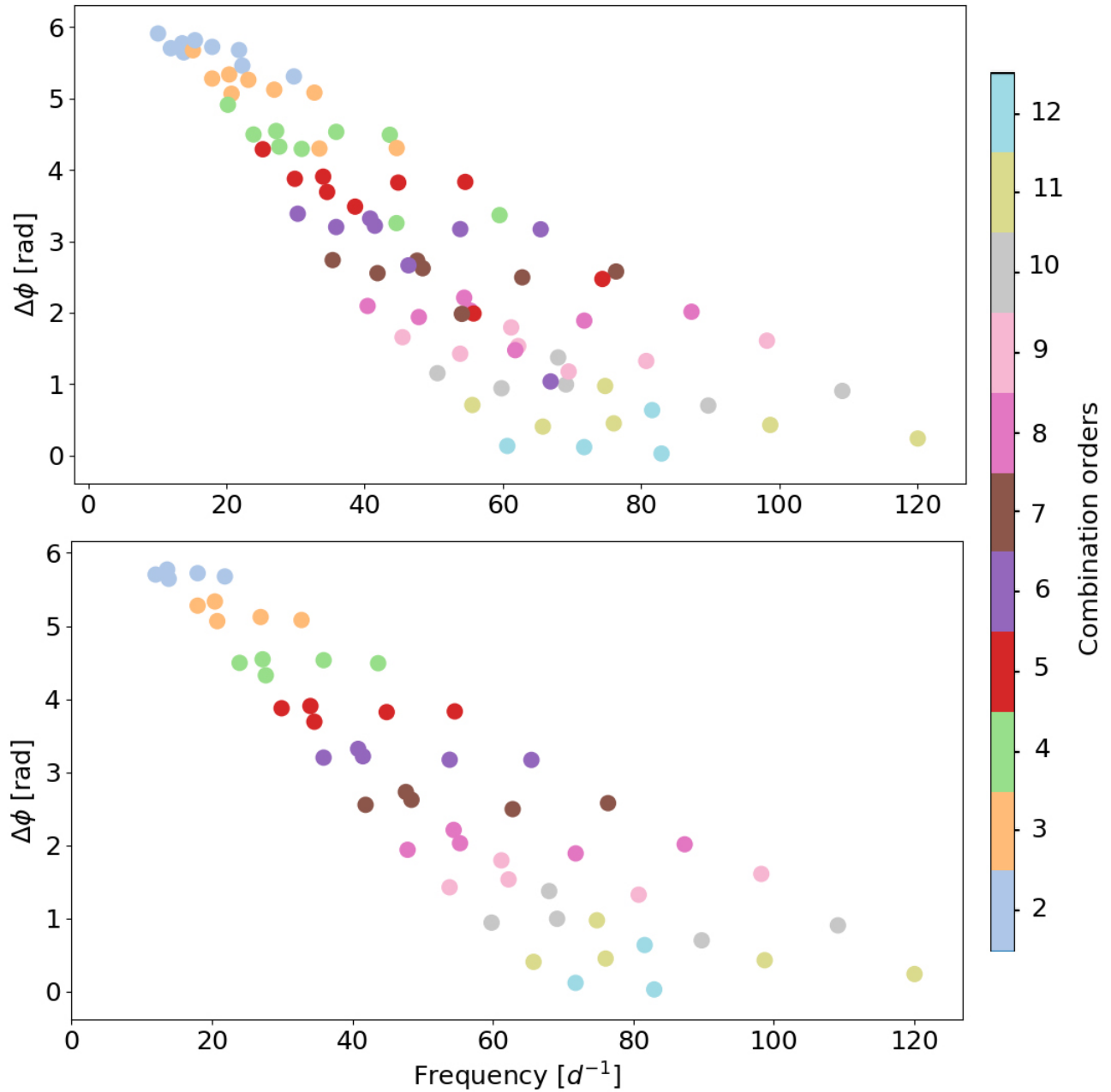
Figure 5.5 Relative phases of 4 peculiar mono-periodic HADS

For a detailed inspection, the relative phases of the 17 HADS can be separated in mono-
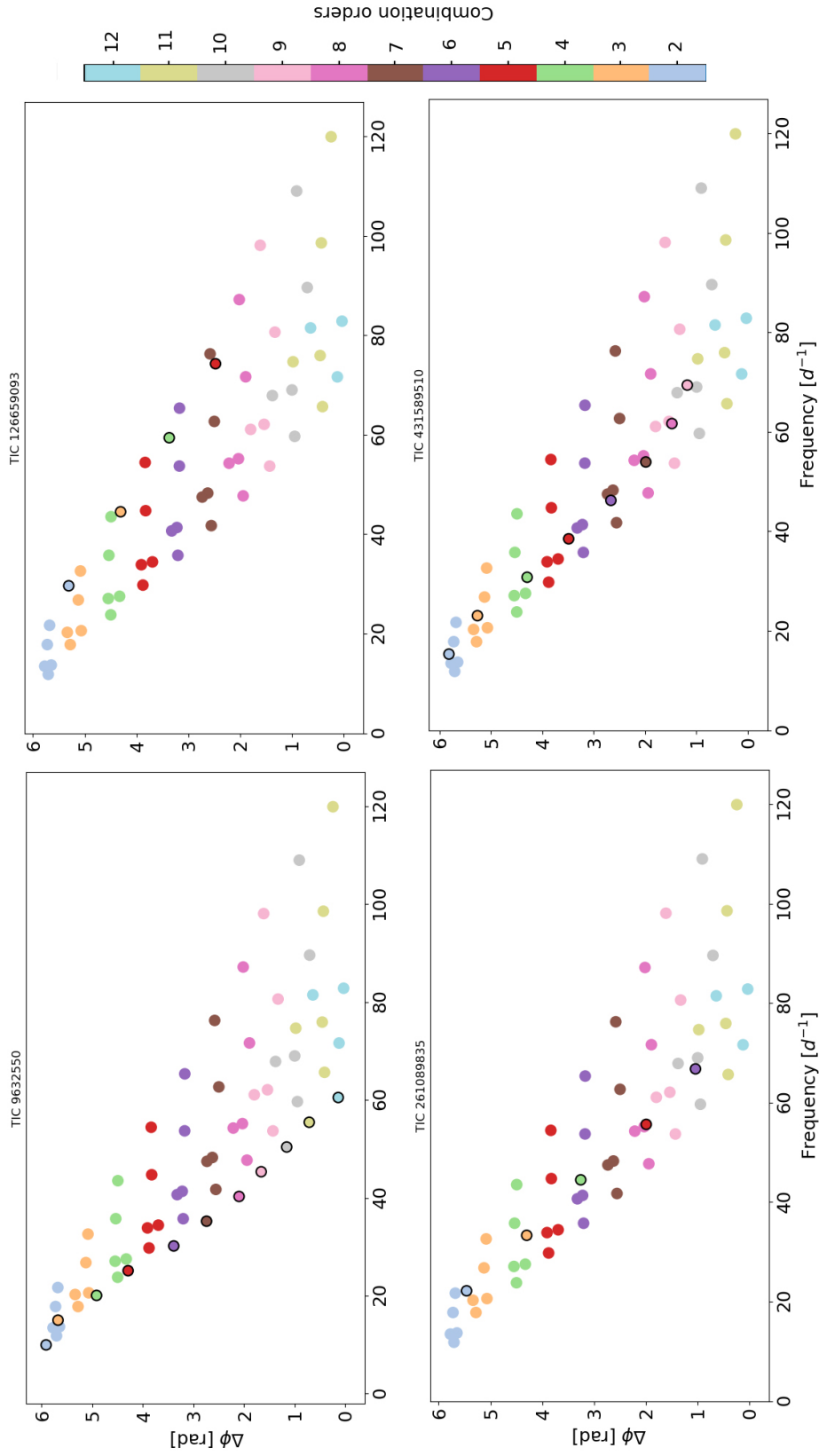
Figure 5.6 Relative phases plot of 9 mono-periodic HADS (Upper panel). In the bottom panel 4 peculiar mono-periodic HADS are removed.
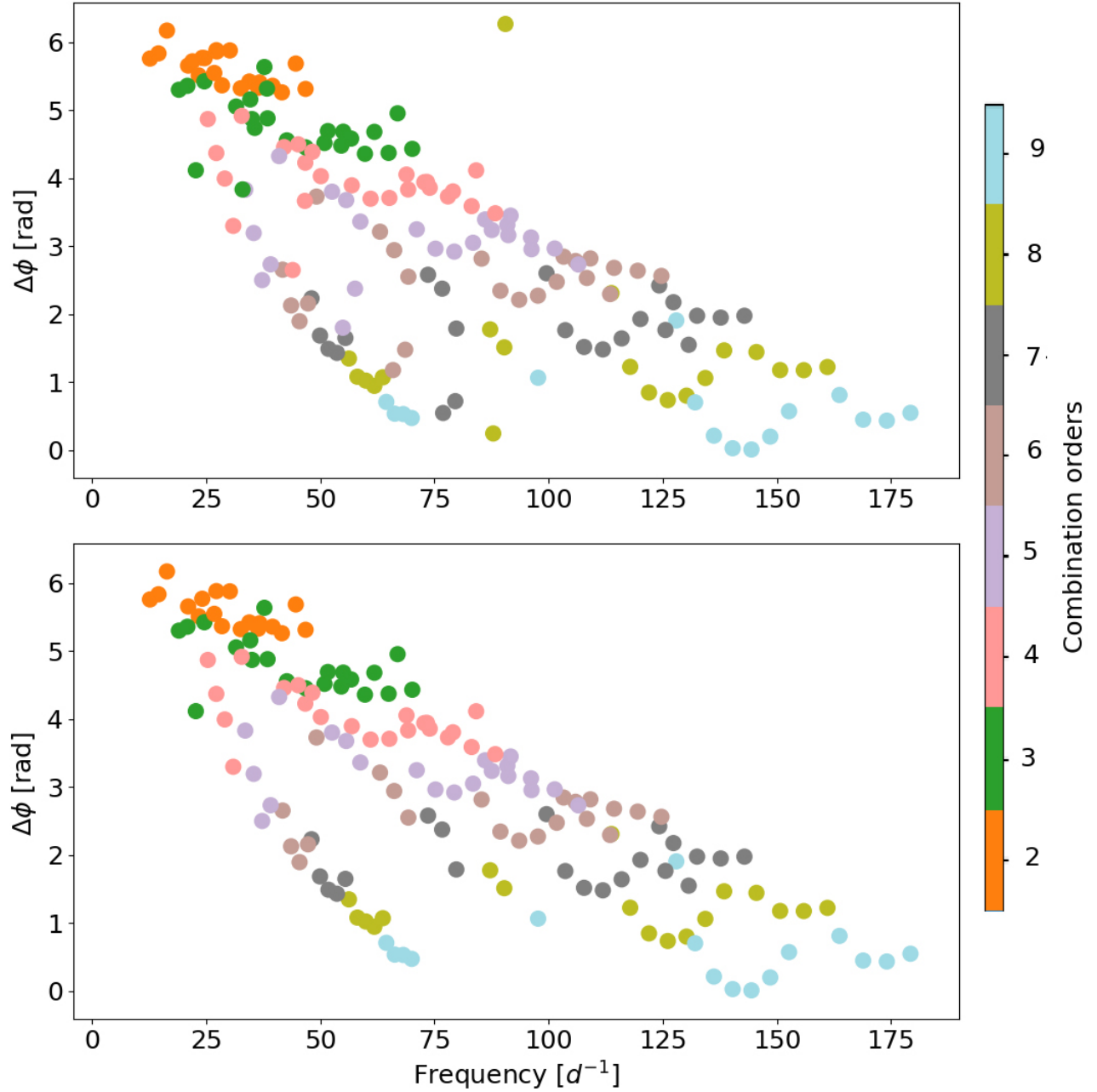
Figure 5.7 Relative phases plot of 8 double-mode HADS (Upper panel). In the bottom panel 2 peculiar double-mode HADS are removed.

periodic HADS and double-mode HADS plots. Except for a few peculiar mono-periodic HADS, the arguments of the Γ_O functions for mono-periodic HADS do hold Garrido's hypothesis of constant Γ_O (see Fig. 5.5). The peculiar mono-periodic HADS are the ones that

do not match the general pattern. It is not the overlapping of the higher orders what makes them peculiar, it is a distortion of the pattern from the lowest order to the highest.

It is widely known that near-degeneracy on the frequencies becomes very important for rotational velocities larger than about $15 - 20\ Km\ s^{-1}$ (Suárez et al., 2007), and although HADS stars are typically slow rotators, two of these peculiar stars (TIC 9632550, TIC 126659093, upper row of Fig. 5.6) happen to have high rotational velocities (see Table A1 from Antoci et al. (2019)). This might be the cause of distortion in the relative phases plot, allowing to infer high rotational velocities in other stars which have similar deviations in their relative phases plot (e.g. TIC 261089835 and TIC 431589510, bottom row of Fig. 5.6, from which no rotation values are available).

When dealing with two dominant modes, both strongly non-sinusoidal, the Γ_O functions represent the non-linear interaction with parabola shapes. The higher points of the parabola branches, determined by the harmonics of the corresponding O, and the base of the parabola, determined by the sum of harmonics (of $\equiv \frac{O}{2}$), create the bands of possible relative phases values for each combination order O. In Fig. 5.7, the bands can be seen, except for a couple of peculiar double-mode HADS showing pattern distortions which are pointing to the same explanation regarding high rotational velocities.

In the case of the HADS KIC 9408694 (bottom panel of Fig. 5.8), identified as a fast rotator by Balona et al. (2012), the pattern is visibly distorted possibly by its fast rotation nature. In the case of TIC 260654645, the parents almost follow the fundamental and first overtone period ratio expected for a δ Sct star of that mass (Stellingwerf, 1979), so the pattern may be distorted if the parents do not follow the ratio $\frac{P_1}{P_0}$ strictly (see upper panel of Fig. 5.8). Many possibilities can explain the change in the theoretical period ratio: small deviation of the frequencies due to fast rotation can induce change in period ratio relation of about $0.01\ d^{-1}$, which is the case of TIC 260654645. Although there is no obvious way on how can rotation alter phase of combination frequencies, this empirical correlation is something to be explored.
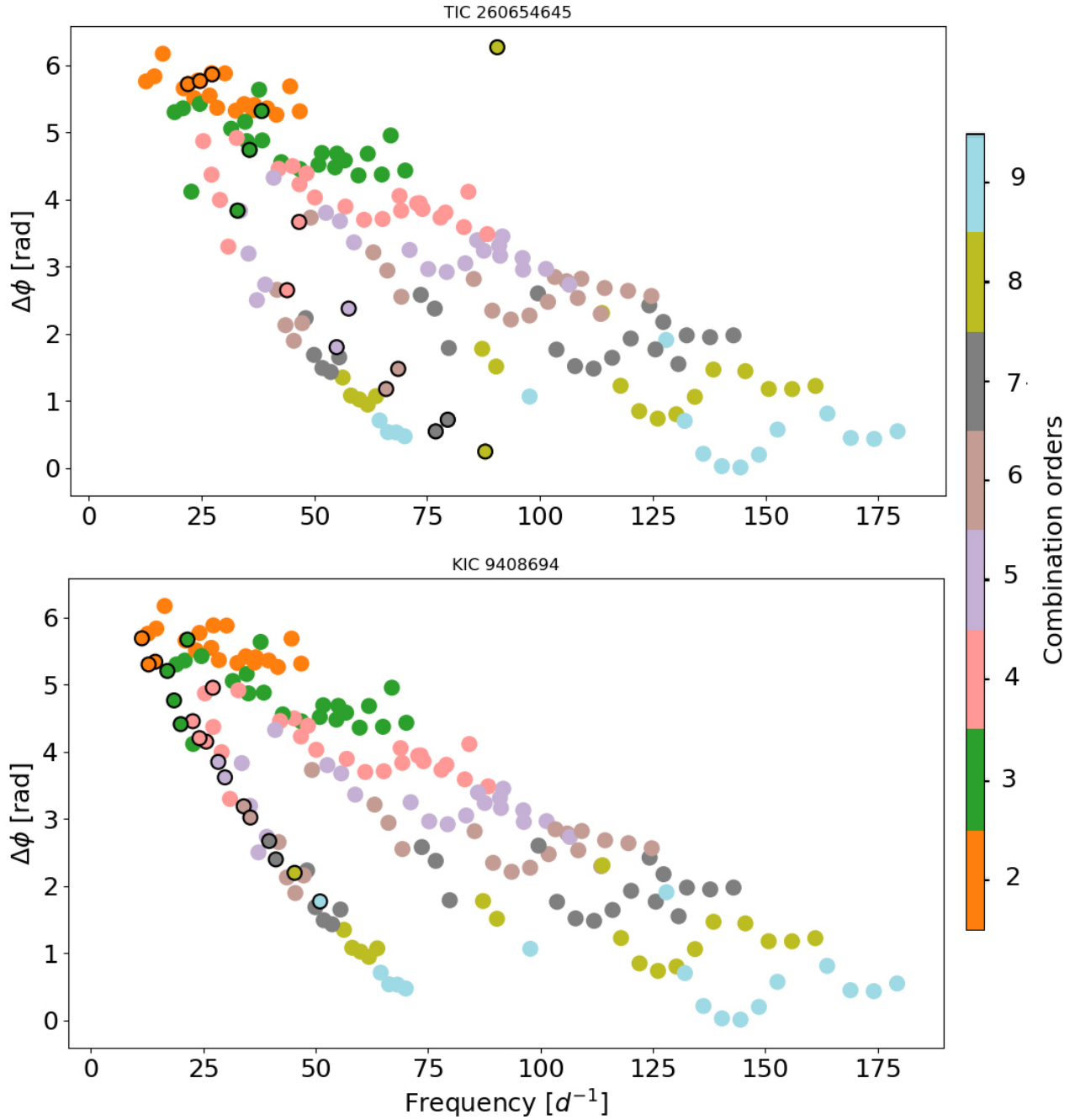
Figure 5.8 Relative phases of 2 peculiar double-mode HADS

Future work involving statistical analysis is required to complete the empirical charac-
terization of the arguments of the generalised transfer functions. Nonetheless, the obtained
results so far in this line of investigation are revealing. Combination frequencies of HADS

follow a very specific pattern in their relative phases, supporting the assumption that they are non-linearities from the same nature. On the other hand, it is important to emphasize the fact that for each combination order, the relative phase is almost the same, independently of the frequency or the star. The only parameter changing from star to star is the slope of the linear correlations of the relative phase with the frequency, which is due to the level of asymmetry of the light curve of the dominant frequency (Balona, 2012).

A rough characterization of the arguments of the generalized transfer functions was made by constraining their value to a certain range, depending on the order of the non-linearity. Truly, the pattern suffers dispersion, possibly due to parents not following Stellinwerf's period relations, or, in some cases, possibly because of fast rotation. Discriminate fast rotation with these plots is just one of the possible practical applications, other potential applications are going to be explained in Section 5.3.

5.2 Amplitude relation of HADS combination frequencies

The general form for the module of the Γ_O functions (Eq.5.3) can be understood as measures of the amplitude ratios between parents and children. In sum combinations of two parents, the amplitude ratio is similar to the van Kerkwijk et al. (2000), where he added the n_{ij} correction to make them equivalent to the amplitude ratio of the harmonics. Here, no correction is imposed, and the analysed amplitude ratio is as derived from Priestley's description of a non-linear time series (Section 3.3.3).

From the simple model, it is logical to assume that combination frequencies from non-linear mixing of the modes will have smaller amplitudes than their parents amplitude. Although Kurtz et al. (2015) proved that combination frequencies could have greater amplitudes than their parents (since parents can be non-radial modes, which suffer from cancellation
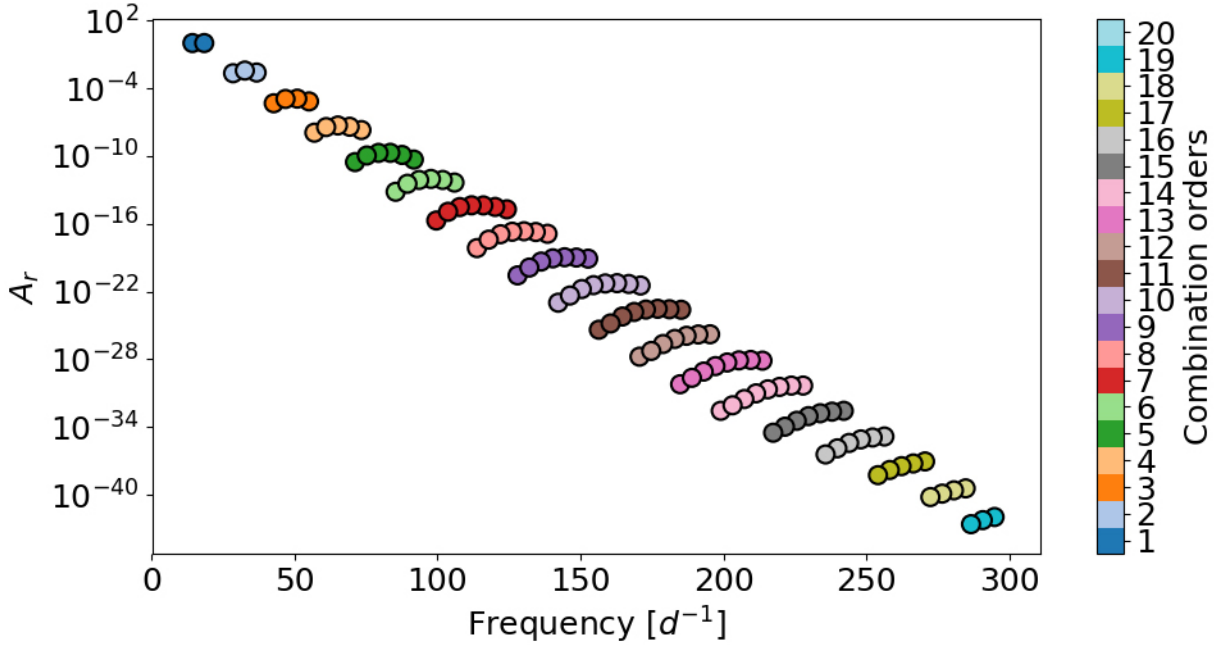
Figure 5.9 Amplitude ratios for the case study HADS star KIC 5950759

effects that could interfere with amplitudes measurements), in HADS stars the simple model amplitude assumption can still hold. The highest amplitude components of these periodograms are usually radial modes, concretely the fundamental and first overtone. This perspective leads us to expect amplitude ratios to decrease with the combination order. In Fig 5.9 the amplitude ratio (or module of the generalised transfer functions) is presented for our case study star, where the order $O = 1$ corresponds to the parent frequencies that by definition are equal to 1. As expected, in the HADS case study the amplitude ratio described by the simple model holds. A zoom of Fig 5.9 is shown in Fig 5.10, where tags over the combinations are given.

The same can be observed when testing the amplitude ratios of the sample of 11 non-peculiar HADS (see Fig. 5.11). The decreasing ratio with increasing order of combinations strengthens the assumption that combination frequencies in HADS are product of the same non-linear process, from the hypothesis taken, due to NLDP. Finally, note the fact that for each combination order the amplitude ratio is almost constant, independently of the
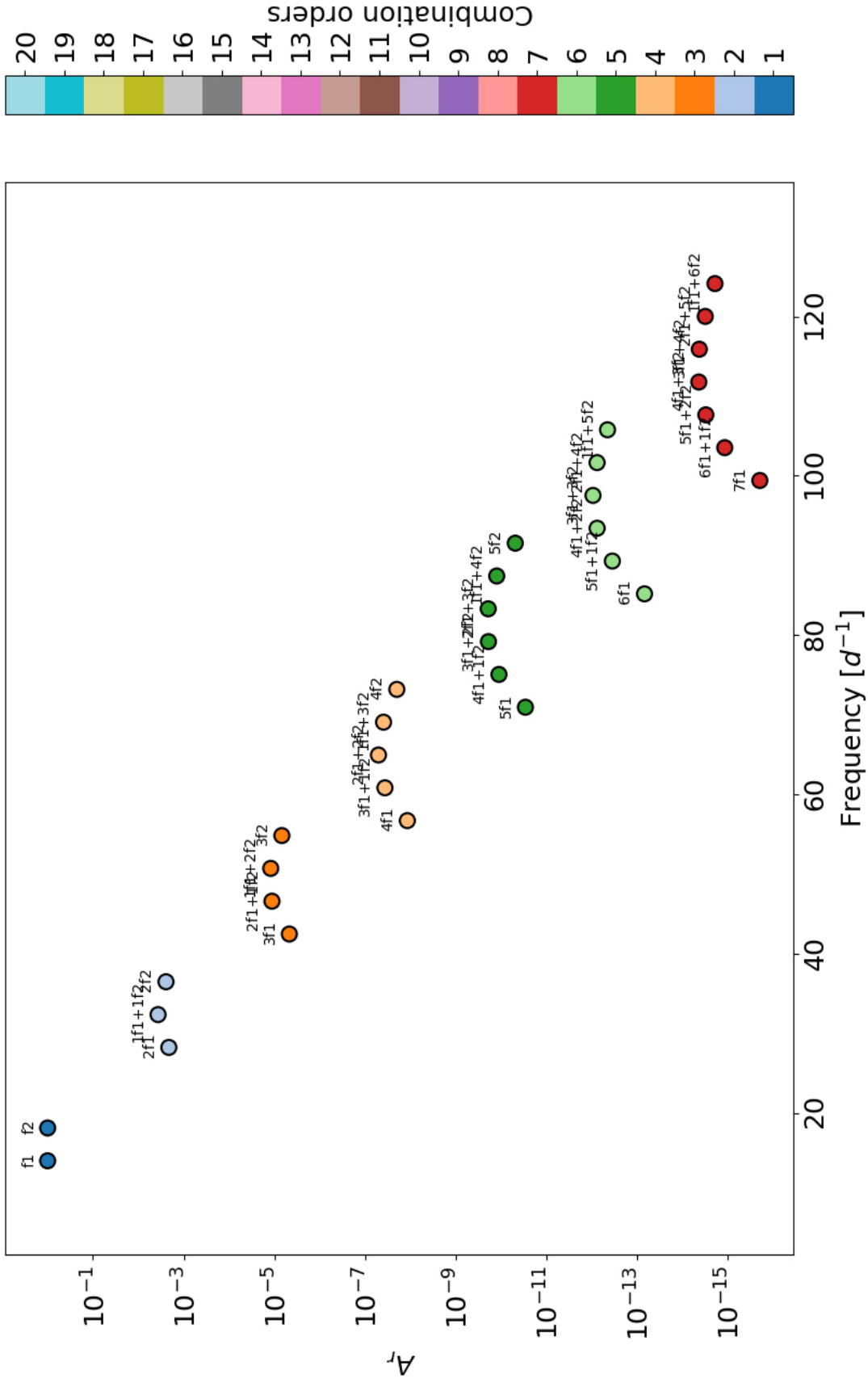
Figure 5.10 Zoom of amplitude ratios for the case study HADS star KIC 5950759
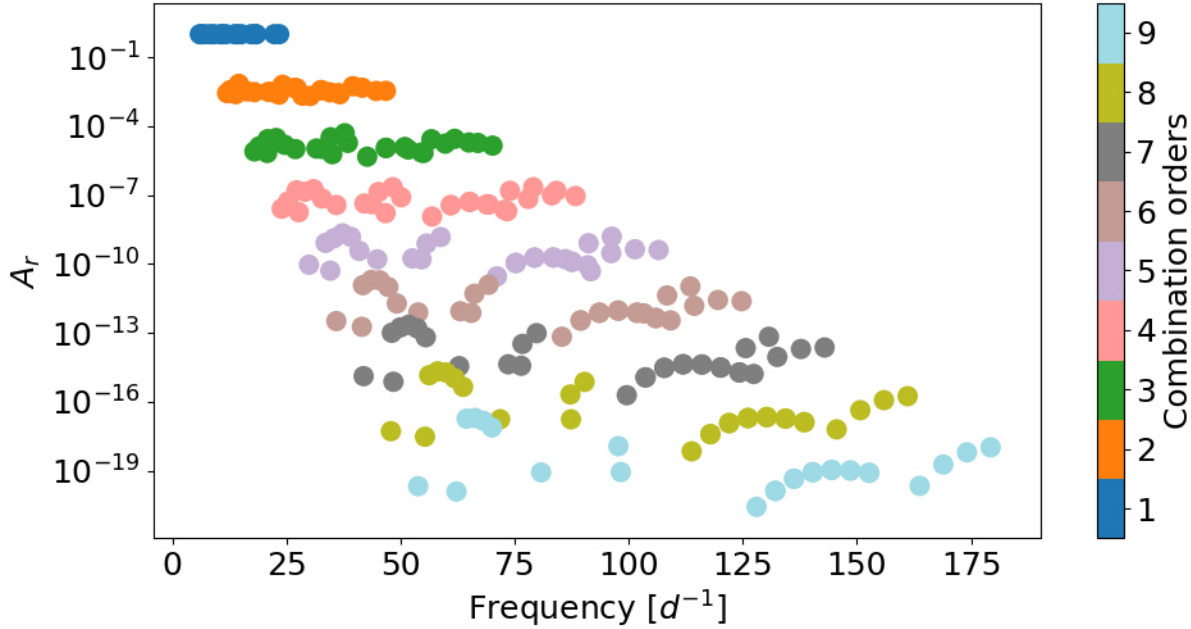
Figure 5.11 Amplitude ratios of the sample of 11 non-peculiar HADS stars.

frequency or the star.

5.3   Practical applications: unambiguous non-linearity identification

Despite all the efforts done (Balona, 2012, 2016, Balona and Dziembowski, 2011, Balona et al., 2012, Buchler et al., 1997), combination frequencies do not yet have any asteroseismic use for δ Sct stars. When a combination frequency is owed to nonlinear response of the stellar flux, it is just a mathematical consequence of the distorted light curve, so, it is not a solution of the perturbed stellar structure equations. If the combination frequency is due to resonant mode coupling, it is considered a stable mode that becomes unstable because of a resonance condition being met, and for example, in the case on non-radial parent modes can be useful for mode identification (Buchler et al., 1997, Goupil et al., 1998). That is why combination frequencies studies in δ Sct stars have been centered in unambiguously

identifying the nature of a combination frequency (Barceló Forteza et al., 2015, Bowman and Kurtz, 2014, Bowman et al., 2016, Breger and Lenz, 2008, Breger and Montgomery, 2014, Degroote et al., 2009) The unambiguous identification has become more and more important for LADS stars, where their usually multi periodic dense and unexplained power spectra have been keeping mode identification in δ Sct stars to be a complex task. This section provides possible new methodology that uses combination frequencies as proxy variables, allowing to serve relevant purposes such as mode identification in asteroseismic studies of δ Sct stars.

It has already been mentioned several times that the Γ_O functions contain information about the non-linear processes occurring in a variable star. From the relative phases and amplitudes ratio patterns seen for HADS stars, empirical inference over the Γ_O functions can be made. As combination frequencies of HADS stars are most likely to be from a non-linear distortion nature (see discussion in the beginning of this chapter), the pattern of the relative phases and the pattern of the amplitude ratios can be associated to these non-linear processes. In this sense, a different physical origin of the combination frequencies (e.g. mode coupling) will be described by different Γ_O functions, consequently, different patterns in the relative phases and amplitudes ratio plots.

As the relative phases and amplitude ratios do not seem to depend on frequency (top panel and bottom panel, respectively in Fig. 5.12), it is possible to merge them to plot what is considered a *Template of combination frequencies from NLDP* (Fig. 5.13) or *Non-linear distortion template*. The nature of a combination frequency detected in a LADS star can be determined by plotting its relative phase and its amplitude ratio over the corresponding template. Such plots are going to be called *Diagnostic plots*, since they will be testing that their position matches the pattern that combination frequencies from NLDP follow. This empirical methodology was tested in the set of 117 A-F stars observed by the TESS space satellite analysed in the first light results of this mission (Antoci et al., 2019).

The BPM was computed for each star of the set, using the first two highest amplitude frequencies (because there is a slight tendency to find more combination frequencies the bigger
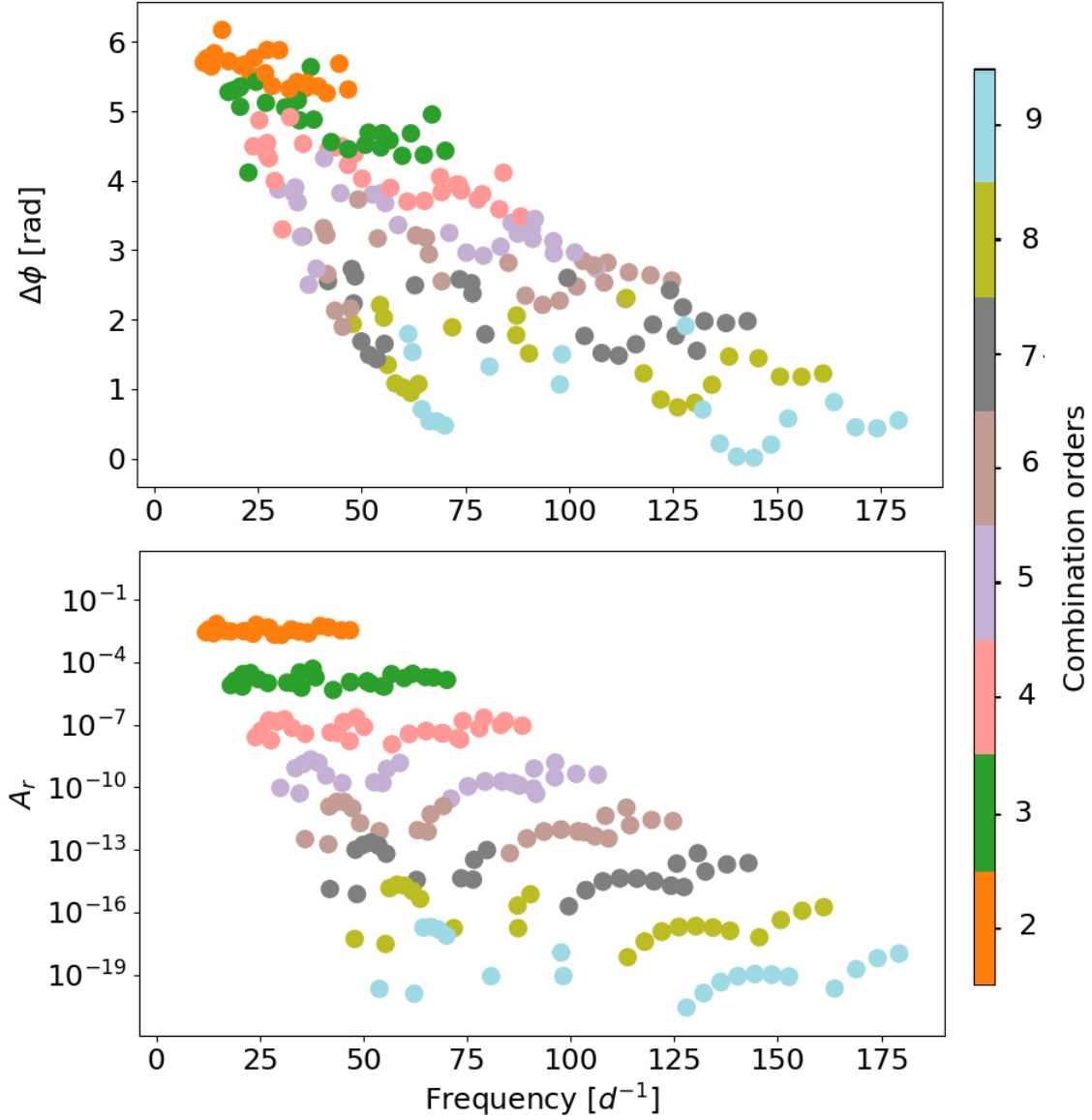
Figure 5.12 First phasor cycle of the relative phases (top panel) and amplitude ratios (bottom panel) plots of alleged NLDP non-linearities of 11 HADS stars (5 monoperiodic and 6 double-mode).

the amplitude of the parents, see Balona 2016), or when it was possible, a pair of frequencies that follow any of the period relations ($\frac{P_0}{P_1}, \frac{P_0}{P_2}$ or $\frac{P_0}{P_3}$, to make sure that the combination frequencies were from eigenmodes and not taking as parents other combinations). Table C shows the resulting best parents for each star. In the set of 117 A-F stars, 74 were identified
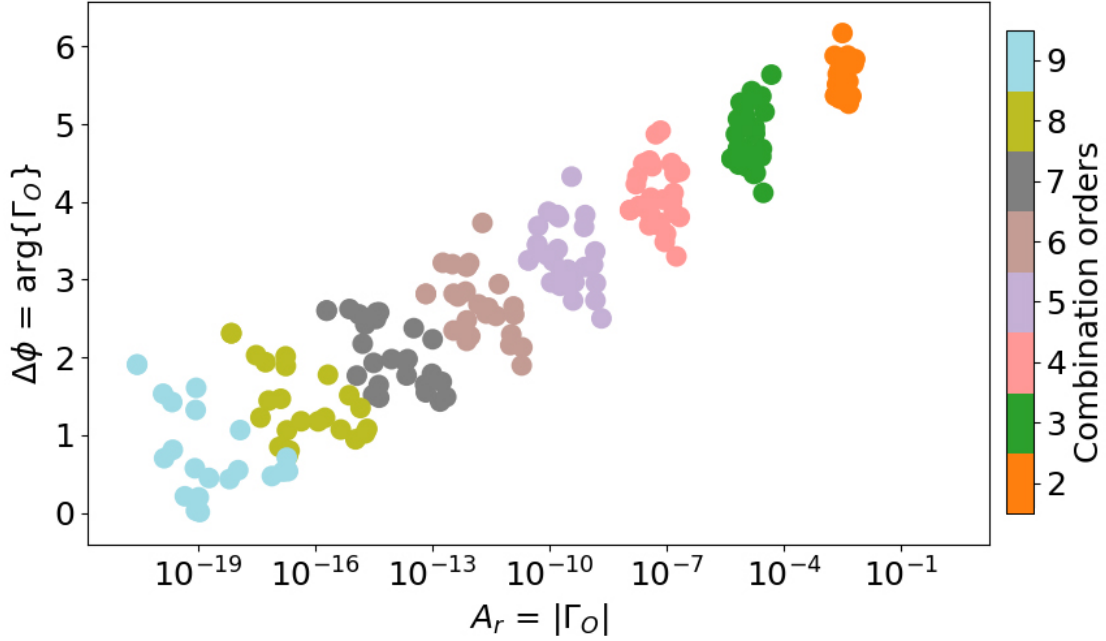
Figure 5.13 Alleged template of combination frequencies from non-linear distortion processes. Concretely, the first phasor cycle of the relative phases and amplitudes ratios of 11 HADS stars (5 mono-periodic and 6 double-mode).

in Antoci et al. (2019) as δ Sct stars (or hybrids). Few combination frequencies were found in the set of 74 low amplitude δ Sct stars. Combination frequencies for each of the 74 LADS stars, found by the BPM method and the unambiguous non-linearity identification, are also given in Table C. Note that the study was constrained to the children of the two highest amplitude frequencies, or when a pair of frequencies followed any period ratio relationship, so maybe more combinations frequencies (from other parents) might be present.

5.3.1 Possible mode identification using non-linearities in p-mode pulsators

Before discussing the diagnostic plots, it is important to remember Kurtz et al. (2015) statement about the possibility of children having higher amplitudes than their parents. When dealing with radial modes, as it is the case in HADS stars, the amplitude ratios pattern does

benchmark the amplitudes of non-linearities from NLDP. However, when analysing LADS stars, the highest amplitude peaks in their spectra (which are taken as parent frequencies) can be non-radial. Cancellation effects affecting non-radial modes could be messing the amplitude ratios, leading to wrongly discard the combination frequencies that do not follow the bottom panel of Fig. 5.12 pattern, when they actually are non-linear effects from NLDP. For this reason, amplitude ratio plots patterns are inspected to support identification, but not to discriminate the nature of non-linearities. However, decisive inferences can be made from relative phases plots.

There are several cases or situations to explore. First, the ones that match the pattern of the non-linear distortion template (see Fig. 5.14). In these cases, the combination frequencies can be unambiguously identified as non-linearities, and moreover that they are effects of the NLDP. In some of these stars interesting frequency structure emerges in the residual light curve, which would have to be analysed for a deeper understanding of the pulsational content.

Reasoning for pattern matching not only led to unambiguously identify a combination frequency of non-linear distortion nature, additionally it also means that the parents are radial modes. For example, in Fig. 5.15 for TIC 150394126, the methodology allowed to identify $f_1 + f_2$ as a NLDP non-linearity, but also to make the inference that f_1 and f_2 are radial modes. Assuring that the parents of $f_1 + f_2$ are radial modes adds an extra constrain for identifying the radial order of the radial parents. In the particular case of TIC 150394126, the real orders of f_1 and f_2 can be estimated taking into account Stellingwerf (1979) period relations, and that radial modes are equally separated in the asymptotic regime (*large separation*, $\Delta\nu$). An example of such estimation, made for TIC 150394126 $f_1 + f_2 = 107.67141d^{-1}$ combination frequency, is presented in the following equations knowing that $f_1 = \nu_n = 49.08808d^{-1}$ and $f_2 = \nu_{n+1} = 58.58333d^{-1}$:

$$\Delta\nu = 9.49525 \ d^{-1} \tag{5.7}$$

$$\frac{\nu_n}{\nu_{n+1}} = 0.838 \tag{5.8}$$
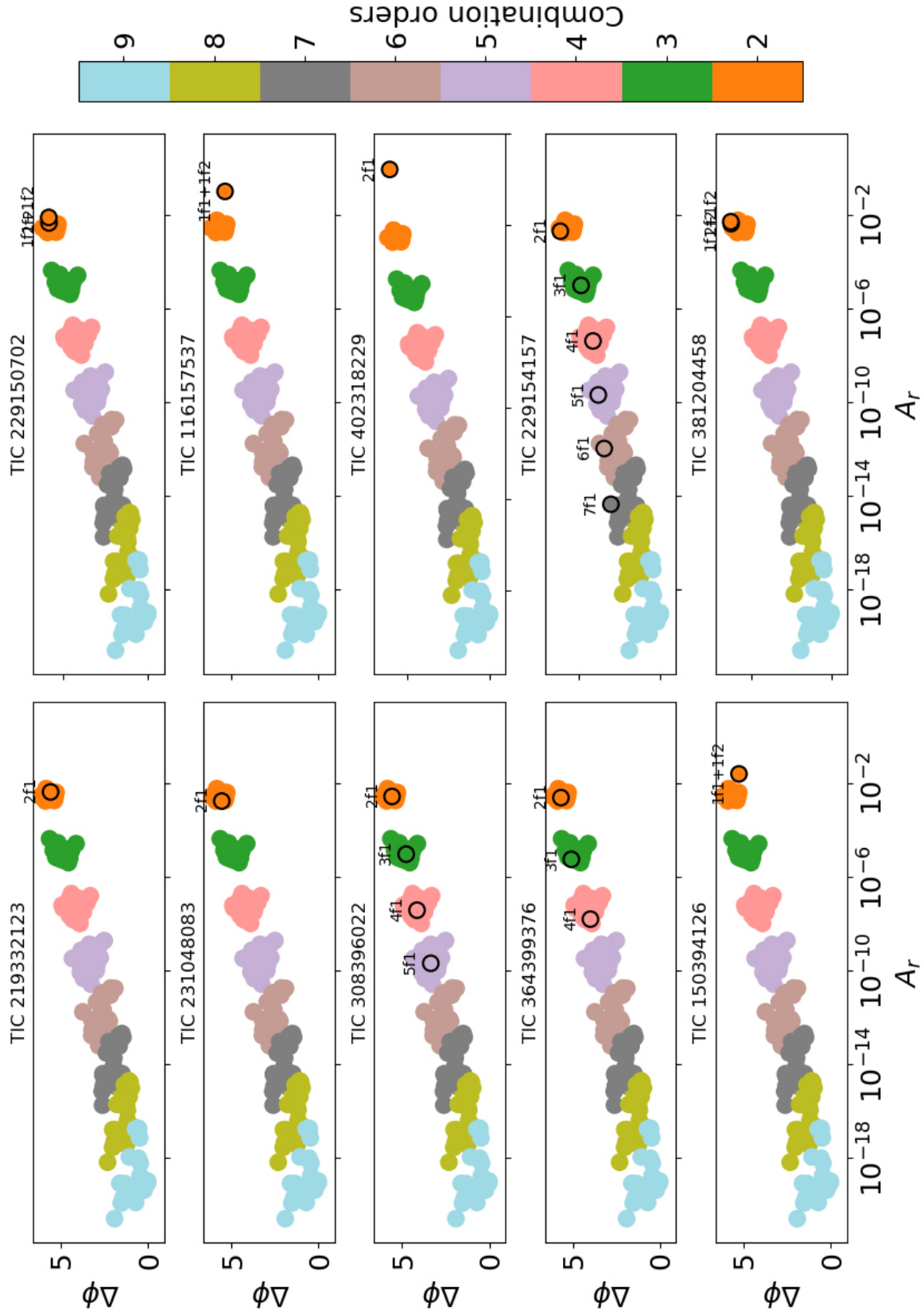
Figure 5.14 Diagnostic plots of combination frequencies matching the non-linear distortion template
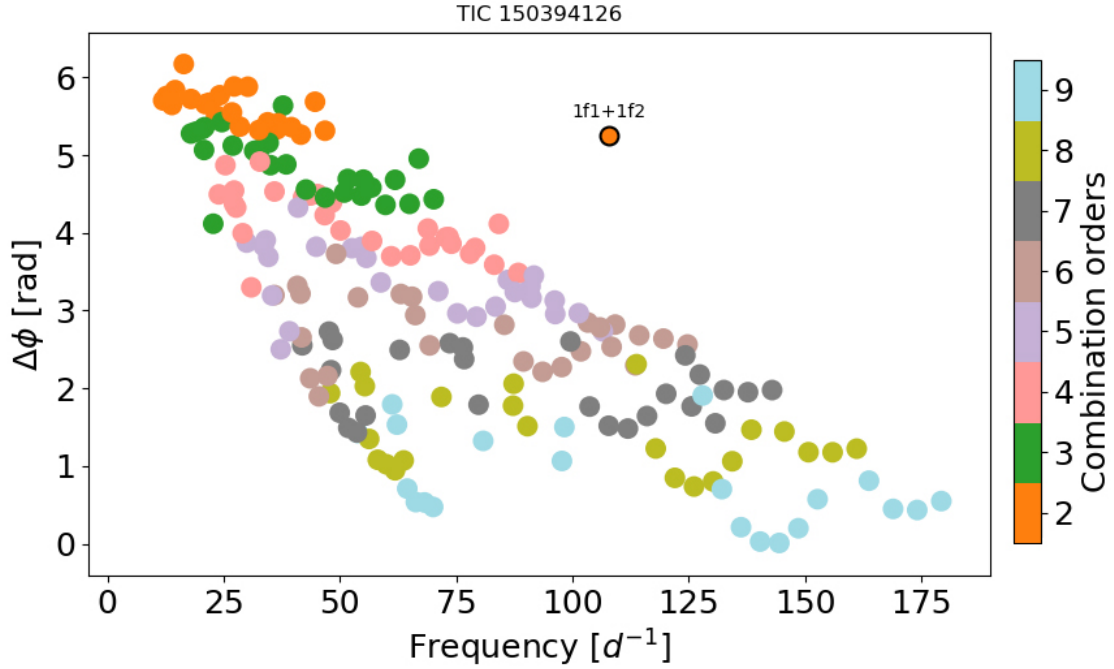
Figure 5.15 Relative phase diagnostic plot for the statistically significant combination frequency $f_1 + f_2$ found in TIC 150394126

and from Stellingwerf's period relations (Eqs. 1.11) it is possible to calculate,

$$0.818 \leq \frac{\nu_2}{\nu_3} \leq 0.831 \tag{5.9}$$

Although it is in the limit of the $\frac{\nu_2}{\nu_3}$ range, error management might allow to identify f_1 to a radial mode of radial order $n = 2$ and f_2 to a radial mode of radial order $n = 3$.

What about when the relative phase does not match the pattern?. One of the situations found is when the chosen as an independent frequency, is actually a combination frequency. In Fig 5.16, one of this cases is shown, where the $2f1$ harmonic is not-matching the relative phase pattern but matching the amplitude ratio expected. Noting that the phase of $f1 = 16.01867\ d^{-1}$ is 5.2855, matching the value as if it were an harmonic of order 2, then the $2f1$ harmonic can be identified with $4f1$. If this was true, the new $f1$ would be around $\approx 8.009335\ d^{-1}$. Such fundamental frequency should be verified calculating an oscillation model with the stellar parameters of the TIC 144387364 δ Sct star.
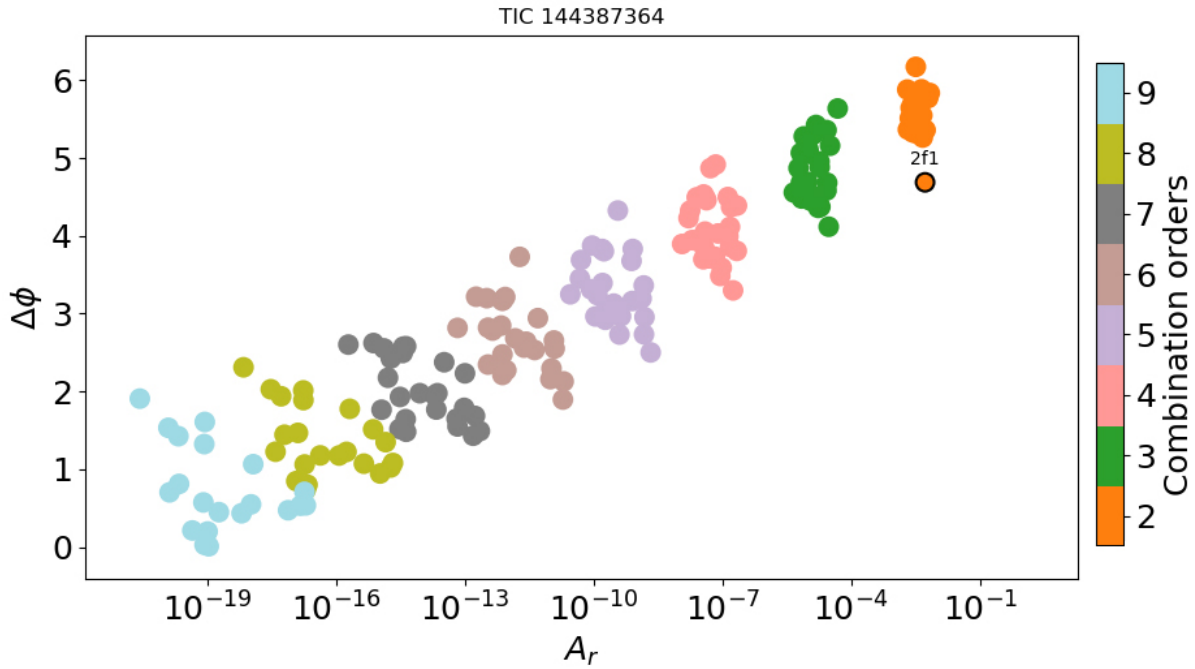
Figure 5.16 Diagnostic plot of the $2f_1$ harmonic in TIC 144387364

5.3.2   Terms from NLDP or resonantly excited coupled modes?
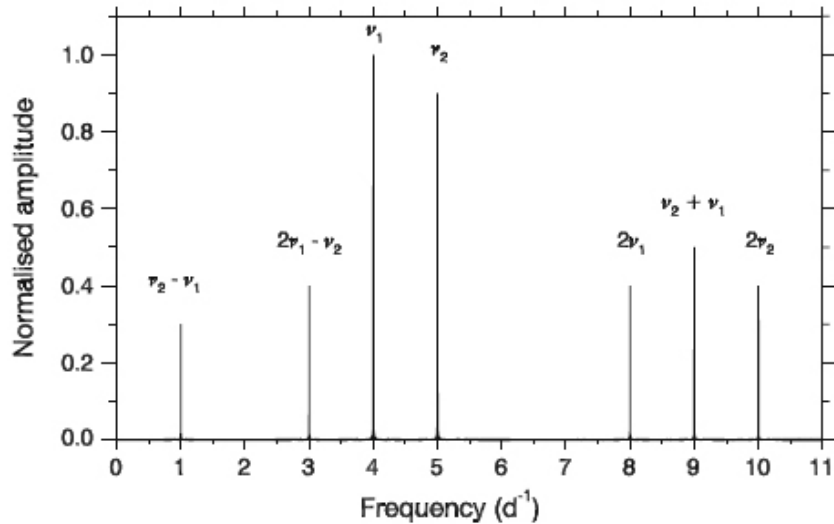
Figure 5.17 Example of fine structure of combination frequencies resembling a rotational splitting. Source (Bowman, 2017)

Resonance (direct, parametric and rotationally induced) can produce similar fine fre-

quency structure as independent modes. For example, in the case of rotationally induced resonance, the frequency structure generated can be very similar to a rotational splitting (see Fig. 5.17 of Bowman, 2017). For this reason, being able to distinguish non-linearities due to NLDP from resonantly excited couple modes and from independent modes, has become so important.

When analysing cases like the ones shown in Fig 5.18, the methodology can only say that Fourier component is not an effect from NLDP produced by the interaction of radial modes. The random relative phase (or simply not matching the template pattern) could indicate that it is:

1. An effect of the NLDP from non-radial parents (whose template is still unknown)

2. A resonantly excited or coupled mode.

3. An independent mode

The 3rd point should yield random diagnostic plots, so the first and second possibility are the ones to be differentiated. Several studies have discussed the nature of combination frequencies in δ Sct stars, to prove the mode coupling theory (Balona et al., 2012, Barceló Forteza et al., 2015, Bowman and Kurtz, 2014, Bowman et al., 2016, Breger et al., 2012, Breger and Lenz, 2008, Breger and Montgomery, 2014, Handler et al., 2000, Nowakowski, 2005). A special highlight to Breger and Montgomery (2014), where a method is presented not only to identify which frequencies are parents and which are children, but to also discriminate whether a combination frequency is a resonantly excited mode or just an effect of NLDP (Section 3.3.2).

The method requires significant amplitude modulation in three similar amplitude modes with large values of μ_c. Searching for this situation is not an easy task because the time variability of each member of the combination has to be studied in detail. The fast rotating δ Sct star KIC 8054146 was analysed by the Breger and Montgomery (2014) method, con-
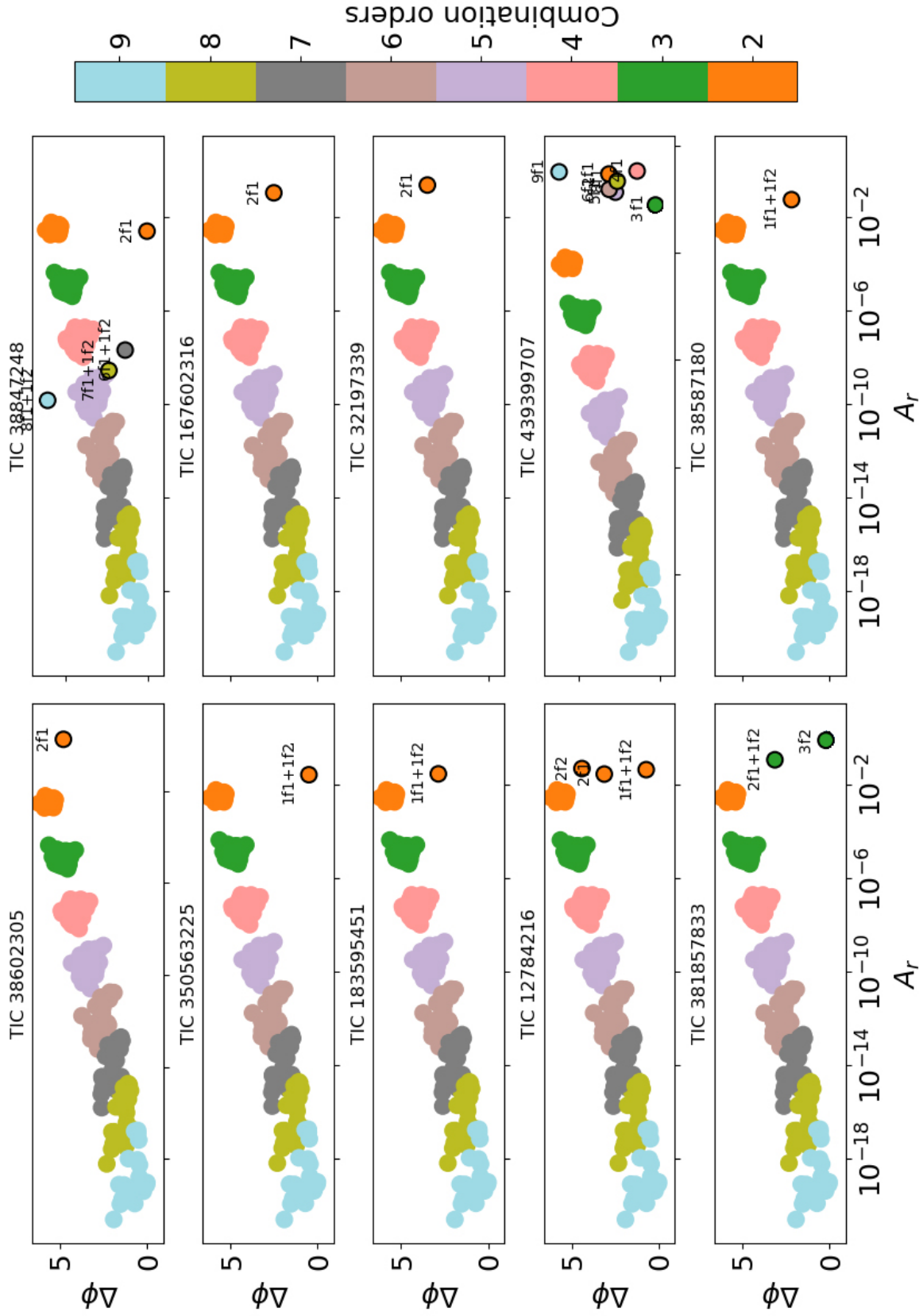
Figure 5.18 Diagnostic plots of combination frequencies not matching the non-linear distortion template
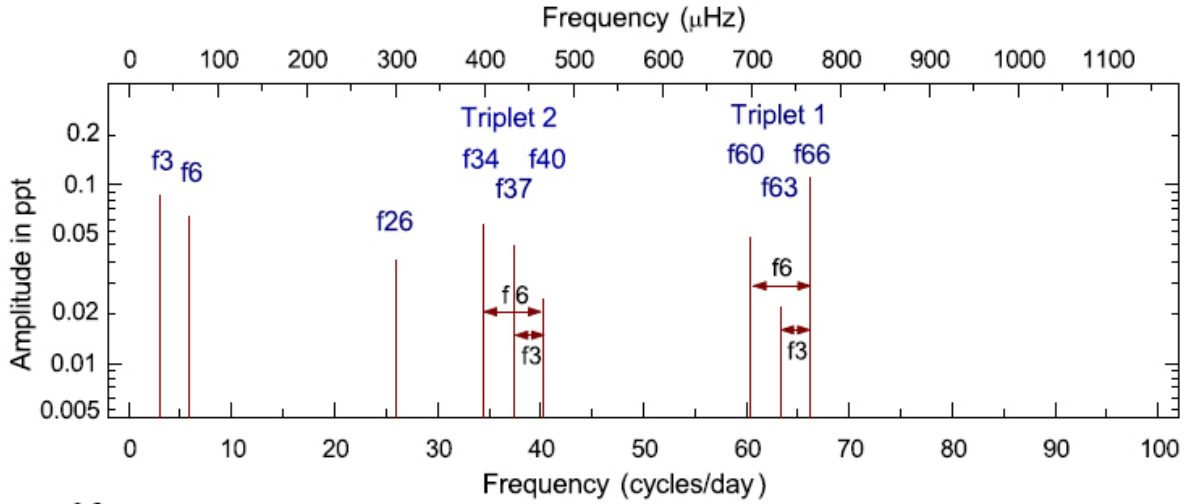
Figure 5.19 Dominant 9 frequencies of the T family (Source: Fig.1 from Breger and Montgomery, 2014))

cluding that the frequency f_{66} is most likely to be a coupled mode, whose parents are f_{40} and f_{26} ($f_{66} = f_{40} + f_{26}$ using the Breger and Montgomery (2014) nomenclature, see Fig 5.19).
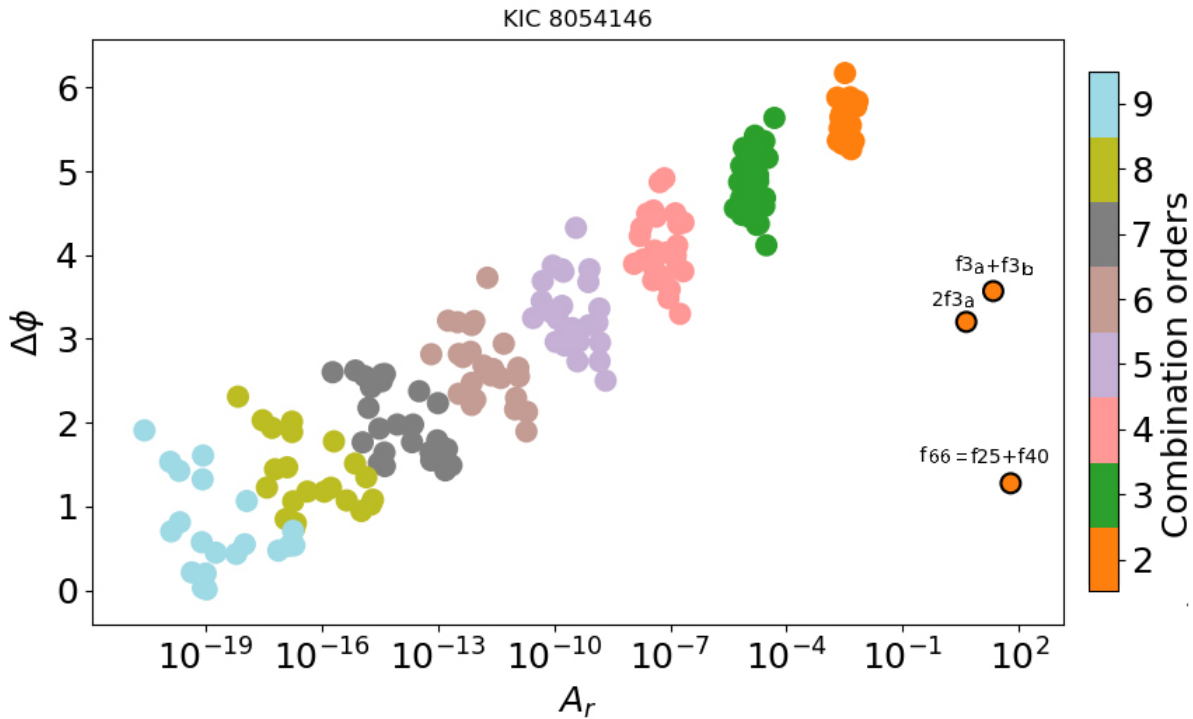
Figure 5.20 Phase diagnostic plot for the statistically significant combination frequencies of triplet 2 (Breger and Montgomery (2014) nomenclature) for KIC 8054146

The diagnostic plot for the f_{66} frequency (Fig.5.20) supports Breger's conclusion. Clearly, the relative phase of f_{66} does not match the relative phase values for combinations of order 2 when the non-linearity is from a non-linear distortion process. Moreover, the dominant low-frequency f_6, is also rejected to be a non-linearity consequence of a non-sinusoidal shaped light-curve. Note that although in Fig. 5.19 f_3 looks like one component, in a closer look it is really two very close frequencies ($f_{3a} = 2.9301d^{-1}$ and $f_{3b} = 2.9340d^{-1}$), so the f_6 component could correspond to a linear combination of the form $2f_{3a}$ or $f_{3a} + f_{3b}$. The relative phase for f_6 is not over the combination order 2 zone of the template, even if this frequency is considered to be $2f_{3a}$ or $f_{3a} + f_{3b}$.

So far, amplitude and phases of each combination frequency are calculated for the entire light curve as if they were constant. Nonetheless, resonant mode coupling induces amplitude modulation of the modes (either from direct, rotationally induced or parametric resonance) (Bowman, 2017). Therefore, it is relevant to discuss if time variability could affect the argumentation exposed until now. It is clear that amplitude modulation of a mode does not influence its phase (nodes and antinodes of a mode, with changing amplitudes in time, remains at same positions), but in regard to phase modulation it is not that clear. If a phase variation as function of time, instead of a constant phase, is introduced in a one component signal $Y(t)$ in the following way:

$$Y(t) = A\cos(\omega t + \phi(t)) \tag{5.10}$$

and the phase function of time can be represented by a Taylor series,

$$\phi(t) \approx \phi_0 + \phi'(t)t + ... \tag{5.11}$$

where $\phi'(t) \equiv \tilde{\omega}$, then

$$Y(t) = A\cos(\omega t + \phi_0 + \phi'(t) + ...) \approx A\cos((\omega + \tilde{\omega})t + \phi_0) \tag{5.12}$$

If the phase variation is small, it translates into a small frequency shift, however, the adjusted phase is going to be the same as if there was no phase variation. Consequently, the

patterns of the relative phase plots are not compromised by neither the amplitude modulation, nor the phase modulation.

To sum up, the combination frequencies of KIC 8054146 do not match the non-linear distortion template. This was expected since in Breger and Montgomery (2014) they were identified as a non-linearities from resonant mode coupling. Their position (near 0 and near π) are similar to other diagnostic plots from Fig. 5.18 (e.g. TIC 381857833, TIC 38587180, TIC 32197339, TIC 183595451, TIC 350563225), guessing that these combination frequencies of these stars are non-linearities from resonant mode coupling as well. However, the pattern of the Γ_O functions for combination frequencies from NLDP of non-radial parents (if these exist), is still unknown. In the next section, the Γ_O functions of combination frequencies in stars pulsating in the g-mode regime (e.g. the γ Dor stars) are examined, since the g-modes are non-radial pulsations, so their study can be revealing.

5.4   Extra: Non-linearities in g-mode pulsators

Combination frequencies in g-mode pulsators have been found useful for asteroseismic inference Buchler et al. (1997), Goupil et al. (1998), Kurtz et al. (2015). For example, in Kurtz et al. (2015), the characteristic shapes of the light curves for γ Dor stars (upward, symmetric or downward shapes) were explained by the phases of the combination frequencies, concretely by computing the relative phase parameter. Buchler et al. (1997) describe a method of identifying modes from constraining conditions over the degree of the mode in relation to the detectable combination frequencies. Regardless of these advances, the characterization of non-linear light curves of g-mode pulsation is far from complete.

In this section, the study of unambiguous identification of the nature of a combination frequency (is it a non-linearity? and if so, is it a non-linearity of resonant mode coupling nature or a convective or surface driven non-linearity?) is extended to g-mode pulsators such as γ Dor stars. A brief study over the characteristics of the Γ_O functions (their arguments

and modulus) for four previously studied γ Dor stars is presented. The motivation is to test the behaviour of a Volterra-based non-linear model for characterization of non-linear light curves of g-mode pulsating stars.

The set of four γ Dor stars used in this section are KIC 8113425 (analysed by Kurtz et al., 2015), KIC 4731916 (analysed by Bowman, 2017), KIC 5608334 (analysed by Saio et al., 2018), and TIC 30531417 (analysed by Antoci et al., 2019). Combination frequencies have been detected in their power spectra by the BPM.

KIC 8113425

The γ Dor of Kurtz et al. (2015) study has a strongly non-linear light curve, whose power spectrum shows the typical frequency groups for this type of variables. The first four highest power components of its power spectrum, and the two-termed combination frequencies generated by them, accounts for $\%CF = 58.04\%$ of all the light variability, meaning that the variance after the fit was reduced considerably. Meeting such fine structure of many combination frequencies by chance or by resonance mode coupling is highly improbable, therefore the strong chance of them being non-linearities from NLDP makes this star an interesting target for the analysis of the relative phases and amplitude ratios.

The relative phases of the statistically significant combination frequencies for KIC 8113425 are shown in the upper panel of Fig. 5.21. The arguments of the complex Γ_O functions, despite taking very different values, seem to follow an increasing trend with the order of the combinations (and with the frequency). Recall that Y-axis of this plot is cyclic, so the statistically significant frequencies of order 5 do not show a discontinuity. Interestingly, relative phases increasing with the frequency in g-mode pulsators, in opposition with the p-mode case (where the relative phases decreased with the frequency), is in agreement with the asteroseismic fact that the radial order n, referring to the order of the mode, increases with the frequency in p-modes, whereas n increases for lower frequencies in g-modes.

In γ Dor stars the children frequencies come from non-radial mode parents, so cancella-
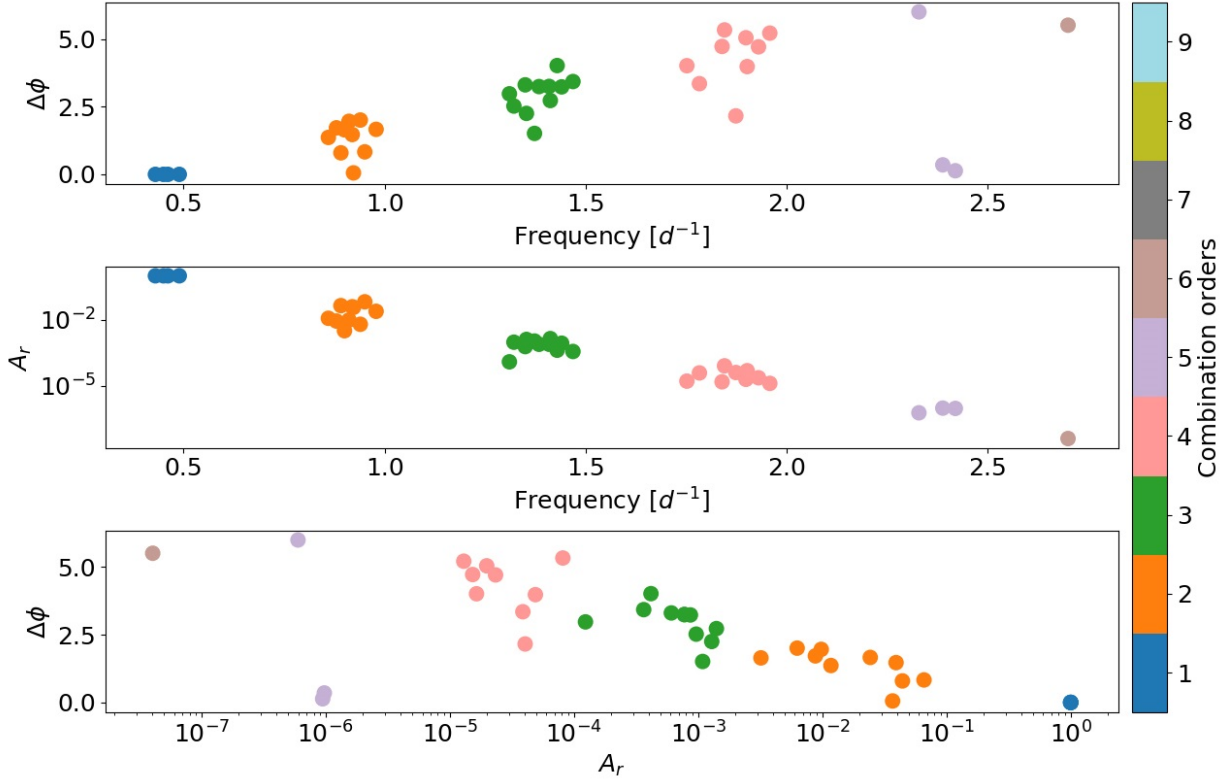
Figure 5.21 Relative phase (upper panel) and amplitude ratio (mid panel) of combination frequencies for KIC 8113425. Relative phases as functions of the amplitude ratios (bottom panel).

tion effects could be affecting the observed amplitudes, enabling the possibility of children frequencies having higher amplitudes than their parents (Kurtz et al., 2015). However, this does not seem to be happening in this star, as it can be seen in the amplitude ratios plot (mid pannel of Fig. 5.21). As in the p-mode case, one can plot relative phases as a function of amplitude ratios, obtaining what can be conjectured to be a non-linear distortion pattern of non-radial parents (Bottom panel of Fig. 5.21).

KIC 4731916

The case of KIC 4731916 was an interesting case of study because of the previous analysis made by Bowman (2017). Tracking plots of the variability of each mode revealed that the combination frequencies did not mimic the parents variability, which is not expected by the

mode coupling theory or by the non-linear distortion model. The amplitude and phases of the combination frequencies remained constant in the entire observation, whereas the parent mode decreased its amplitude over time. The relative phases of the harmonics and sums of KIC 4731916 are discussed in Kurtz et al. (2015). In this study, it was found that the relative phases near 0 or 2π leads to upward light curve shapes, whereas values near π leads to downwards light curves. The conclusion in Kurtz et al. (2015), regarding relative phases of the combination frequencies in KIC 4731916, was that their effects are not very strong in the shape of this star light curve.

Surprisingly, the relative phases and amplitude ratios plots for the combination frequencies exhibit a very interesting pattern including the subtraction combinations (see Fig. 5.22). This is the only star where the subtraction combination shows a clear pattern in their relative phases along with the sums and harmonics. For even combination order, the argument of the generalized transfer function increases. Conversely, for odd combinations it decreases at the same rate. They are seemingly cancelling each other .

The unconserved mode energy in this star was argued by Bowman to be a challenge for the theoretical expectations of combination frequencies. Undoubtedly, this star is very interesting for non-linearities in γ Dor stars studies. In the light of this result, further effort is needed to understand the relative phases plot and amplitude ratios including the subtraction combinations, since the range of possible pulsation content of these stars comprehends the low frequencies zone.

KIC 5608334

Saio et al. (2018) study claimed that the combination frequencies detected in this star were a product of its fast rotation. When the rotation of the star exceeds the pulsation of the mode, resonance conditions can be met inducing the coupling of the modes. The relative phases and amplitude ratios, for the harmonics, sums and subtraction combination frequencies detected in KIC 5608334, are plotted in Fig. 5.23. All combinations of the same order do not have
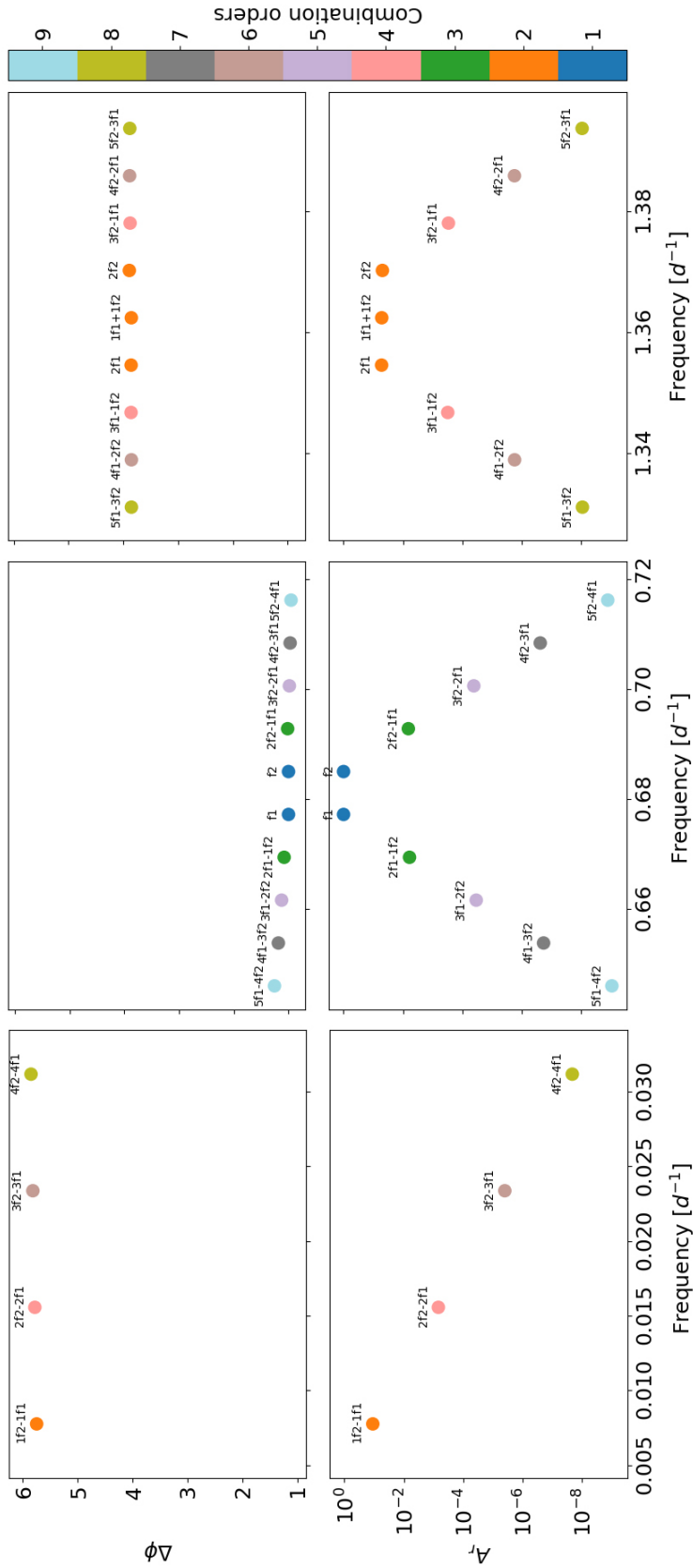
Figure 5.22 Relative phase (upper panels) and amplitude ratio (bottom panels) of harmonics, sums and subtraction combination frequencies of KIC 4731916
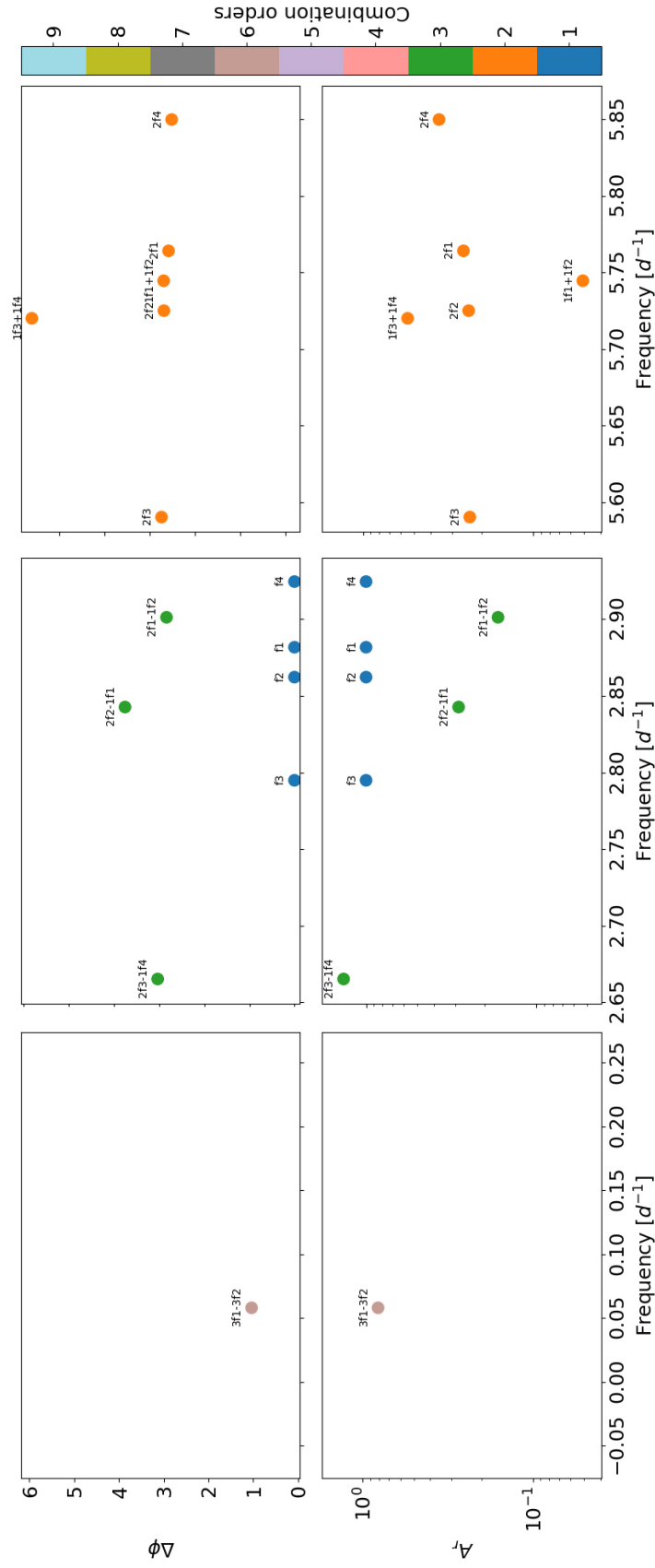
Figure 5.23 Relative phase (upper panels) and amplitude ratio (bottom panels) of harmonics, sums and subtraction combination frequencies of KIC 5608334

similar relative phases evoking the coupling of modes in the δ Sct star cases (see Sec. 5.3.2).

TIC 30531417
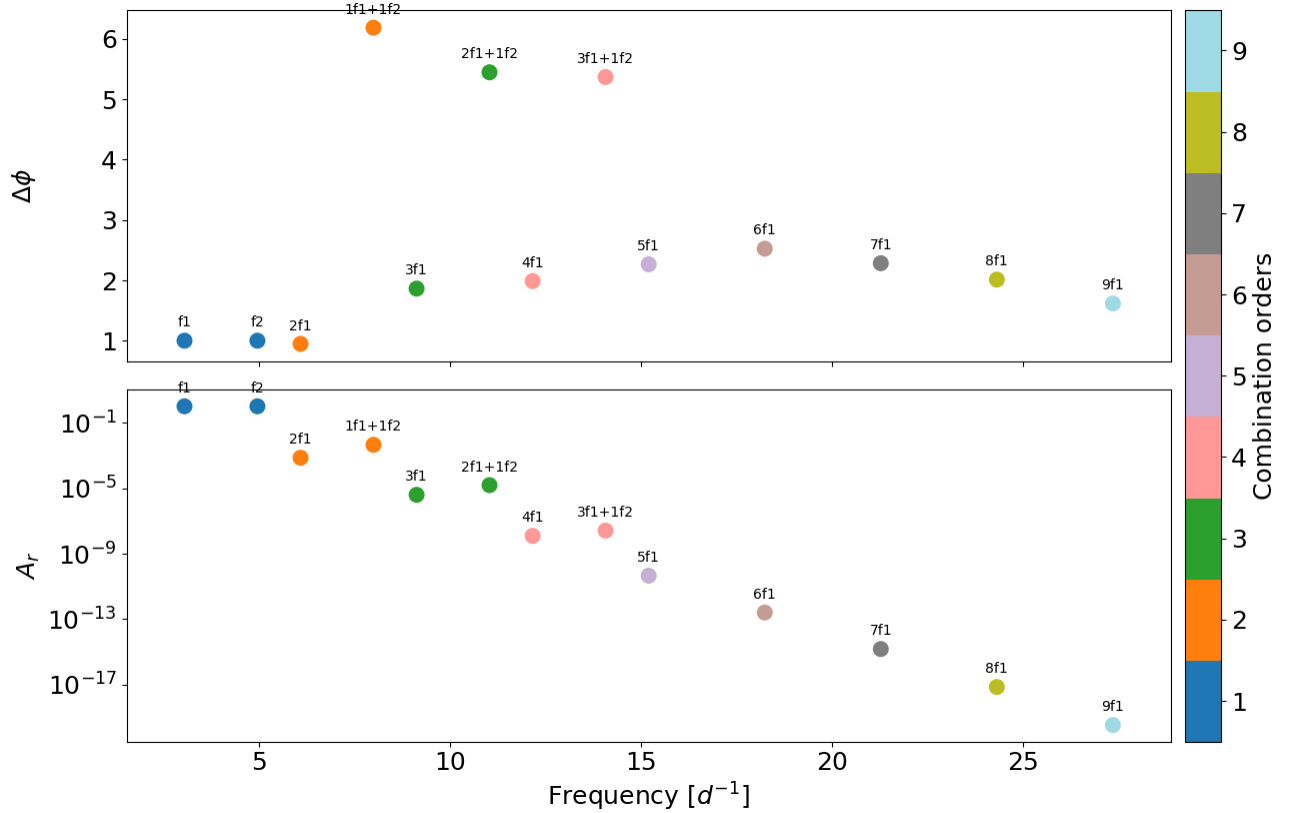
Figure 5.24 Relative phase (upper panel) and amplitude ratio (bottom panel) for sums and harmonics combination frequencies of TIC 30531417

The TIC 30531417 star shows a very regular light curve. The principal component of the power spectrum belongs to the g-mode frequency range $(0.3 < \nu < 3 \ d^{-1})$ but showing high amplitude for a γ Dor star. For this reason, it was baptised by Antoci et al. (2019) as a High Amplitude γ Dor (HAGD) star. The BPM was computed first for the highest amplitude peak, extracting almost all the harmonics. After an inspection of the residual light curve, a second mode was detected at $\nu_2 = 4.96067 \ d^{-1}$.

Expectations over the relative phases were that they must follow the increasing pattern given by the first γ Dor analysed in this section (KIC 8113425), but this hypothesis is not

fulfilled (see Fig. 5.24). The relative phase of the principal component, whose frequency value is in the g-mode regime, seems to be increasing with the higher the frequency value and with the combination order. However, it is not increasing in the same rate as KIC 8113425, and from $6f_1$ it starts to decrease. Regarding ν_2, the second order harmonic seems to be following the non-linear distortion template, so ν_2 is possibly a radial p-mode.

5.5   Chapter Summary

- In this chapter, characterization of non-linearities in terms of their phases and amplitudes was intended. The motivation was that a combination frequency, meeting only the frequency relation between parent and children, does not necessarily mean that it is a non-linearity. The study enables to characterize the non-linearities due to non-linear distortion processes of radial p-mode parents, and exposed the possibility of mode identification and unambiguous non-linearity nature identification (non-linear distortion nature or resonant mode coupling nature). Additionally, the study took the first steps towards the characterization of non-linearities of g-mode and non-radial mode parents.

- HADS stars exhibit so many combination frequencies that they are assumed to be from the non-sinusoidal shape of the light curve due to NLDP. Clear patterns are observed when analysing the relations of phases and amplitudes between these combinations and their parents, under the general Volterra expansion framework.

- The relative phases represent the arguments of the Γ_O complex transfer functions of Volterra expansion. For combination frequencies with radial mode parents, the relative phases showed a decreasing pattern with the frequency and the combinations of the same order shared almost the same relative phase value. Moreover, the pattern is similar for every HADS star. This was tested in a set of 17 HADS stars observed by

the TESS space satellite.

- The distortions in the relative phase patterns, for the few cases where they exist, coincide with stars with high rotation speed and due to slight deviations in the period ratios.

- The amplitude ratio represents the modules of the Γ_O complex transfer functions of Volterra expansion. For combination frequencies with radial mode parents, their amplitude ratio follows a decreasing exponential pattern. Care must be taken when dealing with LADS stars, as generally the parents chosen are most probably non-radial modes where cancellation effect could be hampering the amplitude ratio pattern.

- Subtractions do not meet the relative phases nor the amplitude ratios pattern. The subtractions do not fulfill the commutative property, so the order of the factors in the linear combination of independent mode phases is important. The equations must be revised to resolve this issue.

- Since the patterns do not vary from star to star, in the sense that the combination frequencies of all the HADS were grouped by the order of the combination in the same way, then it was possible to build the non-linear distortion template by plotting all relative phases as a function of their amplitude ratios. From these empirical characterization of NLDP non-linearities, a procedure to unambiguously identify the non-linearities nature was conjectured in terms of their position over the template, namely the diagnostic plots. Although, this reasoning would require more statistical support.

- The combination frequencies of 76 stars from TESS sectors 1 and 2 were analyzed with the diagnostic plots and the results are given in the Table C. It was shown how to estimate radial orders n in some cases where the combination frequency matched the pattern. The no-match cases could be pointing to a resonantly couple mode, so in this

way determining its nature. This was tested for a previously known case of resonant mode coupling, confirming the no-match position of their combination frequencies over the template. Other no-match possible explanation is that those combination frequencies parents are non-radial modes. These motivate the brief study of stars pulsating in g-modes such as γ Dor stars, where all the modes are non-radial.

• The phase and amplitude relationships in pulsating g-modes such as γ Dor stars were explored, yielding interesting results in which to continue working. The phase patterns appear to be clustered but vary for each star. Under the theoretical formulations presented in this work, and in the 4 stars analysed, it was not possible to find a pattern that would unite them all. In any case, the patterns found attracted a lot of attention, especially in the KIC 4731916 γ Dor star, where the subtractions were part of the pattern.

• The Γ_O functions for g-mode pulsators such as the γ Dor stars are far from being characterized. Carrying out the relative phases and amplitude ratios study to a larger sample of γ Dor stars, will allow to know to what extent the generalized Γ_O functions can be characterized for the g-modes. Nevertheless, the results obtained from the chosen γ Dor stars already delivered interesting patterns, so further research in this direction could be promising.

Chapter Six

Conclusions and Future work

6.1   Conclusions

In this chapter, the conclusions drawn from the empirical characterization of non-linear components in δ Sct stars power spectra are presented. Additionally, future work ideas on how to continue this study are given afterwards.

- Characterizing non-linearities in p-modes pulsating stars such as δ Sct has yielded very interesting results. Initially, to face the challenge of correctly identifying them in the power spectra, a method was developed (The BPM) in which it is possible to identify the parents that best describe the light curve in terms of their linear combinations. This is relevant for the analysis of a given light curve, firstly, because it takes into account the non-introduction of spurious information in the process and, at the same time, gives very high precision in the determination of the frequency. In essence it was shown that, when fitting combination frequencies of the parents yielded by the BPM, the residual light-curve is the one with the lowest contributions from these components, and is the only method available nowadays that does this automatically and exhaustively. From the point of view of asteroseismology, it allows us to take a step forward in the understanding of the dense and complex power spectra, characteristic of these stars. For example, considering that non-linearities from NLDP are not solutions

of the perturbed stellar structure equations, one may be interested in extracting these contributions from the spectrum and this method would do it with great efficiency (Lares-Martiz et al., 2020).

- Fitting combination frequencies with the BPM presented in Chapter 4 could help to identify pulsation modes by possibly revealing radial and non-radial frequency patterns, rotational splittings in the periodogram of the residuals, or just frequency and/or amplitude modulations. An example of this was shown in the results for the mono-periodic TIC 9362550, where a possible amplitude modulation was found, and in the SC observations of the HADS star KIC 5950759, where the modulating frequency ω_m became detectable without needing LC super-Nyquist alias analysis, as in Yang et al. (2018). Likewise for the multi-periodic star, where a new unexplained frequency structure emerged from what was considered noise before the combination frequencies extraction.

- With respect to phase and amplitude relationships, the empirical characterization of the Γ_O functions in stars with radial parents proved to be largely constant, regardless of the star analysed. Taking advantage of this fact, it might help to identify non-linearities nature (NLDP or resonant mode coupling). Moreover, it might help to identify the radial nature of an independent mode, in this way providing an extra constrain that would enable mode identification. This finding is relevant because it might be the first time that combination frequencies can be of asteroseismic use in intermediate-mass pulsating stars. Further study and statistical robustness are required to be able to establish the diagnostic plots as a consistent tool for asteroseismic analyses.

- The diagnostic plots of the combination frequencies in 74 δ Sct observed by the TESS satellite were analysed. At least 10 of them showed matching positions to the NLDP non-linearities template pattern, so the conjecture is that they are non-linearities from a non-linear distortion nature. On the other hand, at least 10 stars whose combination

frequencies did not match the NLDP non-linearities template pattern, showed similar positions to the pattern of a previously known resonant mode coupling family detected in the KIC 805414 δ Sct star. If future work succeeds to statistically strengthen this procedure, it would be a faster method to identify the non-linearities nature and with no previous condition needed to apply it. It shows advantages over the Breger and Montgomery (2014) method, where the implicated coupled modes have to be modulated in amplitude and the variations between all the signal components must be tracked.

- The observational characterization of non-linearities in g-mode pulsating stars, particularly for γ Dor stars, yielded interesting but not conclusive results. In some cases the patterns are clear, increasing in relative phases with the order of combination. Making a visual comparison, it is seen that they have similar features between them. For example, in most cases the combination frequencies relative phases have values around 0, π and 2π. We speculate it to be the signature for non-linearities of mode coupling nature, or, still can be from NLDP nature but of non-radial parents. Results for KIC 4731916 (a γ Dor also analysed by Bowman, 2017) are unexpected and challenging. The resulting pattern of the relative phases for the combination frequencies in this star, without modifying the phase relationship in any way, unexpectedly presents a clear pattern including the subtraction combinations. The required research to understand the results for this star are promising to explain a non-linear effect in γ Dor stars.

- The models for stars that display non-linear effects in their power spectra could benefit from this work. The state-of-the-art model regarding non-linearities was the non-linear amplitude equations (AEs in Buchler et al., 1997, Goupil et al., 1998), the work of Van Hoolst (1994), and more recently, the new MESA (Modules for Experiments in Stellar Astrophysics) functionality regarding non-linear radial stellar pulsations (Paxton et al., 2019). Perhaps the key to finally understand δ Sct stars pulsational content

is to develop non-linear models balancing the mechanisms driving and damping the pulsations in the way non-linearities are showing from their Γ_O functions presented in this work. Anyway, a rigorous study to understand the underlying physical meaning of the Γ_O functions is needed.

6.2   Future work

Much remains for the complete characterization of non-linearities. In the course of these work, ramifications of the study came out, some to provide even more rigor to the present study and some to take further the investigation. For example:

- Building a HADS Catalog of Space Observations:

  Although HADS are not very common, efforts need to be made to constitute a bigger catalogue of HADS in order to conduct a statistical robust study and confirm the assumptions made in Chapter 5 about the arguments of the Γ_O functions in HADS stars. For example, observations looking for HADS in the southern hemisphere could help to add HADS located in the Magellanic cloud to the sample used in this monograph (Balona, 2016).

- Spectroscopic follow-up of δ sct stars (HADS and LADS):

  It would confirm the origin of the combinations as non-linearities from NLDP, since they are not real oscillations. For example, they do not produce a real observable displacement in a radial velocity plot (van Kerkwijk et al., 2000), since they are mathematical products of the deviation of the sinusoidal shape of the light curve. Radial velocities taken from a spectroscopic follow-up could bring confirmation on the identifications of NLDP non-linearities from radial parents, and to maybe identify the ones from non-radial parents.

- Time-frequency analysis:

  Conducting time-frequency analysis could help in the identification of a non-linearity nature. It is known that resonant mode coupling can induce amplitude and frequency modulation of the modes (Bowman, 2017, Buchler et al., 1997, Dziembowski, 1982, Nowakowski, 2005) so, this might be a way to confirm or support non-linearities nature identifications.

- Development of the analytical equations:

  The development of the equations and the modeling of the results from the empirical characterization found in this study, may allow us to achieve numerical solutions for the non-linear treatment of temperature, pressure, displacement or any other variable that may present non-linearities.

  The patterns obtained could be modeled to analytically characterize the non-linearities, at least the non-linearities of stars pulsing in radial p-modes such as δ sct stars. The increasing rate of the delay between the observed phases and the phases expected by the simple model can be the starting point to model non-linearities, whose parameters have to be closely linked to the non-linear effect happening in convective layers and star surfaces, or any other non-linear process within the pulsating star. Additionally, better characterizations could be done to the very complete patterns of the case study KIC 5950759. Parabolic functions could be appropriate to model the relative phases and the amplitude ratios.

- Massive application in γ Dor stars:

  To establish statistical criteria that allow us to draw conclusions about the non-linearities in these stars through the procedures presented in this monograph. Also, a study in this direction could be helpful for developing new non-linear theories, since they could possibly be pointing to new non-linear processes happening near the core

of the star.

- Study of the physical meaning of the Γ_O functions:

  They differ enormously when the phases belong to g-modes or p-modes. This strengthens the argument that the Γ_O functions would speak about the different non-linear effects within each physical system. Future research could be focused in understanding the arguments of the Γ_O functions, when the non-linear effect is of a resonant mode coupling nature.

APPENDICES

Appendix A

Relevant information on the time series of the Delta Sct stars used in chapter 4

Table A.1 Relevant time series information. T is the length of the observation in days and δ_t is the cadence or sampling rate in seconds. For the TESS and Kepler light curves, we used the instrumental effects free light curve, resulting from the Pre-Search data Conditioning (PDC) pipeline, accessible in the Mikulski Archive for Space Telescopes (MAST: https://archive.stsci.edu/).

Time series Parameters			
Star Name	T [d]	δ_t [s]	Obs. Sequence
TIC 9632550	27.41	120.01	Sector 2
KIC 5950759	31.04	58.85	Quarter 4
HD 174966	27.20	31.99	Run SRc01

Appendix B

Combination frequencies detected in the Delta Sct stars analysed in chapter 4

Table B.1 Tags of the statistically significant combination frequencies for the mono-periodic δ Sct star TIC 9632550. The frequency values can be calculated with the parent frequency $f0$ resulting from the BPM given in Table 4.3, since the fitted values are the exact combination frequency values

Combination frequencies in TIC 9362550				
2f0	5f0	8f0	11f0	14f0
3f0	6f0	9f0	12f0	
4f0	7f0	10f0	13f0	

Table B.2 Tags of the statistically significant combination frequencies for the double mode HADS star KIC 5059759. The frequency values can be calculated with the given parent frequencies $f0$ and $f1$ resulting from the BPM given in Table 4.4, since the fitted values are the exact combination frequency values.

Combination frequencies of KIC 5059759					
2f0	3f0+2f1	7f0+5f1	11f0+7f1	6f0-3f1	4f1-1f0
3f0	3f0+3f1	7f0+6f1	12f0+1f1	7f0-1f1	4f1-2f0
4f0	3f0+4f1	7f0+7f1	12f0+2f1	7f0-2f1	4f1-3f0
5f0	3f0+5f1	8f0+1f1	12f0+3f1	7f0-3f1	4f1-5f0
					Continued on next page

Table B.2 – continued from previous page					
Non-linearities of KIC 5059759					
6f0	3f0+6f1	8f0+2f1	12f0+4f1	7f0-4f1	5f1-1f0
7f0	3f0+7f1	8f0+3f1	12f0+5f1	7f0-5f1	5f1-2f0
8f0	4f0+1f1	8f0+4f1	12f0+6f1	8f0-1f1	5f1-3f0
9f0	4f0+2f1	8f0+5f1	13f0+1f1	8f0-2f1	5f1-4f0
10f0	4f0+3f1	8f0+6f1	13f0+2f1	8f0-4f1	5f1-6f0
11f0	4f0+4f1	8f0+7f1	13f0+3f1	8f0-6f1	6f1-4f0
12f0	4f0+5f1	9f0+1f1	13f0+4f1	9f0-1f1	6f1-5f0
13f0	4f0+6f1	9f0+2f1	13f0+5f1	9f0-2f1	6f1-6f0
14f0	4f0+7f1	9f0+3f1	13f0+6f1	9f0-6f1	6f1-7f0
2f1	5f0+1f1	9f0+4f1	14f0+1f1	10f0-1f1	7f1-6f0
3f1	5f0+2f1	9f0+5f1	14f0+2f1	10f0-2f1	7f1-7f0
4f1	5f0+3f1	9f0+6f1	14f0+3f1	10f0-4f1	7f1-8f0
5f1	5f0+4f1	9f0+7f1	14f0+4f1	10f0-6f1	7f1-9f0
1f0+1f1	5f0+5f1	10f0+1f1	14f0+5f1	10f0-7f1	8f1-7f0
1f0+2f1	5f0+6f1	10f0+2f1	15f0+4f1	11f0-1f1	8f1-6f0
1f0+3f1	6f0+1f1	10f0+3f1	2f0-1f1	11f0-2f1	8f1-8f0
1f0+4f1	6f0+2f1	10f0+4f1	3f0-1f1	11f0-7f1	8f1-9f0
1f0+5f1	6f0+3f1	10f0+5f1	3f0-2f1	11f0-4f1	9f1-7f0
1f0+6f1	6f0+4f1	10f0+6f1	4f0-1f1	12f0-1f1	9f1-8f0
2f0+1f1	6f0+5f1	10f0+7f1	4f0-2f1	20f0-14f1	15f1-19f0
2f0+2f1	6f0+6f1	11f0+1f1	4f0-3f1	1f1-1f0	16f1-19f0
2f0+3f1	6f0+7f1	11f0+2f1	5f0-1f1	2f1-1f0	17f1-19f0
2f0+4f1	7f0+1f1	11f0+3f1	5f0-2f1	2f1-2f0	18f1-20f0
Continued on next page					

Table B.2 – continued from previous page				
Non-linearities of KIC 5059759				
2f0+5f1	7f0+2f1	11f0+4f1	5f0-3f1	3f1-1f0
2f0+6f1	7f0+3f1	11f0+5f1	6f0-1f1	3f1-2f0
3f0+1f1	7f0+4f1	11f0+6f1	6f0-2f1	3f1-3f0

Table B.3 Tags of the statistically significant combination frequencies for the multi-periodic δ star HD 174966. The frequency values can be calculated with the parents given in Table 4.6 since the fitted values are the exact combination frequency values

Combination frequencies of HD 174966				
2f3	7f0-4f4	8f1-6f4	9f2-7f3	2f4-1f3
1f0+1f1	8f0-5f1	8f1-8f2	1f3-1f1	3f4-2f0
1f0+1f2	8f0-6f2	9f1-9f2	1f3-1f2	3f4-3f0
1f0+1f3	8f0-5f3	2f2-1f0	2f3-3f0	3f4-4f0
1f0+1f4	9f0-6f2	2f2-1f1	2f3-1f4	3f4-3f1
1f1+1f2	9f0-7f2	2f2-1f3	3f3-1f4	3f4-2f3
1f1+1f3	1f1-1f0	3f2-1f0	4f3-5f0	4f4-4f0
1f1+2f3	1f1-1f2	3f2-2f3	4f3-4f1	4f4-4f1
1f1+1f4	3f1-3f0	3f2-1f4	4f3-5f2	4f4-4f2
2f1+1f3	3f1-3f2	4f2-3f3	5f3-5f0	4f4-5f2
2f1+1f4	3f1-2f3	4f2-2f4	5f3-7f0	4f4-4f3
1f2+1f3	4f1-5f0	4f2-3f4	5f3-3f1	5f4-5f3
1f2+1f4	4f1-3f3	5f2-6f0	5f3-5f2	6f4-8f0
1f3+1f4	4f1-2f4	5f2-2f3	5f3-4f4	6f4-7f1
2f0-1f1	5f1-6f0	5f2-3f3	6f3-8f0	6f4-7f2
Continued on next page				

Table B.3 – continued from previous page				
Non-linearities of HD 174966				
2f0-1f3	6f1-7f0	6f2-7f0	6f3-7f2	6f4-6f3
3f0-1f1	6f1-4f3	6f2-2f3	6f3-4f4	7f4-7f1
3f0-3f1	6f1-5f4	6f2-4f3	7f3-7f2	7f4-8f1
3f0-1f4	7f1-8f0	6f2-4f4	7f3-8f2	7f4-9f2
4f0-3f2	7f1-9f0	7f2-6f1	8f3-8f1	8f4-8f1
5f0-3f2	7f1-7f2	7f2-4f4	8f3-9f1	8f4-8f2
5f0-2f3	7f1-6f3	8f2-9f0	1f4-1f2	8f4-9f2
5f0-2f4	8f1-8f0	8f2-6f3	1f4-1f3	9f4-8f2
6f0-3f1	8f1-9f0	8f2-6f4	2f4-2f0	
7f0-4f3	8f1-8f2	9f2-6f3	2f4-2f2	

Appendix C

Combination frequencies detected in a set of light curves obtained by the TESS mission and their non-linearity unambiguous identifications.

Table C.1 Combination frequencies detected in the stars of the set analysed in Antoci et al. (2019). Variability type column is extracted from Antoci et al. (2019) A1 table. In column 2, the Best Parents resulting from the BPM in cycles per day. In the 4th column, the combination frequency values can be calculated with the given parent frequencies resulting from BPM in column 2, since the fitted values are the exact combination frequency values. (M) means that the combination matches the NLDP non-linearities template. (N-M) means no-matching the NLDP non-linearities template.

TICs	Variability Type	Best Parents [d^{-1}]	Combinations
TIC 102090493	δSct/Ap/binary?	$f_1 =$23.79306 $f_2 =$24.47857	only subtractions
TIC 116157537	δ Sct	$f_1 =$2.72392 $f_2 =$4.44156	$f_1 + f_2$ (M) and a few subtractions
TIC 12784216	δ Sct / hybrid?	$f_1 =$12.65818 $f_2 =$16.70634	$2f_1$, $2f_2$, $f_1 + f_2$ (N-M) and a few subtractions
			Continued on next page

Combination frequencies detected in a set of light curves obtained by the TESS mission and their non-linearity unambiguous identifications.

Table C.1 – continued from previous page

TICs	Variability Type	Best Parents [d^{-1}]	Combinations
TIC 137796620	δ Sct	$f_1 =$29.79899 $f_2 =$40.49900	No combinations
TIC 139825582	δ Sct / hybrid?	$f_1 =$5.93556 $f_2 =$7.93856	$2f_1$ (N-M) and a few subtractions
TIC 144387364	δ Sct / hybrid?	$f_1 =$16.01867 $f_2 =$16.70819	$2f_1$ (N-M) and a few subtractions
TIC 147085268	δ Sct / hybrid?	$f_1 =$13.94128 $f_2 =$22.55033	only subtractions
TIC 150101501	δ Sct	$f_1 =$42.75621 $f_2 =$45.93556	1 subtraction
TIC 150394126	δ Sct / hybrid?	$f_1 =$49.08808 $f_2 =$58.58333	$f_1 + f_2$ (M)
TIC 152864226	δ Sct / hybrid?	$f_1 =$32.62299 $f_2 =$41.57444	1 subtraction
TIC 161172103	δ Sct	$f_1 =$7.93333 $f_2 =$14.77690	only subtractions
TIC 166808854	δ Sct	$f_1 =$21.63202 $f_2 =$37.34444	only subtractions
TIC 167602316	δ Sct / hybrid?	$f_1 =$1.41631 $f_2 =$5.74444	$2f_1$, $2f_2$, $3f_2$, $5f_2$, $7f_2$, $9f_2$, $10f_2$ $f_1 + f_2$, $f_1 + 4f_2$, $f_1 + 5f_2$ (N-M) and a few subtractions
			Continued on next page

Table C.1 – continued from previous page

TICs	Variability Type	Best Parents $[d^{-1}]$	Combinations
TIC 183595451	δ Sct	$f_1 = 10.70333$ $f_2 = 11.93333$	$f_1 + f_2$ (N-M) and a few subtractions
TIC 197686479	δ Sct	$f_1 = 8.27070$ $f_2 = 9.19179$	only subtractions
TIC 197759259	δ Sct / hybrid?	$f_1 = 24.47584$ $f_2 = 26.28570$	only subtractions
TIC 198035211	δ Sct	$f_1 = 19.74444$ $f_2 = 31.05598$	only subtractions
TIC 201250317	δ Sct	$f_1 = 26.92956$ $f_2 = 34.69396$	only subtractions
TIC 211379298	δ Sct / binary	$f_1 = 22.46870$ $f_2 = 32.13282$	No combinations
TIC 219332123	δ Sct / hybrid?	$f_1 = 28.24515$	$2f_1$ (M)
TIC 224285142	δ Sct	$f_1 = 20.17758$ $f_2 = 22.44444$	1 subtraction
TIC 229059574	δ Sct	$f_1 = 18.59344$ $f_2 = 30.20444$	only subtractions
TIC 229150702	δ Sct	$f_1 = 25.21282$ $f_2 = 26.80444$	$2f_1$, $f_1 + f_2$ (M) and a few subtractions
TIC 229154157	δ Sct	$f_1 = 10.98872$	$2f_1$, $3f_1$, $4f_1$, $5f_1$, $6f_1$, $7f_1$ (M)
TIC 231014033	δ Sct	$f_1 = 23.59567$ $f_2 = 30.61971$	only subtraction

Table C.1 – continued from previous page

TICs	Variability Type	Best Parents [d^{-1}]	Combinations
TIC 231020078	δ Sct / hybrid?	$f_1 =$17.98733 $f_2 =$32.76667	only subtractions
TIC 231048083	developed δSct?	$f_1 =$6.29135	$2f_1$ (M)
TIC 234498473	δ Sct	$f_1 =$16.30171 $f_2 =$18.63009	only subtractions
TIC 234516307	δ Sct	$f_1 =$20.00806 $f_2 =$30.11556	only subtractions
TIC 234528371	δ Sct	$f_1 =$32.10399 $f_2 =$37.97444	only subtractions
TIC 234548714	δ Sct / hybrid?	$f_1 =$15.43207 $f_2 =$17.87356	only subtractions
TIC 237318602	δ Sct	$f_1 =$7.27344 $f_2 =$23.30243	only subtractions
TIC 237881239	δ Sct / hybrid?	$f_1 =$16.79003 $f_2 =$21.77969	only subtractions
TIC 253917376	δ Sct	$f_1 =$9.14444 $f_2 =$13.33404	only subtractions
TIC 260353074	δ Sct/ hybrid?	$f_1 =$12.00606 $f_2 =$14.60759	only subtractions
TIC 265566844	δ Sct? 1 peak	$f_1 =$5.63108	$2f_1$, $3f_1$ (N-M)
TIC 269994543	δ Sct / hybrid?	$f_1 =$19.43133 $f_2 =$23.13667	only subtractions
			Continued on next page

Table C.1 – continued from previous page

TICs	Variability Type	Best Parents $[d^{-1}]$	Combinations
TIC 277682809	δ Sct / hybrid?	$f_1 = 22.89667$ $f_2 = 46.46667$	only subtractions
TIC 279361762	δ Sct	$f_1 = 6.71667$ $f_2 = 10.76687$	only subtractions
TIC 279613634	δ Sct	$f_1 = 12.65844$ $f_2 = 20.61042$	only subtractions
TIC 303584611	δ Sct	$f_1 = 8.84756$ $f_2 = 17.63556$	$2f_1$ (N-M) and a few subtractions
TIC 308396022	δ Sct /HADS/ hybrid?	$f_1 = 13.20347$	$2f_1$, $3f_1$, $4f_1$, $5f_1$ (M)
TIC 32197339	γ Dor (unre-solved)	$f_1 = 2.76196$	$2f_1$
TIC 30531417	HAGD	$f_1 = 3.03967$ $f_2 = 4.96067$	$2f_1$, $3f_1$, $4f_1$, $5f_1$, $6f_1$ $7f_1$, $8f_1$, $9f_1$, $f_1 + f_2$, $2f_1 + f_2$, $3f_1 + f_2$
TIC 33911462	δ Sct	$f_1 = 5.66125$ $f_2 = 8.54603$	only subtractions
TIC 348762920	δ Sct / hybrid?	$f_1 = 12.28199$ $f_2 = 15.58145$	only subtractions
TIC 348772511	δ Sct	$f_1 = 6.67509$	$2f_1$ (N-M)
TIC 350431472	δ Sct	$f_1 = 27.37762$ $f_2 = 23.97945$	only subtractions
			Continued on next page

Combination frequencies detected in a set of light curves obtained by the TESS mission and their non-linearity unambiguous identifications.

Table C.1 – continued from previous page

TICs	Variability Type	Best Parents [d^{-1}]	Combinations
TIC 350563225	δ Sct	$f_1 =$15.12392 $f_2 =$26.82290	$f_1 + f_2$ (N-M)
TIC 358070081	δ Sct	$f_1 =$24.67471 $f_2 =$27.86013	No combinations
TIC 364399376	δ Sct	$f_1 =$7.07729	$2f_1$, $3f_1$, $4f_1$ (M)
TIC 381204458	δ Sct / binary	$f_1 =$25.60145 $f_2 =$27.56295	$2f_1$, $f_1 + f_2$ (M)
TIC 381857833	δ Sct	$f_1 =$9.86770 $f_2 =$13.00469	$3f_1$, $2f_1 + f_2$ (N-M)
TIC 38587180	δ Sct	$f_1 =$8.89994 $f_2 =$9.60006	$f_1 + f_2$ (N-M)
TIC 38602305	binary or multiple system	$f_1 =$2.11512	$2f_1$ (N-M)
TIC 38847248	δ Sct / EB	$f_1 =$0.27791 $f_2 =$15.85333	$2f_1$, $4f_1 + f_2$, $6f_1 + f_2$, $7f_1 + f_2$, $8f_1 + f_2$, $11f_1 + f_2$, $12f_1 + f_2$, $14f_1 + f_2$, $16f_1 + f_2$ (N-M)
TIC 394015973	δ Sct / hybrid?	$f_1 =$18.13799 $f_2 =$21.89067	only subtractions
TIC 396720223	δ Sct / hybrid?	$f_1 =$14.63695 $f_2 =$23.42661	only subtractions
TIC 402318229	δ Sct / hybrid?	$f_1 =$19.12031 $f_2 =$25.30510	$2f_1$ (M)
			Continued on next page

Table C.1 – continued from previous page

TICs	Variability Type	Best Parents [d^{-1}]	Combinations
TIC 439399707	δ Sct / binary / flares	$f_1 = 0.30121$	$2f_1$, $3f_1$, $4f_1$, $5f_1$, $6f_1$, $8f_1$, $9f_1$, $10f_1$, $13f_1$, $14f_1$, $17f_1$ (N-M)
TIC 441110063	δ Sct	$f_1 = 26.22285$ $f_2 = 34.47330$	No combinations
TIC 44627561	δ Sct / binary / Ap?	$f_1 = 0.32056$	$[1\text{-}6]f_1$, $59f_1$, $[61\text{-}66]f_1$, $74f_1$ (N-M)
TIC 469844770	δ Sct	$f_1 = 43.58022$ $f_2 = 50.23215$	No combinations
TIC 469933721	γ Dor / δ Sct / hybrid?	$f_1 = 4.58435$	$2f_1$ (N-M)
TIC 49677785	δ Sct / binary	$f_1 = 0.62718$	$[1\text{-}10]f_1$, $[12\text{-}14]f_1$, $32f_1$, $33f_1$, $43f_1$ (N-M)
TIC 52244754	δ Sct	$f_1 = 20.33117$ $f_2 = 23.37295$	No combinations
TIC 52258534	δ Sct	$f_1 = 8.87822$ $f_2 = 9.04222$	only subtractions
TIC 66434034	δ Sct	$f_1 = 39.76912$ $f_2 = 41.13685$	No combinations
TIC 71334169	δ Sct	$f_1 = 22.46268$ $f_2 = 22.96432$	only subtractions

Combination frequencies detected in a set of light curves obtained by the TESS mission and their non-linearity unambiguous identifications.

Table C.1 – continued from previous page

TICs	Variability Type	Best Parents [d^{-1}]	Combinations
TIC 80474886	δ Sct	$f_1 =$14.82019 $f_2 =$18.17329	No combinations
TIC 88277481	γDor/hybrid/1 peak only in δ Sct regime	$f_1 =$28.05811	No combinations
TIC 89464315	δ Sct	$f_1 =$6.00045 $f_2 =$8.01266	only subtractions
TIC 89542582	δ Sct	$f_1 =$22.16419 $f_2 =$28.29050	only subtractions
TIC 92734713	δ Sct	$f_1 =$49.69298 $f_2 =$54.40333	No combinations
TIC 399572664	δ Sct / binary? / rot?	$f_1 =$2.23314	$2f_1$ (N-M)
TIC 99839685	δ Sct / hybrid?	$f_1 =$7.54644 $f_2 =$13.81373	$2f_1$ (N-M)

Bibliography

Aerts, C., Christensen-Dalsgaard, J., and Kurtz, D. W. (2010). *Asteroseismology.*

Antoci, V., Cunha, M. S., Bowman, D. M., Murphy, S. J., Kurtz, D. W., Bedding, T. R., Borre, C. C., Christophe, S., Daszyńska-Daszkiewicz, J., Fox-Machado, L., García Hernández, A., Ghasemi, H., Handberg, R., Hansen, H., Hasanzadeh, A., Houdek, G., Johnston, C., Justesen, A. B., Kahraman Alicavus, F., Kotysz, K., Latham, D., Matthews, J. M., Mønster, J., Niemczura, E., Paunzen, E., Sánchez Arias, J. P., Pigulski, A., Pepper, J., Richey-Yowell, T., Safari, H., Seager, S., Smalley, B., Shutt, T., Sódor, A., Suárez, J. C., Tkachenko, A., Wu, T., Zwintz, K., Barceló Forteza, S., Brunsden, E., Bognár, Z., Buzasi, D. L., Chowdhury, S., De Cat, P., Evans, J. A., Guo, Z., Guzik, J. A., Jevtic, N., Lampens, P., Lares Martiz, M., Lovekin, C., Li, G., Mirouh, G. M., Mkrtichian, D., Monteiro, M. J. P. F. G., Nemec, J. M., Ouazzani, R. M., Pascual-Granado, J., Reese, D. R., Rieutord, M., Rodon, J. R., Skarka, M., Sowicka, P., Stateva, I., Szabó, R., and Weiss, W. W. (2019). The first view of δ Scuti and γ Doradus stars with the TESS mission. *Monthly Notices of the Royal Astronomical Society*, 490(3):4040–4059.

Antonello, E., Broglia, P., Conconi, P., and Mantegazza, L. (1986). Fourier decomposition of the light curves of high amplitudes delta Scuti and SX Phe stars. *Astronomy & Astrophysics*, 169:122–132.

Auvergne, M., Bodin, P., Boisnard, L., Buey, J.-T., Chaintreuil, S., Epstein, G., Jouret, M., Lam-Trong, T., Levacher, P., Magnan, A., Perez, R., Plasson, P., Plesseria, J., Peter, G.,

Steller, M., Tiphène, D., Baglin, A., Agogué, P., Appourchaux, T., Barbet, D., Beaufort, T., Bellenger, R., Berlin, R., Bernardi, P., Blouin, D., Boumier, P., Bonneau, F., Briet, R., Butler, B., Cautain, R., Chiavassa, F., Costes, V., Cuvilho, J., Cunha-Parro, V., De Oliveira Fialho, F., Decaudin, M., Defise, J.-M., Djalal, S., Docclo, A., Drummond, R., Dupuis, O., Exil, G., Fauré, C., Gaboriaud, A., Gamet, P., Gavalda, P., Grolleau, E., Gueguen, L., Guivarc'h, V., Guterman, P., Hasiba, J., Huntzinger, G., Hustaix, H., Imbert, C., Jeanville, G., Johlander, B., Jorda, L., Journoud, P., Karioty, F., Kerjean, L., Lafond, L., Lapeyrere, V., Landiech, P., Larqué, T., Laudet, P., Le Merrer, J., Leporati, L., Leruyet, B., Levieuge, B., Llebaria, A., Martin, L., Mazy, E., Mesnager, J.-M. M., Michel, J.-P. P., Moalic, J.-P. P., Monjoin, W., Naudet, D., Neukirchner, S., Nguyen-Kim, K., Ollivier, M., Orcesi, J.-L. L., Ottacher, H., Oulali, A., Parisot, J., Perruchot, S., Piacentino, A., da Silva, L., Platzer, J., Pontet, B., Pradines, A., Quentin, C., Rohbeck, U., Rolland, G., Rollenhagen, F., Romagnan, R., Russ, N., Samadi, R., Schmidt, R., Schwartz, N., Sebbag, I., Smit, H., Sunter, W., Tello, M., Toulouse, P., Ulmer, B., Vandermarcq, O., Vergnault, E., Wallner, R., Waultier, G., Zanatta, P., Pinheiro da Silva, L., Platzer, J., Pontet, B., Pradines, A., Quentin, C., Rohbeck, U., Rolland, G., Rollenhagen, F., Romagnan, R., Russ, N., Samadi, R., Schmidt, R., Schwartz, N., Sebbag, I., Smit, H., Sunter, W., Tello, M., Toulouse, P., Ulmer, B., Vandermarcq, O., Vergnault, E., Wallner, R., Waultier, G., and Zanatta, P. (2009). The CoRoT satellite in flight: description and performance. *Astronomy & Astrophysics*, 506(1):411–424.

Baglin, A., Breger, M., Chevalier, C., Hauck, B., Le Contel, J. M., Sareyan, J. P., and Valtier, J. C. (1973). Delta Scuti stars. *Astronomy & Astrophysics*, 23:221.

Balona, L. A. (2012). Combination frequencies in δ Scuti stars. *Monthly Notices of the Royal Astronomical Society*, 422(2):1092–1097.

Balona, L. A. (2014). Low frequencies in Kepler δ Scuti stars. *Monthly Notices of the Royal Astronomical Society*, 437(2):1476–1484.

Balona, L. A. (2016). Combination frequencies in high-amplitude δ Scuti stars. *Monthly Notices of the Royal Astronomical Society*, 459(1):1097–1103.

Balona, L. A. (2018). Gaia luminosities of pulsating A-F stars in the Kepler field. *Monthly Notices of the Royal Astronomical Society*, 479(1):183–191.

Balona, L. A., Daszyńska-Daszkiewicz, J., and Pamyatnykh, A. A. (2015). Pulsation frequency distribution in δ Scuti stars. *Monthly Notices of the Royal Astronomical Society*, 452(3):3073–3084.

Balona, L. A. and Dziembowski, W. A. (2011). Kepler observations of δ Scuti stars. *Monthly Notices of the Royal Astronomical Society*, 417(1):591–601.

Balona, L. A., Lenz, P., Antoci, V., Bernabei, S., Catanzaro, G., Daszyńska-Daszkiewicz, J., di Criscienzo, M., Grigahcène, A., Handler, G., Kurtz, D. W., Marconi, M., Molenda-Żakowicz, J., Moya, A., Nemec, J. M., Pigulski, A., Pricopi, D., Ripepi, V., Smalley, B., Suárez, J. C., Suran, M., Hall, J. R., Kinemuchi, K., and Klaus, T. C. (2012). Kepler observations of the high-amplitude δ Scuti star V2367 Cyg. *Monthly Notices of the Royal Astronomical Society*, 419(4):3028–3038.

Barceló Forteza, S., Michel, E., Roca Cortés, T., and García, R. A. (2015). Evidence of amplitude modulation due to resonant mode coupling in the δ Scuti star KIC 5892969. A particular or a general case? *Astronomy & Astrophysics*, 579:A133.

Bevington, P. R. and Robinson, D. K. (2003). *Data reduction and error analysis for physical sciences*. McGraw-Hill, New York, NY.

Bowman, D. M. (2017). *Amplitude Modulation of Pulsation Modes in Delta Scuti Stars*.

Bowman, D. M. and Kurtz, D. W. (2014). Pulsational frequency and amplitude modulation in the δ Sct star KIC 7106205. *Monthly Notices of the Royal Astronomical Society*, 444(2):1909–1918.

Bowman, D. M., Kurtz, D. W., Breger, M., Murphy, S. J., and Holdsworth, D. L. (2016). Amplitude modulation in δ Sct stars: Statistics from an ensemble study of Kepler targets. *Monthly Notices of the Royal Astronomical Society*, 460(2):1970–1989.

Brassard, P., Fontaine, G., and Wesemael, F. (1995). The Modeling of Energy Distributions and Light Curves of ZZ Ceti Stars. I. Basic Theory and Semianalytic Expressions for the Emergent Flux. *The Astrophysical Journal Supplement Series*, 96(3):545–580.

Breger, M., Fossati, L., Balona, L., Kurtz, D. W., Robertson, P., Bohlender, D., Lenz, P., Müller, I., Lüftinger, T., Clarke, B. D., Hall, J. R., and Ibrahim, K. A. (2012). Relationship between Low and High Frequencies in δ Scuti Stars: Photometric Kepler and Spectroscopic Analyses of the Rapid Rotator KIC 8054146. *The Astrophysical Journal*, 759(1):62.

Breger, M. and Lenz, P. (2008). Amplitude variability and multiple frequencies in 44 Tauri: 2000-2006. *Astronomy & Astrophysics*, 488(2):643–651.

Breger, M. and Montgomery, M. H. (2014). Evidence of Resonant Mode Coupling and the Relationship between Low and High Frequencies in a Rapidly Rotating a Star. *The Astrophysical Journal*, 783(2):89.

Breger, M., Pamyatnykh, A. A., Pikall, H., and Garrido, R. (1999). The delta Scuti star FG Virginis. IV. Mode identifications and pulsation modelling. *Astronomy & Astrophysics*, 341:151–162.

Breger, M., Stich, J., Garrido, R., Martin, B., Jiang, S. Y., Li, Z. P., Hube, D. P., Ostermann, W., Paparo, M., and Scheck, M. (1993). Nonradial pulsation of the delta Scuti star BU CANCRI in the Praesepe cluster. *Astronomy & Astrophysics*, 271:482–486.

Brickhill, A. J. (1992). The pulsations of ZZ Ceti stars - V. The light curves. *Monthly Notices of the Royal Astronomical Society*, 259:519–528.

Buchler, J. R., Goupil, M. J., and Hansen, C. J. (1997). On the role of resonances in nonradial pulsators. *Astronomy & Astrophysics*, 321:159–176.

Christensen-Dalsgaard, J. (1997). Lecture notes on stellar oscillations. *Institut for Fysik og Astronomi, Aarhus Universitet, Denmark*.

Christy, R. F. (1962). Energy Transport in the Hydrogen Ionization Zone of Giant Stars. *The Astrophysical Journal*, 136:887.

Christy, R. F. (1964). The Calculation of Stellar Pulsation. *Reviews of Modern Physics*, 36(2):555–571.

Christy, R. F. (1966). A Study of Pulsation in RR Lyrae Models. *The Astrophysical Journal*, 144:108.

Christy, R. F. (1967). The Non-Linear Calculations for Pulsating Stars. In Thomas, R. N., editor, *Aerodynamic Phenomena in Stellar Atmospheres*, volume 28, page 105.

Claverie, A., Isaak, G. R., McLeod, C. P., van der Raay, H. B., and Cortes, T. R. (1979). Solar structure from global studies of the 5-minute oscillation. *Nature*, 282:591–594.

Cooley, J. W. and Tukey, J. W. (1965). An algorithm for the machine calculation of complex fourier series. *Mathematics of computation*, 19(90):297–301.

Cunha, M. S., Aerts, C., Christensen-Dalsgaard, J., Baglin, A., Bigot, L., Brown, T. M., Catala, C., Creevey, O. L., Domiciano de Souza, A., Eggenberger, P., Garcia, P. J. V., Grundahl, F., Kervella, P., Kurtz, D. W., Mathias, P., Miglio, A., Monteiro, M. J. P. F. G., Perrin, G., Pijpers, F. P., Pourbaix, D., Quirrenbach, A., Rousselet-Perraut, K., Teixeira, T. C., Thévenin, F., and Thompson, M. J. (2007). Asteroseismology and interferometry. *Astronomy & Astrophysicsr*, 14(3-4):217–360.

De Franciscis, S., Pascual-Granado, J., Suárez, J. C., García Hernández, A., and Garrido, R. (2018). Fractal analysis applied to light curves of δ Scuti stars. *Monthly Notices of the Royal Astronomical Society*, 481(4):4637–4649.

Deeming, T. J. (1975). Fourier Analysis with Unequally-Spaced Data. *Astrophysics and Space Science*, 36(1):137–158.

Degroote, P., Aerts, C., Ollivier, M., Miglio, A., Debosscher, J., Cuypers, J., Briquet, M., Montalbán, J., Thoul, A., Noels, A., De Cat, P., Balaguer-Núñez, L., Maceroni, C., Ribas, I., Auvergne, M., Baglin, A., Deleuil, M., Weiss, W. W., Jorda, L., Baudin, F., and Samadi, R. (2009). CoRoT's view of newly discovered B-star pulsators: results for 358 candidate B pulsators from the initial run's exoplanet field data. *Astronomy & Astrophysics*, 506(1):471–489.

Dupret, M. A., Grigahcène, A., Garrido, R., Gabriel, M., and Scuflaire, R. (2005). Convection-pulsation coupling. II. Excitation and stabilization mechanisms in δ Sct and γ Dor stars. *Astronomy & Astrophysics*, 435(3):927–939.

Dziembowski, W. and Krolikowska, M. (1985). Nonlinear mode coupling in oscillating stars. II - Limiting amplitude effect of the parametric resonance in main sequence stars. *Acta Astronomica*, 35:5–28.

Dziembowski, W. a. (1982). Nonlinear mode coupling in oscillating stars. I - Second order theory of the coherent mode coupling. *Acta Astronómica*, 32:147.

Eddington, A. S. (1917). The pulsation theory of Cepheid variables. *The Observatory*, 40:290–293.

Eddington, A. S. (1920). The Internal Constitution of the Stars. *Nature*, 106(2653):14–20.

Eddington, A. S. (1926). *The Internal Constitution of the Stars.*

Eggen, O. J. (1956). ρ Puppis: A New Short-Period Variable Star. *Publications of the Astronomical Society of the Pacific*, 68(402):238.

García Hernández, A., Moya, A., Michel, E., Suárez, J. C., Poretti, E., Mart\'\in-Ru\'\iz, S., Amado, P. J., Garrido, R., Rodr\'\iguez, E., Rainer, M., Uytterhoeven, K., Rodrigo, C., Solano, E., Rodón, J. R., Mathias, P., Rolland, A., Auvergne, M., Baglin, A., Baudin, F., Catala, C., and Samadi, R. (2013). An in-depth study of HD 174966 with CoRoT photometry and HARPS spectroscopy. Large separation as a new observable for δ Scuti stars. *Astronomy & Astrophysics*, 559:A63.

Garrido, R. and Rodriguez, E. (1996). Microvariability in high-amplitude delta Scuti radially pulsating stars. *Monthly Notices of the Royal Astronomical Society*, 281(2):696–702.

Gilliland, R. L., Brown, T. M., Christensen-Dalsgaard, J., Kjeldsen, H., Aerts, C., Appourchaux, T., Basu, S., Bedding, T. R., Chaplin, W. J., Cunha, M. S., De Cat, P., De Ridder, J., Guzik, J. A., Handler, G., Kawaler, S., Kiss, L., Kolenberg, K., Kurtz, D. W., Metcalfe, T. S., Monteiro, M. J. P. F. G., Szabó, R., Arentoft, T., Balona, L. A., Debosscher, J., Elsworth, Y. P., Quirion, P.-O., Stello, D., Suárez, J. C., Borucki, W. J., Jenkins, J. M., Koch, D., Kondo, Y., Latham, D. W., Rowe, J. F., and Steffen, J. H. (2010). Kepler Asteroseismology Program: Introduction and First Results. *Publications of the Astronomical Society of the Pacific*, 122(888):131–143.

Goodricke, J. and Englefield, H. C. (1785). Observations of a New Variable Star. By John Goodricke, Esq.; Communicated by Sir H. C. Englefield, Bart. F. R. S. and A. S. *Philosophical Transactions of the Royal Society of London Series I*, 75:153–164.

Goupil, M. J., Dziembowski, W. A., and Fontaine, G. (1998). On Some Observational Consequences of Nonlinearities in Stellar Pulsations. *Baltic Astronomy*, 7:21–41.

Grigahcène, A., Antoci, V., Balona, L., Catanzaro, G., Daszyńska-Daszkiewicz, J., Guzik, J. A., Handler, G., Houdek, G., Kurtz, D. W., Marconi, M., Monteiro, M. J. P. F. G.,

Moya, A., Ripepi, V., Suárez, J. C., Uytterhoeven, K., Borucki, W. J., Brown, T. M., Christensen-Dalsgaard, J., Gilliland, R. L., Jenkins, J. M., Kjeldsen, H., Koch, D., Bernabei, S., Bradley, P., Breger, M., Di Criscienzo, M., Dupret, M. A., García, R. A., García Hernández, A., Jackiewicz, J., Kaiser, A., Lehmann, H., Martín-Ruiz, S., Mathias, P., Molenda-Żakowicz, J., Nemec, J. M., Nuspl, J., Paparó, M., Roth, M., Szabó, R., Suran, M. D., and Ventura, R. (2010). Hybrid γ Doradus-δ Scuti Pulsators: New Insights into the Physics of the Oscillations from Kepler Observations. *The Astrophysical Journall*, 713(2):L192–L197.

Guzik, J. A., Kaye, A. B., Bradley, P. A., Cox, A. N., and Neuforge, C. (2000). Driving the Gravity-Mode Pulsations in γ Doradus Variables. *The Astrophysical Journal*, 542(1):L57–L60.

Handler, G., Arentoft, T., Shobbrook, R. R., Wood, M. A., Crause, L. A., Crake, P., Podmore, F., Habanyama, A., Oswalt, T., Birch, P. V., Lowe, G., Sterken, C., Meintjes, P., Brink, J., Claver, C. F., Medupe, R., Guzik, J. A., Beach, T. E., Martinez, P., Leibowitz, E. M., Ibbetson, P. A., Smith, T., Ashoka, B. N., Raj, N. E., Kurtz, D. W., Balona, L. A., O'Donoghue, D., Costa, J. E. S., and Breger, M. (2000). Delta Scuti Network observations of XX Pyx: detection of 22 pulsation modes and of short-term amplitude and frequency variations. *Monthly Notices of the Royal Astronomical Society*, 318(2):511–525.

Jeffery, C. S. (2008). The impact of asteroseismology on the theory of stellar evolution. *Communications in Asteroseismology*, 157:240–248.

Kallinger, T., Reegen, P., and Weiss, W. W. (2008). A heuristic derivation of the uncertainty for frequency determination in time series data. *Astronomy & Astrophysics*, 481(2):571–574.

Kurtz, D. W., Shibahashi, H., Murphy, S. J., Bedding, T. R., and Bowman, D. M. (2015). A unifying explanation of complex frequency spectra of γ Dor, SPB and Be stars: com-

bination frequencies and highly non-sinusoidal light curves. *Monthly Notices of the Royal Astronomical Society*, 450(3):3015–3029.

Lares-Martiz , M., Garrido, R., and Pascual-Granado, J. (2020). Self-consistent method to extract non-linearities from pulsating star light curves - I. Combination frequencies. *Monthly Notices of the Royal Astronomical Society*, 498(1):1194–1204.

Lee, Y.-H., Kim, S. S., Shin, J., Lee, J., and Jin, H. (2008). Incidence of High-Amplitude δ Scuti-Type Variable Stars. *Publications of the Astronomical Society of Japan*, 60(3):551–555.

Lenz, P. and Breger, M. (2004). Period04: A software package to extract multiple frequencies from real data. *Proceedings of the International Astronomical Union*, 224:786–790.

Lorimer, D. R. and Kramer, M. (2004). *Handbook of Pulsar Astronomy*, volume 4 of *Cambridge observing handbooks for research astronomers*.

Mantegazza, L., Poretti, E., Michel, E., and others (2012). Pulsation spectrum of δ Scuti stars: the binary HD 50870 as seen with CoRoT and HARPS. *Astronomy & Astrophysics*, 542:A24.

Mathias, P., Gillet, D., Aerts, C., and Breitfellner, M. G. (1997). A spectroscopic study of the delta Scuti star rho Puppis. *Astronomy & Astrophysics*, 327:1077–1086.

McNamara, D. (1997). Luminosities of SX Phoenicis, Large-Amplitude Delta Scuti, and RR Lyrae Stars. *Publications of the Astronomical Society of the Pacific*, 109:1221–1232.

Michel, E., Dupret, M.-A., Reese, D., Ouazzani, R.-M., Debosscher, J., Hernández, A. G., Belkacem, K., Samadi, R., Salmon, S., Suarez, J. C., and Forteza, S. B. (2017). What CoRoT tells us about δ Scuti stars. Existence of a regular pattern and seismic indices to characterize stars. In *European Physical Journal Web of Conferences*, volume 160 of *European Physical Journal Web of Conferences*, page 03001.

Montgomery, M. H. (2005). A New Technique for Probing Convection in Pulsating White Dwarf Stars. *The Astrophysical Journal*, 633(2):1142–1149.

Moulton, F. R. (1909). On Certain Implications of Possible Changes in the Form and Dimensions of the Sun, and Some Suggestions Toward Explaining Certain Phenomena of Variable Stars. *The Astrophysical Journal*, 29:257.

Murphy, S. J., Pigulski, A., Kurtz, D. W., Suárez, J. C., Handler, G., Balona, L. A., Smalley, B., Uytterhoeven, K., Szabo, R., Thygesen, A. O., Elkin, V., Breger, M., Grigahcene, A., Guzik, J. A., Nemec, J. M., and Southworth, J. (2013). Asteroseismology of KIC 11754974: a high-amplitude SX Phe pulsator in a 343-d binary system. *Monthly Notices of the Royal Astronomical Society*, 432(3):2284–2297.

Nowakowski, R. M. (2005). Multimode Resonant Coupling in Pulsating Stars. *Acta Astronomica*, 55:1–41.

Pascual-Granado, J., Garrido, R., and Suárez, J. C. (2015a). Limits in the application of harmonic analysis to pulsating stars. *Astronomy & Astrophysics*, 581:A89.

Pascual-Granado, J., Garrido, R., and Suárez, J. C. (2015b). MIARMA: A minimal-loss information method for filling gaps in time series. Application to CoRoT light curves. *Astronomy & Astrophysics*, 575:A78.

Pascual-Granado, J., Suárez, J. C., Garrido, R., Moya, A., García Hernández, A., Rodón, J. R., and Lares-Martiz, M. (2018). Impact of gaps in the asteroseismic characterization of pulsating stars. I. The efficiency of pre-whitening. *Astronomy & Astrophysics*, 614:A40.

Paxton, B., Smolec, R., Schwab, J., Gautschy, A., Bildsten, L., Cantiello, M., Dotter, A., Farmer, R., Goldberg, J. A., Jermyn, A. S., Kanbur, S. M., Marchant, P., Thoul, A., Townsend, R. H. D., Wolf, W. M., Zhang, M., and Timmes, F. X. (2019). Modules for

Experiments in Stellar Astrophysics (MESA): Pulsating Variable Stars, Rotation, Convective Boundaries, and Energy Conservation. *The Astrophysical Journal Supplement Series*, 243(1):10.

Payne, C. H. (1925). *Stellar Atmospheres; a Contribution to the Observational Study of High Temperature in the Reversing Layers of Stars.* PhD thesis, RADCLIFFE COLLEGE.

Pesnell, W. D. (1987). A New Driving Mechanism for Stellar Pulsations. *The Astrophysical Journal*, 314:598.

Poleski, R., Soszyński, I., Udalski, A., Szymański, M. K., Kubiak, M., Pietrzyński, G., Wyrzykowski, Ł., Szewczyk, O., and Ulaczyk, K. (2010). The Optical Gravitational Lensing Experiment. The OGLE-III Catalog of Variable Stars. VI. Delta Scuti Stars in the Large Magellanic Cloud. *Acta Astronomica*, 60(1):1–16.

Poretti, E. (2003). Asteroseismology of HADS stars: V974 Oph, a radial pulsator flavoured by nonradial components. *Astronomy & Astrophysics*, 409:1031–1035.

Poretti, E., Michel, E., Garrido, R., Lefèvre, L., Mantegazza, L., Rainer, M., Rodríguez, E., Uytterhoeven, K., Amado, P. J., Martín-Ruiz, S., Moya, A., Niemczura, E., Suárez, J. C., Zima, W., Baglin, A., Auvergne, M., Baudin, F., Catala, C., Samadi, R., Alvarez, M., Mathias, P., Paparò, M., Pápics, P., and Plachy, E. (2009). HD 50844: a new look at δ Scuti stars from CoRoT space photometry. *Astronomy & Astrophysics*, 506(1):85–93.

Priestley, M. B. (1988). *Non-linear and non-stationary time series analysis*. Academic Press.

Pápics, P. (2012). The puzzle of combination frequencies found in heat-driven pulsators. *Astronomische Nachrichten*, 333(10):1053–1056.

Reegen, P. (2007). SigSpec I. Frequency- and phase-resolved significance in Fourier space. *Astronomy & Astrophysics*, 467(3):1353–1371.

Reegen, P. (2011). Combine User's Manual. *Communications in Asteroseismology*, 163:119.

Ricker, G. R., Winn, J. N., Vanderspek, R., Latham, D. W., Bakos, G. A., Bean, J. L., Berta-Thompson, Z. K., Brown, T. M., Buchhave, L., Butler, N. R., Butler, R. P., Chaplin, W. J., Charbonneau, D., Christensen-Dalsgaard, J., Clampin, M., Deming, D., Doty, J., De Lee, N., Dressing, C., Dunham, E. W., Endl, M., Fressin, F., Ge, J., Henning, T., Holman, M. J., Howard, A. W., Ida, S., Jenkins, J. M., Jernigan, G., Johnson, J. A., Kaltenegger, L., Kawai, N., Kjeldsen, H., Laughlin, G., Levine, A. M., Lin, D., Lissauer, J. J., MacQueen, P., Marcy, G., McCullough, P. R., Morton, T. D., Narita, N., Paegert, M., Palle, E., Pepe, F., Pepper, J., Quirrenbach, A., Rinehart, S. A., Sasselov, D., Sato, B., Seager, S., Sozzetti, A., Stassun, K. G., Sullivan, P., Szentgyorgyi, A., Torres, G., Udry, S., and Villasenor, J. (2014). Transiting Exoplanet Survey Satellite. *Journal of Astronomical Telescopes, Instruments, and Systems*, 1(1):014003.

Rodríguez, E., López-González, M. J., and López de Coca, P. (2000). A revised catalogue of delta Sct stars. *Astronomy & Astrophysics*, 144:469–474.

Saha, M. N. (1920). Ionisation in the Solar Chromosphere. *Nature*, 105(2634):232–233.

Saio, H., Bedding, T. R., Kurtz, D. W., Murphy, S. J., Antoci, V., Shibahashi, H., Li, G., and Takata, M. (2018). An astrophysical interpretation of the remarkable g-mode frequency groups of the rapidly rotating γ Dor star, KIC 5608334. *Monthly Notices of the Royal Astronomical Society*, 477(2):2183–2195.

Scargle, J. D. (1982). Studies in astronomical time series analysis. II. Statistical aspects of spectral analysis of unevenly spaced data. *The Astrophysical Journal*, 263:835–853.

Scargle, J. D. (1989). Studies in Astronomical Time Series Analysis. III. Fourier Transforms, Autocorrelation Functions, and Cross-Correlation Functions of Unevenly Spaced Data. *The Astrophysical Journal*, 343:874.

Scargle, J. D. (2020). Studies in Astronomical Time Series Analysis: VII. An Enquiry Concerning Non-Linearity, the RMS-Mean Flux Relation, and log-Normal Flux Distributions. *Preprint (arXiv-ph.IM/08314v1)*.

Scargle, J. D., Way, M. J., and Gazis, P. R. (2017). Structure in the 3D Galaxy Distribution. III. Fourier Transforming the Universe: Phase and Power Spectra. *The Astrophysical Journal*, 839(1):40.

Shapley, H. (1914). On the Nature and Cause of Cepheid Variation. *The Astrophysical Journal*, 40:448.

Simon, N. R. and Lee, A. S. (1981). THE STRUCTURAL PROPERTIES OF CEPHEID LIGHT CURVES. *The Astrophysical Journal*, 248(1):291–297.

Stellingwerf, R. F. (1979). Pulsation in the lower Cepheid strip. I. Linear survey. *The Astrophysical Journal*, 227:935–942.

Stellingwerf, R. F. (1980). *Nonlinear delta Scuti models - The main sequence catastrophe*, volume 125, pages 50–54.

Sterken, C. (2005). The O-C Diagram: Basic Procedures. In Sterken, C., editor, *The Light-Time Effect in Astrophysics, Proceedings of ASP Conference Series, Vol. 335, held in Brussels 19-22 July 2004. Edited by C. Sterken. San Francisco: Astronomical Society of the Pacific, 2005, p. 3.*, volume 335 of *Astronomical Society of the Pacific Conference Series*, page 3.

Strömgren, B. (1932). The opacity of stellar matter and the hydrogen content of the stars. *Zeitschrift für Astrophysik*, 4:118.

Suárez, J. C., Garrido, R., and Moya, A. (2007). The role of rotation on Petersen diagrams. II. The influence of near-degeneracy. *Astronomy & Astrophysics*, 474(3):961–967.

Unno, W., Osaki, Y., Ando, H., Saio, H., and Shibahashi, H. (1989). *Nonradial oscillations of stars.*

Uytterhoeven, K., Moya, A., Grigahcène, A., Guzik, J. A., Gutiérrez-Soto, J., Smalley, B., Hand ler, G., Balona, L. A., Niemczura, E., Fox Machado, L., Benatti, S., Chapellier, E., Tkachenko, A., Szabó, R., Suárez, J. C., Ripepi, V., Pascual, J., Mathias, P., Martín-Ruíz, S., Lehmann, H., Jackiewicz, J., Hekker, S., Gruberbauer, M., García, R. A., Dumusque, X., Díaz-Fraile, D., Bradley, P., Antoci, V., Roth, M., Leroy, B., Murphy, S. J., De Cat, P., Cuypers, J., Kjeldsen, H., Christensen-Dalsgaard, J., Breger, M., Pigulski, A., Kiss, L. L., Still, M., Thompson, S. E., and van Cleve, J. (2011). The Kepler characterization of the variability among A- and F-type stars. I. General overview. *Astronomy & Astrophysics*, 534:A125.

Van Cleve, J. E., Christiansen, J. L., Jenkins, J. M., Caldwell, D. A., Barclay, T., Bryson, S. T., Burke, C. J., Cambell, J., Catanzarite, J., Clarke, B. D., Coughlin, J. L., Girouard, F., Haas, M. R., Klaus, T. C., Kolodziejczak, J. J., Li, J., McCauliff, S. D., Morris, R. L., Mullally, F., Quintana, E. V., Rowe, J., Sabale, A., Seader, S., Smith, J. C., Still, M. D., Tenenbaum, P. G., Thompson, S. E., Twicken, J. D., Kamal Uddin, A., and Zamudio, K. (2016). Kepler Data Characteristics Handbook. Kepler Science Document KSCI-19040-005.

Van Hoolst, T. (1994). Coupled-mode equations and amplitude equations for nonadiabatic, nonradial oscillations of stars. *Astronomy & Astrophysics*, 292:471–480.

van Kerkwijk, M. H., Clemens, J. C., and Wu, Y. (2000). Surface motion in the pulsating DA white dwarf G29-38. *Monthly Notices of the Royal Astronomical Society*, 314(2):209–219.

VanderPlas, J. T. (2018). Understanding the Lomb-Scargle Periodogram. *The Astrophysical Journals*, 236(1):16.

Wu, Y. (2001). Combination frequencies in the Fourier spectra of white dwarfs. *Monthly Notices of the Royal Astronomical Society*, 323(1):248–256.

Yang, T., Esamdin, A., Song, F., Niu, H., Feng, G., Zong, P., Zeng, X., Liu, J., Liu, J., Ma, L., and Zhao, F. (2018). A Weak Modulation Effect Detected in the Light Curves of KIC 5950759: Intrinsic or Instrumental Effect? *The Astrophysical Journal*, 863(2):195.

Zhevakin, S. (1953). To the Theory of the Cepheids. I. *Astronomical Magazine.*, 30:161–179.

Zong, W., Charpinet, S., Fu, J.-N., Vauclair, G., Niu, J.-S., and Su, J. (2018). Oscillation Mode Variability in Evolved Compact Pulsators from Kepler Photometry. I. The Hot B Subdwarf Star KIC 3527751. *The Astrophysical Journal*, 853(2):98.

Zong, W., Charpinet, S., and Vauclair, G. (2016). Signatures of nonlinear mode interactions in the pulsating hot B subdwarf star KIC 10139564. *Astronomy & Astrophysics*, 594:A46.

Zwintz, K., Neiner, C., Kochukhov, O., Ryabchikova, T., Pigulski, A., Müllner, M., Steindl, T., Kuschnig, R., Handler, G., Moffat, A. F. J., Pablo, H., Popowicz, A., and Wade, G. A. (2020). β Cas: The first δ Scuti star with a dynamo magnetic field$\star$. *Astronomy & Astrophysics*, 643:A110.